AD-A042 478 AEROVIRONMENT INC PASADENA CALIF F/G 20/4
AIRCRAFT VORTEX WAKE DECAY NEAR THE GROUND.(U)
MAY 77 I TOMBACH, P B LISSAMAN, J B MULLEN DOT-TSC-1008
UNCLASSIFIED AV-FR-668 FAA-RD-77-46 NL

1 OF 2
AD A042478

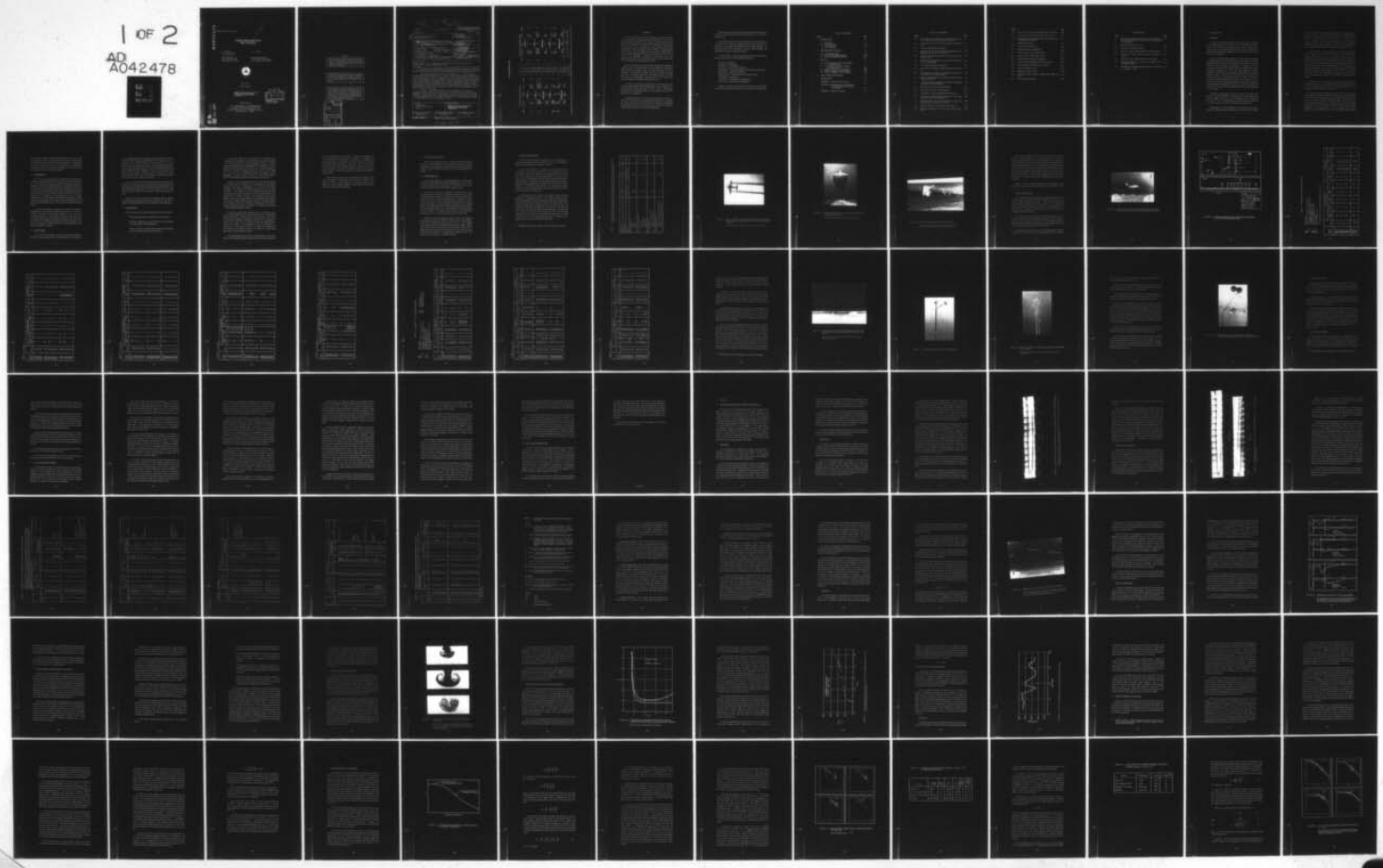

REPORT NO. FAA-RD-77-46

AIRCRAFT VORTEX WAKE DECAY NEAR THE GROUND

I. Tombach
P.B.S. Lissaman
J.B. Mullen

AEROVIRONMENT INC.
145 Vista Avenue
Pasadena CA 91107

S.J. Barker

POSEIDON RESEARCH
11777 San Vicente Blvd.
Los Angeles CA 90049

MAY 1977

FINAL REPORT

Prepared for

U.S. DEPARTMENT OF TRANSPORTATION
FEDERAL AVIATION ADMINISTRATION
Systems Research and Development Service
Washington DC 20591

NOTICE

This document is disseminated under the sponsorship of the Department of Transportation in the interest of information exchange. The United States Government assumes no liability for its contents or use thereof.

The United States Government does not endorse products or manufacturers. Trade or manufacturers' names appear herein solely because they are considered essential to the object of this report.

The contents of this report reflect the views of AeroVironment Inc., which is responsible for the facts and the accuracy of the data presented herein. The contents do not necessarily reflect the official views or policy of the Department of Transportation. This report does not constitute a standard, specification, or regulation.

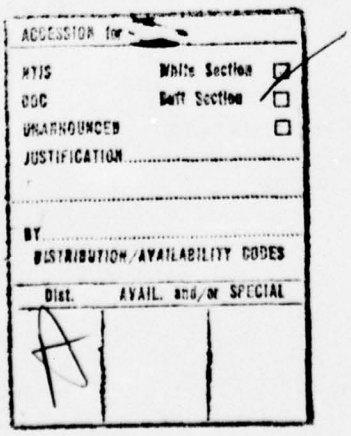

(18) FAA-RD, TSC

(19) 77-46, FAA-77-8

Technical Report Documentation Page

1. Report No.	2. Government Accession No.	3. Recipient's Catalog No.
FAA-RD-77-46		(12) 158 p.

4. Title and Subtitle	5. Report Date
(6) AIRCRAFT VORTEX WAKE DECAY NEAR THE GROUND.	(11) May 1977
	6. Performing Organization Code
7. Author(s) (10) I. Tombach, P.B.S. Lissaman, J.B. Mullen and S.J. Barker	8. Performing Organization Report No. DOT-TSC-FAA-77-8 (14) AV-FR-668
9. Performing Organization Name and Address	10. Work Unit No. (TRAIS)
AeroVironment Inc.* and Poseidon Research 145 Vista Avenue 11777 San Vicente Blvd. Pasadena CA 91107 Los Angeles CA 90049	FA705/R7126
	(15) 11. Contract or Grant No. DOT-TSC-1008 new
12. Sponsoring Agency Name and Address	13. Type of Report and Period Covered
U.S. Department of Transportation Federal Aviation Administration - Systems Research and Development Service, Washington DC 20591	(9) Final Report. June 1975 - September 1976
	14. Sponsoring Agency Code

15. Supplementary Notes

*Under contract to U.S. Department of Transportation, Transportation Systems Center, Kendall Square, Cambridge MA 02142

16. Abstract

A multi-faceted experimental and analytical research program was carried out to explore the details of aircraft wake vortex breakdown under conditions representative of those which would prevail at low altitudes in the vicinity of airports.

Three separate approaches were taken simultaneously. Flight tests with Lockheed L-18 Lodestar and Boeing 747 aircraft flying over ground-based instrumentation provided data on overall vortex behavior, on the vortex ages at the time of onset of instabilities, and on the changes in the vortex velocity fields which resulted from vortex breakdowns. Analytical work on stability theories identified conditions under which vortices could undergo unstable decay. Experimental tests in a water tank looked at the internal instability of vortices, and also shed light on vortex motion near the ground. Finally, a heuristic modeling approach resulted in a simple representation of the relationship between the times of vortex breakdowns and the ambient turbulence levels.

Although a detailed mechanism for vortex breakdowns was not found, a universal function, usable for all aircraft, was developed for predicting vortex breakdown times within a factor of two error. It was also shown that vortex breakdowns do not generally result in total dissipation of the vortex energy, but rather a residual organized motion of significant intensity often persists after bursting of a smokemarked vortex has been noted to occur.

17. Key Words	18. Distribution Statement
Waketurbulence Aircraft wake vortices Vortices	DOCUMENT IS AVAILABLE TO THE U.S. PUBLIC THROUGH THE NATIONAL TECHNICAL INFORMATION SERVICE, SPRINGFIELD, VIRGINIA 22161

19. Security Classif. (of this report)	20. Security Classif. (of this page)	21. No. of Pages	22. Price
Unclassified	Unclassified	162	

Form DOT F 1700.7 (8-72) Reproduction of completed page authorized

390 463

1B

METRIC CONVERSION FACTORS

Approximate Conversions to Metric Measures

Symbol	When You Know	Multiply by	To Find	Symbol
		LENGTH		
in	inches	2.5	centimeters	cm
ft	feet	30	centimeters	cm
yd	yards	0.9	meters	m
mi	miles	1.6	kilometers	km
		AREA		
in^2	square inches	6.5	square centimeters	cm^2
ft^2	square feet	0.09	square meters	m^2
yd^2	square yards	0.8	square meters	m^2
mi^2	square miles	2.6	square kilometers	km^2
	acres	0.4	hectares	ha
		MASS (weight)		
oz	ounces	28	grams	g
lb	pounds	0.45	kilograms	kg
	short tons (2000 lb)	0.9	tonnes	t
		VOLUME		
tsp	teaspoons	5	milliliters	ml
Tbsp	tablespoons	15	milliliters	ml
fl oz	fluid ounces	30	milliliters	ml
c	cups	0.24	liters	l
pt	pints	0.47	liters	l
qt	quarts	0.95	liters	l
gal	gallons	3.8	liters	l
ft^3	cubic feet	0.03	cubic meters	m^3
yd^3	cubic yards	0.76	cubic meters	m^3
		TEMPERATURE (exact)		
°F	Fahrenheit temperature	5.9 (after subtracting 32)	Celsius temperature	°C

Approximate Conversions from Metric Measures

Symbol	When You Know	Multiply by	To Find	Symbol
		LENGTH		
mm	millimeters	0.04	inches	in
cm	centimeters	0.4	inches	in
m	meters	3.3	feet	ft
m	meters	1.1	yards	yd
km	kilometers	0.6	miles	mi
		AREA		
cm^2	square centimeters	0.16	square inches	in^2
m^2	square meters	1.2	square yards	yd^2
km^2	square kilometers	0.4	square miles	mi^2
ha	hectares (10,000 m^2)	2.5	acres	
		MASS (weight)		
g	grams	0.035	ounces	oz
kg	kilograms	2.2	pounds	lb
t	tonnes (1000 kg)	1.1	short tons	
		VOLUME		
ml	milliliters	0.03	fluid ounces	fl oz
l	liters	2.1	pints	pt
l	liters	1.06	quarts	qt
l	liters	0.26	gallons	gal
m^3	cubic meters	35	cubic feet	ft^3
m^3	cubic meters	1.3	cubic yards	yd^3
		TEMPERATURE (exact)		
°C	Celsius temperature	9/5 (then add 32)	Fahrenheit temperature	°F

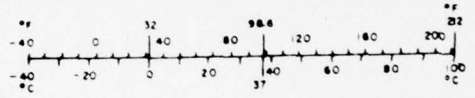

PREFACE

The work on vortex wakes which is described in this report is an evolutionary outgrowth of work begun under the sponsorship of the Air Force Office of Scientific Research in 1970. Support of AeroVironment's research by the U. S. Department of Transportation, Transportation Systems Center which started in 1972 has enabled both more extensive and intensive investigation of wake vortex behavior in the atmosphere. Through the years, the focus of the work has changed from analysis of wake behavior aloft to the more operationally significantly area of wake behavior in the lowest 100 meters of the atmosphere. Concurrently, the aircraft sizes in the experimental portions of the studies have increased so as to simulate better the aircraft wakes of greatest operational concern.

Most of the aircraft (Lockheed Lodestar, Cessna 182, and Hughes 269 helicopter) used in the flight test portion of this program were provided by Flight Systems Inc., Newport Beach, Ca., under subcontract from AeroVironment. The cooperation of Flight Systems Inc. personnel, especially Gary Hall in experiment coordination and Kenneth Anderson in aircraft modifications, was indispensable. James Nieukirk flew the Lodestar, Bill Evans the Hughes 269, and Peter Phelps the Cessna 182.

The research also involved the cooperation of the National Aeronautics and Space Administration Dryden Flight Research Center at Edwards, Ca., which provided and flew the Boeing 747 aircraft. Marvin "Russ" Barber coordinated the NASA-DFRC efforts and Fitzhugh Fulton and Tom McMurtry flew the Boeing 747.

An important portion of the study involved testing of vortices in a water tank. This work was performed by Poseidon Research of Los Angeles, Ca., under a subcontract from AeroVironment. The work was conducted by Steven Barker, one of the authors of this report. Significant contributions were provided by Steven Crow, who authored Appendix A.

Meteorological forecasts for the special wind and stability conditions required for these tests were provided by John Aldrich, as a consultant to AeroVironment.

The cooperation of the Air Force Flight Test Center at Edwards Air Force Base, Ca , in making Rosamond Dry Lake and the airspace above it available for these flight tests helped make the program possible. Of particular note were the cooperation of Joe Reif, Airfield Manager, and Albert Lambert, Program Requirements Officer.

At AeroVironment, the key participating individuals other than the authors, and their roles, included (in alphabetical order):

John Blair – photography.
Kurt Bumiller – photography,
David Felt – instrumentation engineering,
Paul Ferguson – helicopter photography and computer programming,
Ronald Glass – program administration,
Paul MacCready – overall coordination of program phases,
Trang Nguyen – data analysis,
Jerry Thelen – photography and field operations,
Bruce Wright – field operations management.

Finally, the guidance and assistance of James Hallock of DOT-TSC, who was technical monitor of the work under this contract, are appreciated.

TABLE OF CONTENTS

LIST OF ILLUSTRATIONS

LIST OF TABLES

1. INTRODUCTION

1.1 Background

The extent of the operational hazard to air traffic which is presented by the trailing vortices from aircraft in flight is ultimately limited by a decay of the strength of the organized vortical motion. Several experimental studies have established that this decay can have several forms, generally occurs rapidly once it begins, and is a consequence of an instability in the vortex configuration.

The best understood mode of decay is a mutual induction instability involving both vortices, which has been analytically modeled by Crow (1970). Subsequent flight test research by Tombach (1973) showed a correlation between the rate of growth of the instability, as measured by the time required for the vortex pair to break up into vortex rings, and the ambient atmospheric turbulence level. Crow's theory was expanded to include a turbulent forcing function (Crow and Bate, 1976), and shows reasonable agreement (within a factor of 2) with experimental data collected for various light aircraft, as reported by Tombach, et al (1974). The theory for the mutual induction instability (also known as the "sinuous" or "Crow" instability) has also been tailored for the turbulence field and image effects of the near-ground environment by Tombach, et al (1975) (also reported by Tombach and Crow, 1976), and has compared satisfactorily with experiments in the same study.

The other commonly observed mode of vortex motion decay, often described as vortex "breakdown" or "bursting," is far less understood. This breakdown appears to occur as a result of rapid growth of an instability in the core of the vortex. In experiments with vortices marked by smoke, the vortex often appears to burst when it undergoes this mode of decay.

Descriptions of vortex breakdown for actual aircraft vortices are contained in numerous reports, including work by Garodz (1970), Chevalier

(1973) and Tombach (1973). Chevalier observed that the breakdown appears in two discrete forms, which he called "turbulent" and "stretching" core dissipation. Tombach, et al (1975) noted that the core breakdowns often occur in connection with the sinuous instability, which results in a correlation between vortex breakdown times and ambient turbulence. Breakdowns totally unrelated to the sinuous instability were also observed, and no relationship with atmospheric conditions was apparent for them.

Vortex breakdown has not been treated in the same comprehensive analytical manner as has the sinuous instability. The development of a compact analytical form, even of a semi-empirical nature, for vortex breakdown would contribute a great deal towards the ability to predict and understand vortex behavior. The absence of this form is not due to a lack of effort on the part of investigators, however, but rather to the complexity of the problem and the paucity of detailed observations of the phenomena. As a further consideration, full-scale aircraft vortex wake tests have indicated significant variation in vortex breakdown times from test to test even though major aircraft and meteorological parameters were constant, and thus a purely deterministic theory cannot account for all aspects of such behavior.

In addition to the mutual induction instability and the vortex core instability, slower decay, as by turbulent erosion, aging, or ground friction has also been observed (e.g., Tombach, et al, 1975; Hallock, 1976) and is duscussed at length by Donaldson and Bilanin (1975).

The greatest hazard resulting from aircraft wakes occurs along the final portions of the approach paths to airports, since the air traffic arriving from a distribution of origination points is all funneled along the same path during the final few kilometers preceding landing. Research on the structure and hazard potential of aircraft vortices in this region indicates that the hazard from them appears to diminish when the vortices develop instabilities. Other factors, such as runway crosswinds and the gross properties of the vortex generator aircraft, can also affect the hazard for a

given situation, of course. However, for all situations, the time of vortex decay provides a definite time beyond which the hazard is significantly reduced. Because of this importance of decay mechanisms, the Transportation Systems Center (TSC) of the U.S. Department of Transportation sponsored the research on fundamental mechanisms of wake vortex decay near the ground which is described in this report.

1.2 Study Objectives

This study was concerned with the mechanisms of vortex decay under conditions simulating those present in the vicinity of airports. Although TSC has been studying vortices under operational conditions near airports for several years, much of the fundamental research on wake decay mechanisms has been performed at altitudes well above the ground and with aircraft in a "clean" (flaps up, landing gear up) configuration. Although there were good operational reasons for this emphasis in earlier research, the necessity for measurements in conditions more representative of those of concern mandated that this study emphasize vortices generated by aircraft in landing configuration (landing gear and flaps down) which were generated below the typical glide slope altitude of 60 m at the instrument landing system middle marker.

The specific objective of the study was to achieve some degree of understanding of the phenomena underlying wake decay in the airport terminal environment, with particular emphasis on the vortex core breakdown mode of decay. With regard to that decay mode, the nature of the residual flowfield after the catastrophic breakdown, and the role of axial vortex flows in the breakdown mechanism, were of particular interest. As a goal, some progress in modeling the effect of vortex bursting on vortex strength and lifetime was desired.

1.3 Study Philosophy

At the time this study began in mid-1975, the dynamical mechanisms present in vortex breakdown were not well-understood. It was recognized as

a very complex phenomenon (or, possibly, several phenomena) the results of which had been observed experimentally but not documented in any quantitative way. Possibly because of the limited data, a number of different mechanisms have been proposed. These mechanisms have either been relatively vague and general, or have been complicated mathematically and conceptually; detailed validation of them had not been done, and probably was not possible. More details on this are provided in the review article by Widnall (1975), and in the monograph by Donaldson and Bilanin (1975), as well as in later chapters of this report.

Thus, it was felt that, at this stage, a detailed attempt at theoretical prediction of the mechanism of core bursting would not be worthwhile, since the analysis would be questionable in the absence of good experimental data, while experimental validation of the necessary details of the flow field would be extremely difficult and yet would not meet the objectives of the study.

Instead, it was felt that a fresh look at the phenomenon was required. using controlled experiments to isolate different effects and a new, heuristic approach to analytically identify the main variables and their significance.

1.4 Overall Approach

Within this setting a 3-pronged study approach evolved, consisting of:

Full-scale experiments to provide quantitative information;

Laboratory experiments to explore details of vortex structure and stability under controlled conditions;

Heuristic analysis to meld theoretical concepts and experimental data into a coherent description of the behavior.

The full-scale flight tests were performed to investigate factors influencing vortex wake decay under conditions simulating those prevailing in a terminal environment. The tests employed, primarily, a medium-weight, twin engine aircraft (Lockheed Model L-18 Lodestar) as the vortex generator and were performed in the fall of 1975 in the Mojave Desert of California. The decay of organized vortex motion was monitored through the use of an array of ground-based propeller anemometers and by photography of vortices marked by smoke or small buoyant balloons. Relevant meteorological conditions were measured at the same time.

A portion of the work on this contract involved similar measurements of the vortex wake of a Boeing 747 aircraft operated by the National Aeronautics and Space Administration, so the two aircraft provided independent data relating to the effects of aircraft scale on the decay mechanisms. The Boeing 747 tests had broader objectives than those described above, and thus, in addition to the measurements performed by AeroVironment, the Boeing 747 portion of the experiment also involved Doppler acoustic radar measurements by TSC and Doppler lidar measurements by the Lockheed Missiles and Space Company. This report presents only the Boeing 747 data which is relevant to the objectives of this study; a separate comprehensive report on all aspects of the Boeing 747 experiment is being prepared by Hallock, et al (1977).

The laboratory experiments were performed in a water tank using a unique method of generation of a dye-marked vortex pair. The vortices thus generated were short in length relative to the wavelength of the sinuous mutual-induction instability, causing that instability to be suppressed to allow study of vortex motion and internal structure for extended periods. Because of the nature of this experiment, it was not considered as a simulation of a vortex wake, but rather as an analog model of portions of wake behavior which allowed testing of the effects of various input parameters on vortex stability and motion.

The analysis approach was directed toward defining, on the basis of theory and the field and laboratory experiments, those factors which affect

the vortex breakdown mode of wake decay. A goal was the development of a model giving the best description of the effects of atmospheric and aircraft parameters on the breakdown, and of the effects of the breakdown itself on the strength and lifetime of the vortices. The concepts of vortex core stability theory were reviewed and then coupled with the vortex structure insights of the laboratory experiment to provide a basis for a heuristic approach to the direct analysis of the core breakdowns observed in the flight tests.

These procedural aspects of the study program are discussed in detail in the next chapter. The subsequent chapter reviews the findings of the study, and Chapter 4 then presents an interpretive analysis of the significance of these findings. Appendices contain details of the stability analysis and of the water tank experiment.

2. DESCRIPTION OF PROGRAM

The three major program elements – flight tests, theoretical analysis, and the water tank experiments – were pursued concurrently by different investigators. The methodology which was followed for each of these investigations is described below in this chapter; the results are then presented in Chapter 3.

2.1 In-Flight Experiments

The in-flight experiments involved generation of smoke-marked vortices by Lockheed Model L-18 Lodestar and Boeing 747 aircraft. A total of 5 days of Lodestar tests and 2 days of 747 tests were flown at a test site established on Rosamond Dry Lake on Edwards AFB, California.

Each test day consisted of a sequence of low level passes by the vortex-generating aircraft over a ground-level anemometer array which recorded the velocities induced by the vortices. The behavior of the smoke-marked vortices was recorded photographically by cameras at various locations on the ground and in a helicopter hovering overhead. To provide data on meteorological conditions, soundings were performed by a tethered balloon on a variable length (7-60 m) tether, by pilot balloon launchings, and by a meteorological aircraft which was instrumented to measure temperature and turbulence. Occasionally, buoyant balloons were released from ground level to enter into and mark the axial flow in the vortex cores.

During the two days of Boeing 747 flights, the basic test installation was augmented by an array of monostatic acoustic vortex sensors operated by the DOT Transportation Systems Center and by a laser Doppler velocimeter operated by the Lockheed Missiles and Space Company. Both of these remote sensors monitored velocities in the vortices. Data from these additional sensors was not used for the analyses in this report, and thus their use will not be discussed here. A separate report, (Hallock, et al, 1977) will report in detail on all aspects of the Boeing 747 tests.

Vortex Generating Aircraft

The physical and operational characteristics of the Lockheed L-18 Lodestar and Boeing 747 aircraft are tabulated in Table 2-1. Photographs of these aircraft in flight appear in Figures 2-1 and 2-2.

Both of these aircraft were equipped with smoke generators for visualization of the airflow in the vortices. On the Lodestar, each vortex was marked by smoke from 3 pyrotechnic smoke grenades (red – left vortex; green – right vortex) which burned for approximately 1-1/2 minutes. Each wing carried a smoke generator unit containing 27 grenades, enough for a sortie of 9 passes. A smoke generator was installed underneath each wing at a spanwise point corresponding to the outboard end of the flaps, as shown in Figure 2-3. In addition, 2 violet grenades at the wingtips and 2 yellow grenades at about the midspan point on the flaps were used to illuminate vortex rollup on one run of each sortie.

On the Boeing 747, the vortices were marked by Corvis oil smoke generators* at 8 spanwise locations – each wingtip, outboard ends of outboard flaps, outboard ends of inboard flaps, inboard ends of inboard flaps. (Generator locations are numbered 1 through 8 from left wingtip to right wingtip.) Each generator had enough fuel and oil for about 10 minutes of operation. Not all smoke generators were used on each run, so that a full day's testing was possible without refilling these generators. The generators used to mark the vortices during a given run varied with the flap configuration and run objective, but were generally selected so as to best mark the cores of the vortices generated from the wingtips and, as appropriate, the ends of the outboard and inboard flaps.

---

* Designed and fabricated by Sanders Aircraft, Long Beach, California.

TABLE 2-1. PHYSICAL AND OPERATIONAL CHARACTERISTICS OF THE LOCKHEED L-18 LODESTAR AND BOEING 747 TEST AIRCRAFT, AS OPERATED DURING THIS TEST PROGRAM

Aircraft	L-18	B-747	
Wing span: b	20	60	m
Mass, m	8100-7700	205,000-260,000	kg
Flap settings: δ_f			
Partial	40%	10^o	
Down	70%	30^o	
Nominal true airspeeds: U			
Flaps up	54	110	m/s
Partial flaps	54	81	m/s
Flaps down	54	76	m/s
Vortex spacing, b_v			
Elliptic loading (clean)	16	47	m
Measured, flaps down	12	45	m
Nominal circulation, Γ			
Elliptic loading, flaps down airspeed	77	524	m^2/s
Measured b_v, flaps down airspeed	104	550	m^2/s

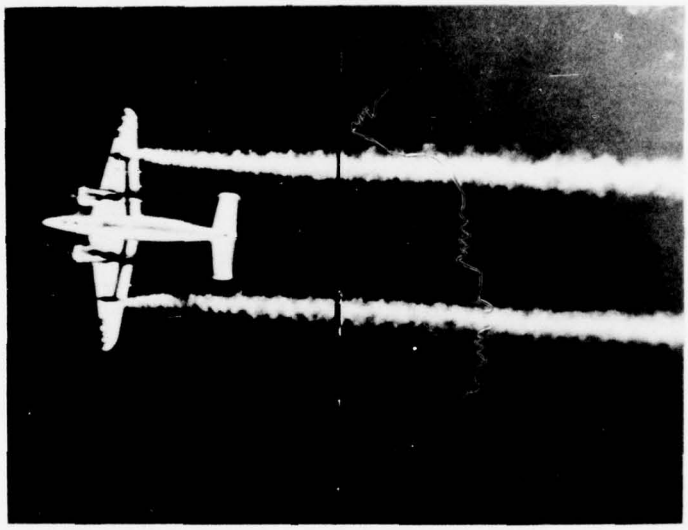

FIGURE 2-1. THE LOCKHEED L-18 LODESTAR TEST AIRCRAFT OVERHEAD WITH THE MAIN SMOKE GENERATORS ON AND WING FLAPS LOWERED

(The dark line was a reference marker above the camera.)

FIGURE 2-2. THE BOEING 747 TEST AIRCRAFT APPROACHING THE INSTRUMENTED ARRAY

(All eight smoke generators have just been turned on.)

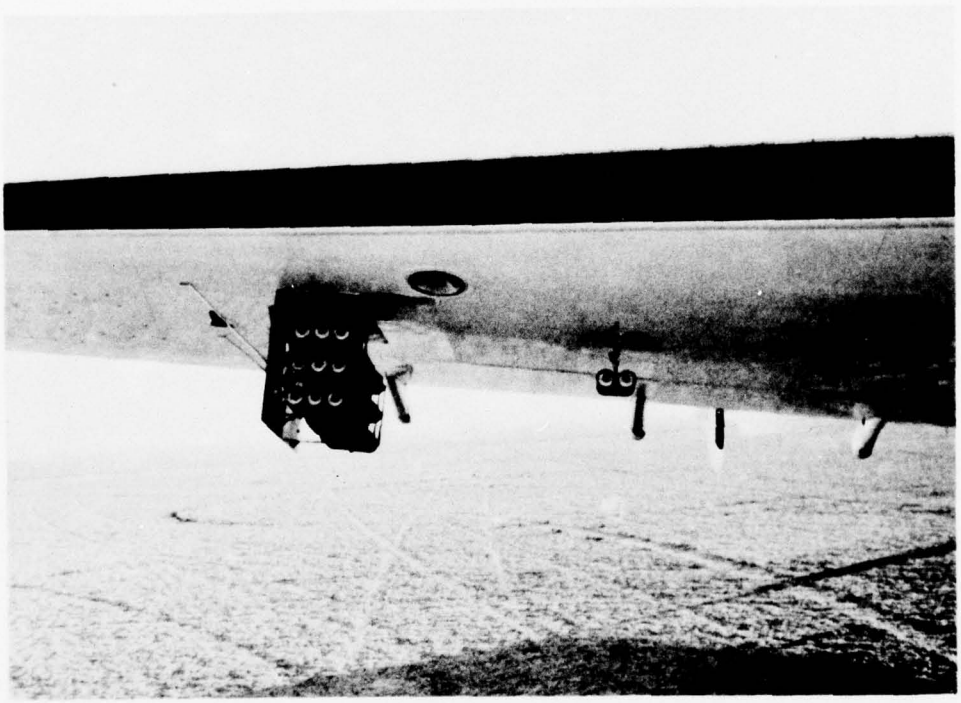

FIGURE 2-3. LODESTAR SMOKE GENERATOR INSTALLATION

(The main rack, consisting of 27 smoke grenades is to the left. The inboard yellow grenade pair is to the right.)

The aircraft configurations varied from run to run, with dominant emphasis on approximating a normal landing configuration as closely as operating conditions would allow. The clean configuration was also studied, and special Boeing 747 flap and spoiler configurations were investigated for vortex alleviation effectiveness. The flight altitudes of the Lodestar ranged from 15 to 60 meters above ground level during the data collection portion of the test; for the Boeing 747 the altitude range was between 30 and 240 meters above the surface. Most passes over the array were made in level flight, as shown in Figure 2-4 , for example, although an occasional run was made with the aircraft descending – as on a landing approach, or climbing as on takeoff.

Table 2-2 contains a complete tabulation of test conditions for each Lodestar run. A similar tabulation for the Boeing 747 runs appears in Table 2-3.

Test Site Data Collection

The test operations took place along an unused runway on Rosamond Dry Lake, with the ground instrumentation straddling this runway and the aircraft flight path following along it. Figure 2-5 shows the ground instrumentation arrangement for the Lodestar tests. The arrangement for the Boeing 747 tests was similar, except that the instrumentation layout was made larger to correspond with the larger size of the 747 and some additional equipment was added.

The major elements of the ground instrumentation system were a number of cameras for recording vortex appearance, an array of anemometers to record vortex-induced velocities, a tethered balloon system for defining low level atmospheric conditions, a pilot balloon (pibal) launch site, and a launch grid for balloons used to mark the vortices.

Two cameras were mounted to the side of the flight path, at distances ranging from 100 to 250 m which varied depending on the experiment

FIGURE 2-4. BOEING 747 TEST AIRCRAFT IN LANDING CONFIGURATION JUST AFTER PASSING OVER THE INSTRUMENTATION ARRAY

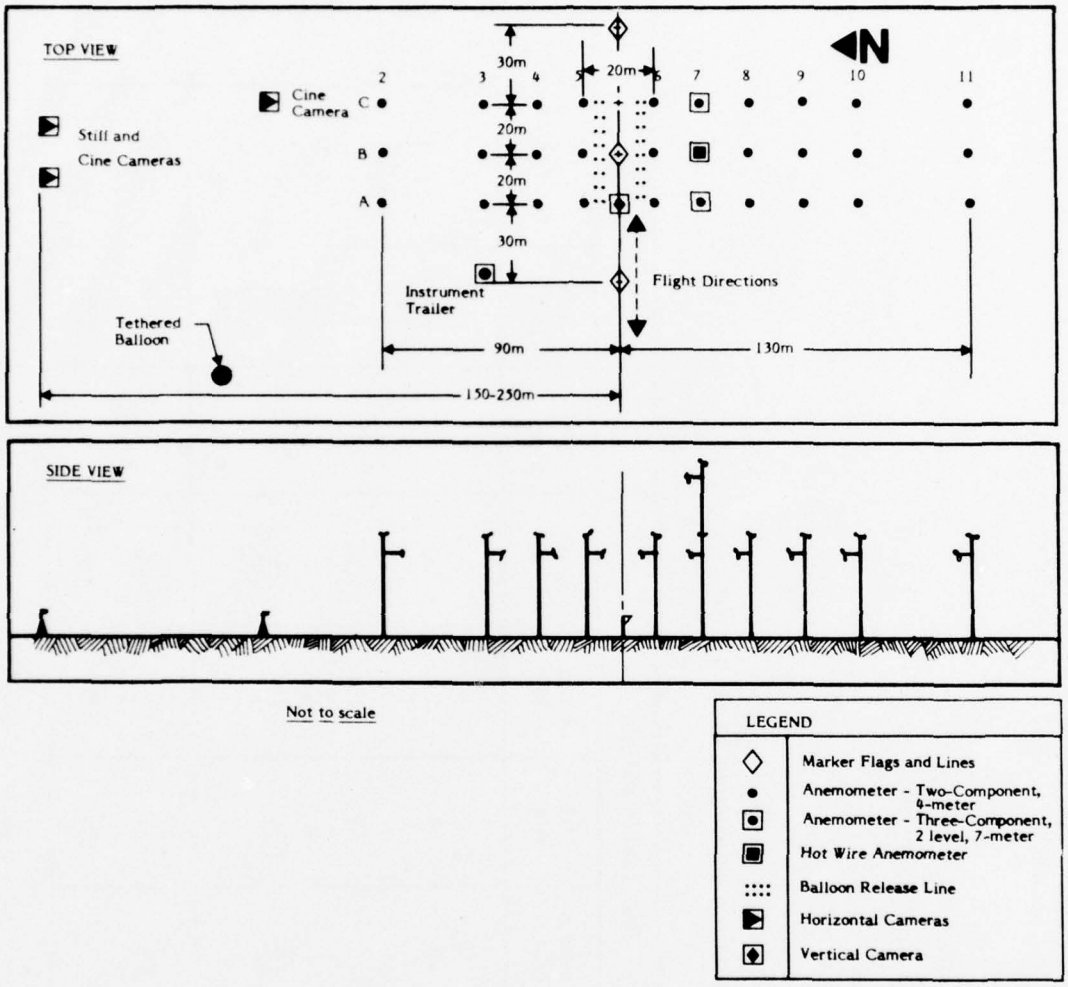

FIGURE 2-5. SCHEMATIC PORTRAYAL OF INSTRUMENTATION ARRAY LAYOUT FOR THE LODESTAR TESTS

TABLE 2-2. LODESTAR TEST CONDITION SUMMARY

WS - Wind speed
WD - Direction from which the wind blows
$\epsilon^{1/3}$ - Atmospheric turbulence dissipation rate
γ - Atmospheric stability, dT/dz
Ldg - Aircraft descending over array
TO - Aircraft climbing over array
TAS - True air speed
PST - Pacific Standard Time

Altitudes given are nominal values assigned to the aircraft.

Time (PST)	Run	Test Configuration					Meteorology			
		Heading (deg)	Altitude (m)	TAS (m/s)	Flaps (%)	Gear	WS (m/s)	WD (deg)	$\epsilon^{1/3}$ ($cm^{2/3}s^{-1}$)	γ (C/100m)
10/24/75										
0747	1	070	15	54	0	Up	0	--	<1.5	7
0754	2	"	"	"	"	"	1	120	<1.5	7
0800	3	"	"	"	"	"	1	120	<1.5	7
0807	4	070	15	54	40	Up	2	110	<1.5	7
0813	5	"	"	"	"	"	2	110	<1.5	7
0819	6	"	"	"	"	"	2	110	<1.5	7
0825	7	070	15	54	70	Up	1	100	<1.5	7
0831	8	"	"	"	"	"	1	100	<1.5	7
0836	9	"	"	"	"	"	1	150	<1.5	7
10/25/75										
0730	10	250	15	54	0	Up	1	10	0.6	4
0734	11	"	"	"	"	"	1	350	0.6	4
0738	12	"	"	"	"	"	1	350	0.5	4

TABLE 2-2. (Continued)

Time (PST)	Run	Test Configuration					Meteorology			
		Heading (deg)	Altitude (m)	TAS (m/s)	Flaps (%)	Gear	WS (m/s)	WD (deg)	$\epsilon^{1/3}$ ($cm^{2/3}s^{-1}$)	γ (C/100m)
0743	13	250	15	54	40	Up	0	--	1.2	5
0748	14	"	"	"	"	"	0	--	1.2	5
0753	15	"	"	"	"	"	0	--	1.3	5
0758	16	"	"	"	"	"	0	--	1.1	6
0803	17	"	"	"	"	"	0	--	1.3	6
0807	18	"	"	"	"	"	0	--	1.5	6
0925	19	070	15	54	40	Up	0	--	1.8	-2
0930	20	"	"	"	"	"	0	--	1.8	-2
0934	21	"	"	"	"	"	0	--	1.7	-2
0938	22	070	30	54	40	Up	0	--	1.9	-2
0942	23	"	"	"	"	"	0	--	2.2	-3
0945	24	"	"	"	"	"	0	--	2.3	-3
0949	25	"	"	"	"	"	0	--	2.1	-3
0953	26	"	"	"	"	"	0	--	2.2	-3
0957	27	"	"	"	"	"	0	--	2.1	-4
1105	28	250	30	54	40	Up	1	220	2.5	-1
1109	29	"	"	"	"	"	1	250	2.8	-1
1113	30	"	"	"	"	"	1	280	2.6	-1
1117	31	250	61	54	40	Up	1	310	2.5	-2
1120	32	"	"	"	"	"	1	340	2.6	-2
1124	33	"	"	"	"	"	1	300	2.4	-2
1128	34	"	"	"	"	"	1	260	2.7	-1
1132	35	"	"	"	"	"	1	220	2.5	-4
1136	36	"	"	"	"	"	0	--	2.6	-1

TABLE 2-2. (Continued)

Time (PST)	Run	Test Configuration					Meteorology			
		Heading (deg)	Altitude (m)	TAS (m/s)	Flaps (%)	Gear	WS (m/s)	WD (deg)	$\epsilon^{1/3}$ ($cm^{2/3}s^{-1}$)	γ (C/100m)
10/26/75										
0711	37	250	30	54	40	Up	1	190	1.5	3
0715	38	"	"	"	"	"	1	200	1.8	3
0719	39	"	"	"	"	"	1	210	1.5	3
0722	40	250	15	54	40	Up	1	210	1.3	4
0726	41	"	"	"	"	"	1	220	1.3	4
0730	42	"	"	"	"	"	1	190	1.3	5
0734	43	"	"	"	"	"	1	160	1.7	5
0738	44	"	"	"	"	"	2	140	1.7	6
0742	45	"	"	"	"	"	2	120	2.3	6
0841	46	250	15	54	70	Up	1	120	3.5	4
0845	47	"	"	"	"	"	1	120	2.9	4
0848	48	"	"	"	"	"	1	120	2.2	3
0852	49	"	"	"	"	"	1	110	2.3	3
0856	50	"	"	"	"	"	1	110	2.4	3
0859	51	"	"	"	"	"	2	110	3.9	3
0903	52	"	"	"	"	"	4	120	3.1	2
0906	53	"	"	"	"	"	5	120	4.3	2
0909	54	250	15	54	40	Up	4	120	3.2	2
12/10/75										
0854	1	250	61	54	40	Up	1	260	2.4	0
0859	2	"	"	"	"	"	1	260	1.8	0
0903	3	"	"	"	"	"	1	270	2.3	0
0906	4	"	"	"	"	"	1	270	2.4	0
0911	5	"	61	54	40	Dn	1	270	2.1	0
0915	6	"	"	"	"	"	1	260	2.3	0
0919	7	"	61	54	70	Up	1	250	1.8	0
0923	8	"	"	"	"	"	1	240	1.9	0
0928	9	"	61	54	70	Dn	1	240	1.2	0

TABLE 2-2. (Continued)

Time (PST)	Run	Test Configuration					Meteorology			
		Heading (deg)	Altitude (m)	TAS (m/s)	Flaps (%)	Gear	WS (m/s)	WD (deg)	$\epsilon^{1/3}$ ($cm^{2/3}s^{-1}$)	γ (C/100m)
1033	10	070	30 (Ldg)	54	40	Dn	1	280	2.4	0
1037	11	"	30	"	"	"	1	280	3.3	0
1041	12	"	30 (Ldg)	"	"	"	1	280	3.5	0
1045	13	"	30	"	"	"	1	290	3.1	0
1049	14	070	30 (Ldg)	54	40	Up	1	290	3.7	0
1053	15	"	30	"	"	"	1	280	4.0	0
1057	16	"	30 (Ldg)	"	"	"	1	270	3.3	0
1102	17	"	30	"	"	"	1	260	4.2	0
1106	18	070	30 (Ldg)	54	40	Dn	1	250	3.3	0
12/11/75										
0651	19	250	30 (TO)	54	0	Up	0	--	1.4	1
0656	20	"	30	"	"	"	0	--	1.3	1
0700	21	250	30 (TO)	54	15	Up	0	--	1.1	1
0704	22	"	30	"	"	"	1	180	0.8	0
0708	23	250	30 (TO)	54	40	Up	1	190	0.3	0
0712	24	"	30	"	"	"	1	170	1.0	0
0717	25	"	15	"	"	"	0	--	0.9	-1
0721	26	"	"	"	"	"	0	--	1.2	-1
0726	27	"	"	"	"	"	0	--	1.3	-1
0824	28	250	30	54	40	Up	1	290	0.9	0
0828	29	"	"	"	"	"	1	290	1.1	0
0832	30	"	"	"	"	"	1	300	0.9	0
0836	31	"	"	"	"	"	0	--	1.6	0
0841	32	"	30	54	40	Dn	0	--	0.8	0
0845	33	"	"	"	"	"	0	--	0.7	0
0850	34	"	30	54	70	Up	1	270	0.9	0
0856	35	"	"	"	"	"	1	240	0.7	0
0900	36	"	30	54	70	Dn	1	210	1.3	0

TABLE 2-2. (Continued)

Time (PST)	Run	Test Configuration					Meteorology			
		Heading (deg)	Altitude (m)	TAS (m/s)	Flaps (%)	Gear	WS (m/s)	WD (deg)	$\epsilon^{1/3}$ ($cm^{2/3}s^{-1}$)	γ (C/100m)
0952	37	070	15 (Ldg)	54	40	Dn	1	30	3.7	0
0956	38	"	15	"	"	"	1	20	4.0	0
1000	39	"	15 (Ldg)	"	"	"	1	20	4.1	0
1004	40	"	15	"	"	"	1	10	4.0	0
1009	41	"	15 (Ldg)	"	"	"	1	10	3.7	0
1014	42	070	15	54	40	Up	1	50	3.6	0
1018	43	"	15 (TO)	"	"	"	1	100	3.3	0
1021	44	"	15	"	"	"	0	--	4.0	0
1026	45	"	15	"	"	"	0	--	3.5	0
1114	46	070	15	54	40	Dn	1	60	3.1	0
1118	47	"	15	"	0	Up	1	60	4.4	0
1123	48	"	30	"	40	Up	1	60	4.4	0
1126	49	"	30	"	0	Up	1	60	4.6	0
1130	50	"	30 (Ldg)	"	40	Dn	1	60	4.0	0
1134	51	"	30 (Ldg)	54	0	Dn	1	50	4.1	0
1137	52	"	30 (Ldg)	"	70	Dn	1	40	3.8	0
1142	53	"	30 TO)	54	40	Up	1	30	4.0	0
1146	54	"	30 (TO)	"	0	Up	1	20	3.7	0

TABLE 2-3. BOEING 747 TEST CONDITION SUMMARY.

WS - Wind speed
WD - Direction from which the wind blows
$\epsilon^{1/3}$ - Atmospheric turbulence dissipation rate
γ - Atmospheric stability, dT/dz
Ldg - Aircraft descending over array
TO - Aircraft climbing over array
* - Nominal altitude assigned to aircraft, not measured.

TAS - True air speed
PST - Pacific Standard Time
EPR - Engine Pressure Ratio

		Test Configuration							Meteorology			
Time (PST)	Run	Altitude (m)	TAS (m/s)	Weight (10^3kg)	Flaps (deg)	Gear	Spoilers	Thrust (EPR)	WS (m/s)	WD (deg)	$\epsilon^{1/3}$ ($cm^{2/3}s^{-1}$)	γ (C/100m)
12/2/75												
0707	1	66	79	255	30/30	Dn	No	1.25	1	190	0.7	12
0713	2	62	79	251	"	"	"	1.21	1	190	1.6	11
0718	3	68	78	250	"	"	"	1.25	1	180	0.7	10
0725	4	65	78	249	"	"	"	1.22	1	180	0.6	9
0730	5	122*	78	248	30/30	Dn	No	1.22	1	210	1.0	9
0735	6	122*	78	247	"	"	"	1.23	1	240	1.5	8
0740	7	244*	77	245	30/30	Dn	No	1.23	1	270	1.2	1
0745	8	244*	77	244	"	"	"	1.20	1	310	0.7	1
0818	9	61*	77	235	30/30	Dn	Yes	1.26	1	140	0.6	1
0823	10	122*	77	234	30/30	Dn	"	1.26	1	210	0.5	2
0824	11	91*	77	233	30/30	Dn	"	1.25	1	280	0.5	5
0835	12	244*	77	231	30/30	Dn	"	1.25	1	0	0.8	3
0841	13	64	77	230	30/30	Dn	"	1.24	1	0	0.5	1
0847	14	65	75	228	30/30	Dn	No	1.20	1	10	2.1	0
0852	15	61*	75	227	"	"	"	1.20	1	10	2.9	0
0858	16	61*	75	226	"	"	"	1.18	1	10	2.7	0

TABLE 2-3. (Continued)

Time (PST)	Run	Test Configuration						Meteorology				
		Altitude (m)	TAS (m/s)	Weight (10^3 kg)	Flaps (deg)	Gear	Spoilers	Thrust (EPR)	WS (m/s)	WD (deg)	$\epsilon^{1/3}$ ($cm^{2/3}s^{-1}$)	γ (C/100m)
0932	17	30*	76	222	30/1	Dn	No	1.19	1	20	3.3	1
0938	18	37	76	217	30/1	Dn	No	1.18	1	60	3.6	1
0942	19	38	76	216	30/1	Up	No	1.18	1	100	3.7	1
0947	20	67	75	215	30/1	Dn	No	1.18	1	130	3.1	0
0951	21	64	75	213	30/1	Up	No	1.16	0	--	2.7	-1
0956	22	91*	75	212	30/1	Dn	No	1.23	0	--	0.8	-1
12/3/75												
0654	23	122*	79	260	30/30	Dn	No	1.24	1	190	0.6	8
0658	24	122*	119	258	0/0	Up	"	1.03	1	190	0.5	8
0703	25	122*	79	257	30/30	Dn	"	1.24	1	180	0.4	7
0707	26	122*	116	256	0/0	Up	"	1.06	1	180	0.6	7
0712	27	67 Ldg	79	255	30/30	Dn	"	1.20	1	180	1.1	6
0716	28	66	79	255	"	"	"	1.20	1	180	0.9	6
0721	29	72 Ldg	79	253	"	"	"	1.14	1	180	0.9	6
0725	30	66	78	251	"	"	"	1.24	1	180	1.0	6
0750	31	106* TO	84	243	10/10	Up	No	1.38	0	--	0.5	5
0801	32	65	84	242	"	"	"	1.11	0	--	0.6	6
0806	33	57 TO	84	241	"	"	"	1.36	1	310	1.4	6
0811	34	59	77	240	"	"	"	1.15	1	320	1.5	6
0816	35	63	77	239	30/30	Dn	"	1.20	1	340	1.9	6
0821	36	68	77	238	"	Up	"	1.20	1	0	1.5	5
0826	37	67	76	237	"	Dn	"	1.21	1	10	0.6	5
0831	38	61*	76	236	"	Up	"	1.22	1	20	0.7	5

TABLE 2-3. (Continued)

Time (PST)	Run	Test Configuration						Meteorology				
		Altitude (m)	TAS (m/s)	Weight (10^3kg)	Flaps (deg)	Gear	Spoilers	Thrust (EPR)	WS (m/s)	WD (deg)	$\epsilon^{1/3}$ ($cm^{2/3}s^{-1}$)	γ (C/100m)
0902	39	47 TO	82	230	10/10	Up	Yes	1.36	0	--	2.4	1
0907	40	46	82	228	"	"	No	1.36	1	110	2.3	1
0913	41	48	81	227	"	"	Yes	1.36	1	120	0.5	1
0919	42	54	81	226	"	"	No	1.40	1	130	1.0	1
0924	43	61*	75	225	30/30	Dn	"	1.24	1	110	0.7	1
0929	44	63 Ldg	75	224	"	"	"	1.12	1	90	0.8	-1
0935	45	50	75	223	"	"	"	1.16	1	80	1.0	-1
0940	46	37	74	222	"	"	"	1.24	1	60	3.0	-1
1012	47	91*	73	215	30/30	Dn	No	1.15	1	160	1.5	0
1016	48	91*	73	214	"	"	Yes	1.20	1	160	1.4	0
1022	49	37	72	212	"	"	Yes	1.20	1	150	3.9	-1
1026	50	91* Ldg	72	211	"	"	No	1.11	1	150	3.6	0
1031	51	122*	108	210	0/0	"	"	1.11	1	140	1.8	2
1035	52	122	108	208	"	Up	"	1.03	1	130	1.3	2
1039	53	122	72	208	30/30	Dn	"	1.22	1	120	1.3	2
1043	54	122	108	207	0/0	Up	"	1.05	1	120	1.7	2

objectives. There, a fixed 35 mm motorized still camera documented vortex behavior and descent at 5 second intervals. A 16 mm motion picture camera mounted on the same tripod recorded the same data with finer temporal resolution. A digital clock, visible to both cameras, provided a timing reference.

An additional motion picture camera, also located to the side of the flight path, was sometimes used to observe the behavior of small buoyant balloons released into the vortices from an array of 32 solenoid-activated balloon holders on the ground directly under the aircraft flight path. Such a balloon release is shown in Figure 2-6, which also shows the anemometer array.

An upward-pointing motorized still camera was used to photograph the lateral drift of a pilot balloon (pibal) released directly above it, from which the wind profiles near the ground were obtained. On some Lodestar tests and on all Boeing 747 tests this camera was located on the centerline of the flight path and also recorded details of vortex rollup whenever the generator aircraft passed directly overhead.

An array of 72 sensitive propeller anemometers* was used to sense the horizontal and vertical velocities induced near the ground by the vortices. The array consisted of 30 support standards, 27 of which were 4 m high and supported a two-component anemometer set, (Figure 2-7), and three of which supported three-component anemometers at both 4 and 7 meters above the ground (Figure 2-8). The two-component anemometers sensed both the horizontal wind component transverse to the flight path and the vertical wind component, i.e., the two wind components which would be most affected by a line vortex along the direction of flight. The 3-component anemometers, which were offset 30 meters from the flight path centerline (at row 7 in Figure 2-5) also sensed the flow component along the

---

* Manufactured by R.M. Young Company, Traverse City, Michigan

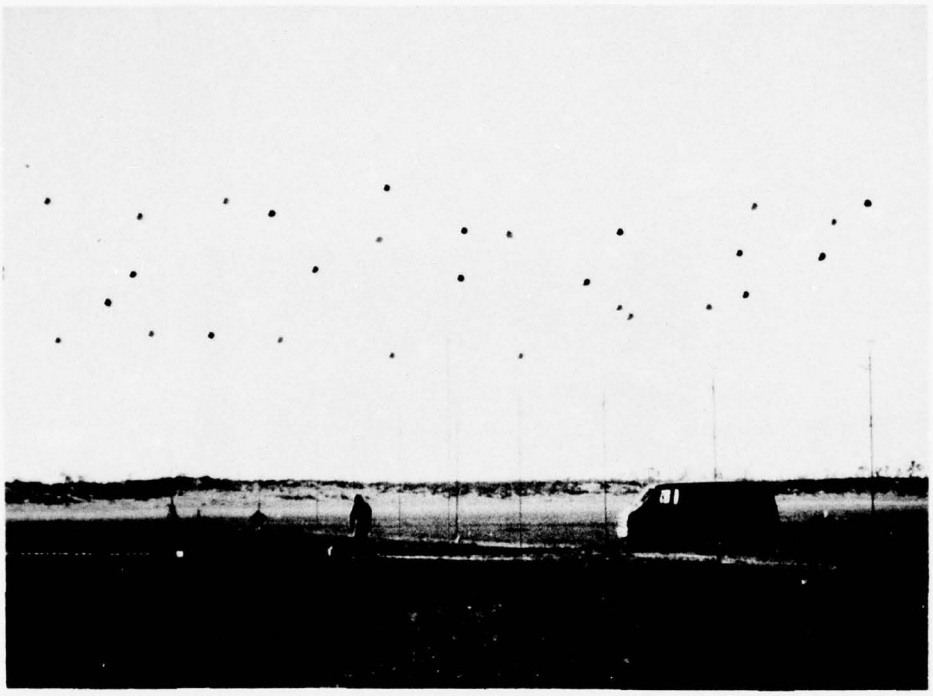

FIGURE 2-6. RELEASE OF BUOYANT BALLOONS, WHICH ASCEND AND ENTER VORTEX CORE (ABOVE PICTURE) TO MARK AXIAL FLOW

(One row of the propeller anemometer array is in the right half of the picture.)

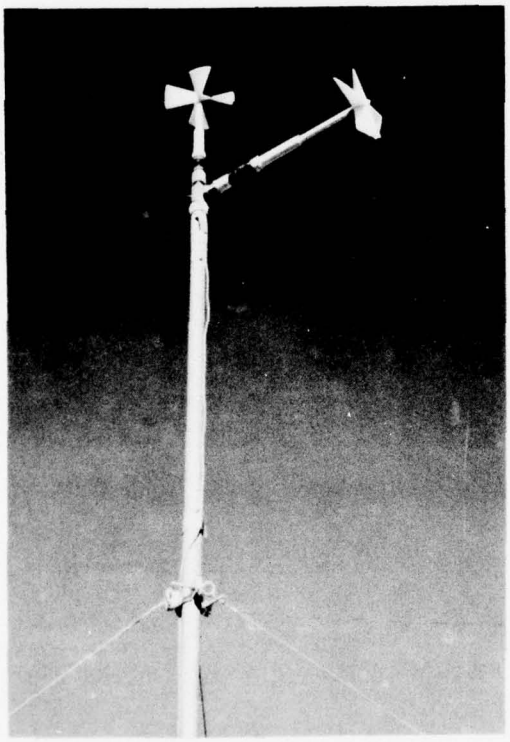

FIGURE 2-7. TWO-COMPONENT PROPELLER ANEMOMETER

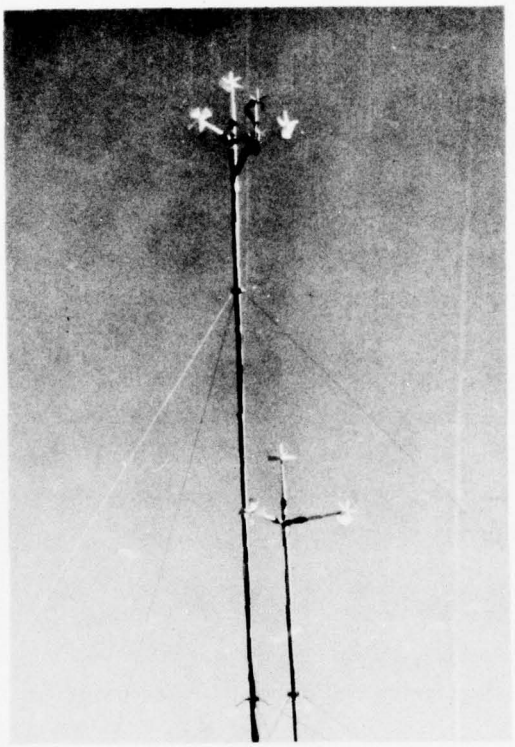

FIGURE 2-8. TWO LEVEL, THREE-COMPONENT PROPELLER ANEMOMETER INSTALLATION

(A three-component hot-wire probe is also installed at the top level.)

axis of the vortices. The anemometers have a response threshold of 0.2 m/s and a response distance of about 1 meter.

One of the 7-meter standards (7B, shown in Figure 2-8), also carried a 3-component hot wire anemometer in addition to the propeller anemometers, to provide data on the fine structure of the flow.

For the Boeing 747 tests the two center rows of anemometers (rows 5 and 6) were removed and were reinstalled 40 meters beyond each end of the array shown in Figure 2-5 (where they then comprised rows 1 and 12).

Signals from all of the sensors in the array were scanned at 0.5 second intervals and were recorded digitally on magnetic tape in an instrumentation trailer. The master clock for the experiment recorded the time on the same tape; the clocks for the various cameras were synchronized with this clock. An event mark was recorded on this tape (as well as on the DOT-TSC and Lockheed tapes during the Boeing 747 tests) to indicate aircraft passage over a marker flag 30 or 40 meters ahead of the first anemometer column reached by the aircraft. Oscillographic recorders also recorded all channels as a backup to the digital system.

Marker flags at various locations in the array provided definite location references for the various ground-based and airborne cameras and were used for calling out timing marks to indicate aircraft passage.

An array of meteorological equipment was suspended beneath a cluster of tethered balloons near the flight path, as shown in Figure 2-9. The sensors suspended beneath the balloons measured the atmospheric turbulence and temperature, using techniques developed by AeroVironment, at heights up to 60 m above the surface. The digital data logging system also recorded the signals from these sensors.

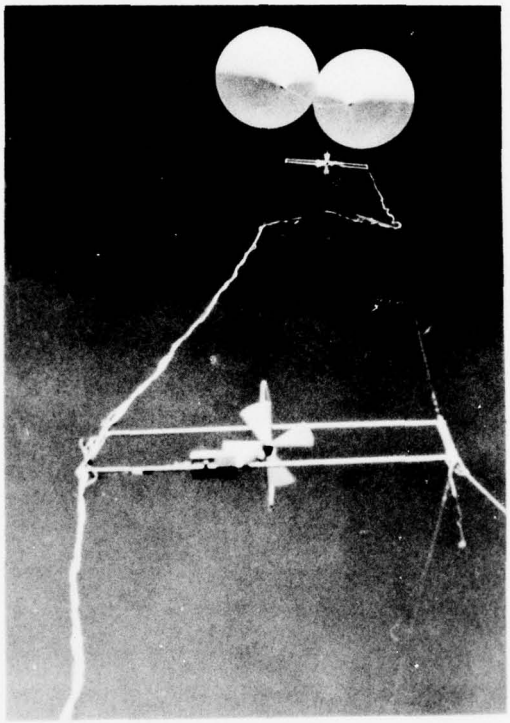

FIGURE 2-9. VIEW UPWARD AT TURBULENCE AND TEMPERATURE SENSORS SUSPENDED BENEATH TWO TETHERED BALLOONS

Airborne Data Collection

Two aircraft in addition to the vortex generating airplane were used on most of the flight tests to photograph the wakes and collect meteorological data. The Lodestar doubled as both a vortex generator and meteorological aircraft on a few early test days; separate aircraft performed these two functions in subsequent tests.

A helicopter was used as a camera platform directly over the array. The helicopter hovered there at a height of about 500 m above the ground and a motorized 35-mm still camera was used to photograph the behavior and lateral motion of the vortices below.

Atmospheric turbulence and temperature profiles from the surface up to 300 m above the ground were obtained by soundings of an instrumented Cessna 182 meteorological aircraft (except for the first few test days, when the Lodestar collected this data). The Cessna 182 also flew alongside the vortex generator aircraft to define the turbulence at the flight level during each pass over the array. The turbulence was measured in terms of the turbulence dissipation rate, $\epsilon^{1/3}$, by a Universal Indicated Turbulence System* (MacCready, 1966). Temperature measurements were by a thermistor probe.

Data Reduction Approach

The data from the various recording media – photographs, magnetic tape, chart records – were analyzed to derive information about vortex behavior to fulfill the objectives of this program and as supporting information for the correlated Boeing 747 program objectives. The amount of data collected during all of these flight tests has been immense and provides

---

* Manufactured by Meteorology Research, Inc., Altadena, California.

data on aspects of wake vortex behavior which were beyond the scope of this study. Thus, not all of the information from all of the sensors has received comprehensive scrutiny, and a fertile data base for further analysis still remains.

The main emphasis of the data reduction approach was on obtaining an understanding of wake decay, especially vortex bursting, near the ground. For this purpose, the primary data sources used were the photographs, which showed visual manifestations of vortex instabilities, and the anemometer array, which reflected any corresponding changes in the velocity fields. Supporting data, such as that from the balloons released into the vortices, was analyzed to further illuminate the decay phenomena.

Analysis of other information about vortex behavior, such as vortex trajectories during descent and over the ground and the details of vortex rollup immediately behind the aircraft, was carried out only insofar as it contributed to the analysis of vortex decay, except that a complete set of Boeing 747 vortex trajectories was prepared for the analyses in Hallock, et al (1977).

The meteorological information was a critical element of the decay analyses, and thus received considerable attention.

The specific analysis techniques used for deriving information will be described as the results are presented in the succeeding chapters.

2.2 Core-bursting Analysis Approach

As noted in the Introduction, the wake vortex system of an aircraft is subject to two forms of instability – sinuous instability and core-bursting instability. These instabilities often occur simultaneously, but are also frequently observed separately and can therefore be presumed to be independent phenomena. To provide a basis for discussion we will briefly describe some of the experimental and theoretical features of these instabilities according to the current state of knowledge.

The sinuous mode, known as Crow Instability, is a vortex pair phenomenon, and requires the velocity field of a neighboring vortex to induce instability and subsequent linking of the pair. When near the ground, a single vortex can undergo instability by interaction with its ground induced image and actually link with the image, so that the vortex has the appearance of a semicircular loop, with both ends terminating on the ground.

The motion of the vortex pair in Crow Instability is predominantly an inviscid response. This had been anticipated in the earliest work on the subject (Crow, 1970) in which the basic parameters controlling the vortex motion were Γ, the trailing vortex strength, and b_v, the trailing vortex span. Both the sinuous behavior and the ground looping can be adequately described by the inviscid model.

It has been observed (Tombach, 1973; Tombach, et al, 1974) that the sinuous instability is excited and driven by the ambient atmospheric turbulence, and the magnitude of this turbulence can be directly related to time-to-link. Good correlation has been achieved using ϵ, the turbulent energy dissipation rate per unit mass, as the index of atmospheric turbulence magnitude. If one assumes that the atmospheric eddies which cause perturbations in the vortex shape are of a scale comparable to about nine times the vortex span (based on Crow's analysis) and lie in the inertial subrange where the turbulence spectrum obeys Kolmogorov scaling, then the turbulence properties can be fully defined by ϵ.

Crow and Bate (1976) have included a turbulent forcing function of this form to develop a universal time-to-link equation, dependent only on the inviscid parameters defined above. The Crow-Bate model incorporates two analyses. One assumes that the turbulence is so strong that it dominates the vortex induced motions, so that linking occurs when the turbulence has driven the vortices into coalescence. In the second case the turbulence is assumed to be a small stochastic disturbing field driving the vortex induced stability. The predictions for wake lifetime (time-to-link) based on these two approaches have been combined into a composite function which fits quite well to the rather limited and scattered flight test data.

on one vortex occurring apparently independently of the other member of the pair. This suggests that one form of core-bursting is a local phenomenon related principally to the approximately axisymmetric structure of a single line vortex of finite core size. There are also frequent occurrences of core-bursting in conjunction with the sinuous instability, however, in which case the sinuous vortex deformation appears to induce core-bursting.

Much effort has been expended in attempting to analyze the fluid mechanics of core-breakdown. An excellent state-of-the-art review of the theoretical aspects of this problem is given in a monograph by Donaldson and Bilanin (1975), which summarizes results to date; some of our following discussion is taken from that publication. Our object here is not to produce yet another analysis, but rather to determine a simple formula or rule by which the time to vortex-breakdown can be approximated from the basic aerodynamic parameters of the generating aircraft and atmospheric properties, in much the same way that the sinuous instability can be predicted. Since Donaldson and Bilanin point out that there are no acceptable rational methods at present which can give these predictions, the approach used here relies heavily on theoretical insight supported by experimental data.

A brief discussion on core-breakdown dynamics will set the stage for the development of this rule. If core bursting is considered as a local internal core effect, we expect that it must be related to details of this core structure, namely, the tangential and axial velocity profiles. Apparently inertial waves can exist and propagate in this three-dimensional axisymmetric flow field and these waves are the precursors of the breakdown. It was surmised by Donaldson and Bilanin (1975) that these waves can be "trapped" at a critical station, where upstream conditions are such that the waves cannot penetrate further upstream. The waves then become of significant amplitude (involving non-linear interactions) and conditions similar to a hydraulic jump occur.

The natural mathematical approach to this problem is to assume a tangential and axial velocity profile and to study the propagation of an

In ground effect, it might be expected that the ground boundary conditions and the different turbulence spectra would have some effect on the sinuous time-to-link. An analysis of this effect, considering both a modified turbulent forcing function and the presence of the ground image, has been made by Tombach, et al (1975). The essential conclusions, which are summarized by Tombach and Crow (1976), are that although the life span, or time-to-link, is reduced by the presence of the ground, the effect is small (not more than about 10%) when comparable vortices at different heights in the same atmospheric boundary layer are compared with each other.

The other important mode of catastrophic instability, vortex breakdown or core-bursting, is poorly understood to the extent that a precise meaning for the description is not agreed upon, nor is it clear whether there are one or more phenomena under this umbrella description. Most experimental data on this effect have been obtained from visual observation of the behavior of a smoke-marked vortex (Chevalier. 1973; Tombach, 1973; Tombach, et al, 1974; Tombach, et al, 1975). The experiments show that the smoke-marked vortex appears to "bunch up" and "break;" that is, the marked core abruptly increases in diameter and then appears to burst, with the burst moving quite rapidly along the vortex axis. Often the smoke which marked the core rapidly dissipates and is no longer visible. Occasionally, a much diminished smaller core remains after the bursting process. The effect of bursting on the velocity fields has not been measured, although inferences from indirect measurements of vortex strength (Hallock, 1976) and from the motion of a vortex after its mate had burst (Tombach, 1973) suggest significant changes in the structure of the vortical core flow field. On the other hand, in studies of other columnar vortices, Mullen and Maxworthy (1976) have observed that highly disruptive core phenomena have had little effect on the outer flow.

It appears likely that core-bursting is a single vortex phenomenon, in the sense that it is not necessarily connected with induced flows associated with the other vortex of the pair. There are observations of core-bursting

infinitesimal general disturbance by determining the dispersion relations. Thus one can determine the frequency/wave number dependence. The fundamental concepts of such a stability analysis for some simple vortex configurations appear in Appendix A of this report.

If this approach is applied to a simple real vortex having a Rankine-type tangential velocity field and a uniform axial flow field, it turns out that an infinite number of modes is possible. However, upstream propagation of disturbances depends upon the swirl velocity ratio, S, defined here as $S = \Gamma/RW_o$ where Γ is the circulation, W_o is the axial velocity along the vortex centerline, and R is the radius at which the maximum tangential velocity, $V_{T\ max}$, occurs. (This velocity ratio can also be written as $S = V_{Tmax}/W_o$.) Generally speaking a family of critical values of S can be defined; for each particular mode upstream propagation is not possible if S is smaller than the appropriate critical value.

Now, the general aging process in an aircraft wake vortex will always cause the swirl velocities to reduce, while the effect on the axial term is believed to be relatively small. Specific information on the downstream variation of the axial velocity is notably lacking, however. Batchelor (1964) shows that far downstream it reduces like (ln x)/x where x is the downstream distance. However, this analysis is for a constant uniform viscosity (that is, a laminar type flow) and is intended to describe events many spans downstream from the wing. For turbulent momentum transfer the ordering with respect to x and the magnitude of the decay can be expected to be different.

On the other hand, the wind tunnel experiments by Corsiglia, et al (1973) show the axial velocity to be wake-like at about 20% of freestream speed with no significant downstream variation in the near wing field for about 31 spans downstream. This is also suggested by recent theoretical results by Donaldson and Bilanin (1975). Their calculations (made for a representative vortex core) show a small wake-like flow of about 15% of the freestream speed with very little variation for the first 15 spans downstream, which the authors suggest is caused by the fact that the swirl flow

decay produces a pressure rise along the vortex centerline which tends to maintain the original axial velocity defect. This would not be the case for a wake without swirl, where the usual axial velocity decay might be expected The Donaldson and Bilanin results are well supported by the experimental data of Corsiglia, et al.

Thus in general we assume the swirl-to-axial velocity ratio will reduce so that it may be expected that during the aging process conditions conducive to core-bursting will ultimately always occur on a solitary vortex However, the presence of the other member of the pair can introduce other phenomena which may preempt this core-bursting. Here we should again note that sinuous instability has been observed to precede, and thus preempt core-bursting, while under very, very calm atmospheric conditions it appears that neither core-bursting nor sinuous instability occur, with the vortex pair instead undergoing so-called regular dissipation (Lissaman, et al, 1973) under which a general two-dimensional vorticity-filled cell develops containing both vortices

2.3 Water Tank Analog Experiments

In order to study the internal turbulence generation, and its effect on vortices near the ground an analog experiment was designed. For this experiment a short "slice" of a vortex pair was generated in a water tank The flow was bounded by two vertical surfaces, which would correspond to planes cutting the vortices and lying normal to the flight path for the vortex pair shed from an actual aircraft. Thus an effective two dimensional transverse section of the vortex pair was created, so that both Crow instability and axial flow were suppressed. The object was to study the gross motion of this pair in the presence of a ground plane, to investigate the apparent change in strength of the vortices under these conditions, and to explore the internal turbulence generation in the pair

For the experiment a vortex pair was formed by a specially designed fluid mechanical generator which produces a flow field more representative

of actual vortex pairs than would result from a simple "puffing" or impulsively-moved-plate type generator. The vortex pair then proceeded to move under its self-induction towards a wall which represented the ground plane. A number of parameters were varied from experiment to experiment, including the roughness of the ground plane and the initial turbulence within the vortex cell. The fluid within the vortex cell was marked with a fluorescent dye, and the entire flow field recorded with high speed motion photography.

More details of the experiment are noted in Appendix B. The results are discussed in the following Section.

3. RESULTS

3.1 Qualitative Description of Vortex Flight Test Observations

All of the flight tests were performed under a wide range of meteorological conditions, which resulted from the natural evolution of the meteorology from calm and stable conditions at sunrise to windier and more unstable conditions at the termination of each day of tests. During the program a variety of aircraft configurations and heights above the ground were explored by each aircraft, although the preponderance of tests were in the normal landing configuration in level flight at a height of 30 m AGL for the Lodestar and 60 m AGL for the Boeing 747. The large range of meteorological conditions and configurations limited the amount of data collected under identical conditions, and thus assessment of whether a variation in results between two runs was random or systematic was often difficult. Nevertheless, several vortex behavior patterns emerged from the data analysis; these are discussed qualitatively in this section, with quantitative analysis appearing later in this chapter.

Meteorology

The meteorology which apparently most affects vortex behavior is defined by vertical profiles of temperature and turbulence and by a three-dimensional description of the wind vector field. The information previously presented in Tables 2-2 and 2-3 characterizes these conditions for the Lodestar and Boeing 747 flight tests, respectively.

By way of interpretation, the temperature profiles at the beginning of a test day (usually dawn) generally indicated a very stable atmosphere. The lowest temperatures were encountered at the ground level, which had cooled by radiation during the night. Consequently, the near-ground air temperature usually increased with altitude to some inversion height, above which the temperature decreased adiabatically with height. After sunrise, the ground and the air above it gradually warmed until, by mid-morning, the

temperature profile was neutrally stable (decreasing adiabatically with height). Further ground heating by the sun caused the atmosphere to become unstable when the warmer-than-adiabatic air near the ground rose vertically and caused a turbulent overturning motion in the atmosphere.

Thus, the turbulence levels at the low flight altitudes generally increased as the atmosphere became less stable as the morning progressed. An anomalous situation was sometimes encountered in the very stable early morning period, however, when drainage flow from nearby mountains caused stable layers to slide over one another and the resulting shears generated high levels of turbulence in spite of the very stable density distribution. This situation has been discussed by Tombach, et al (1974).

The desert winds were generally light in the early morning and were mainly caused by drainage. The wind increased as the morning progressed, and was soon dominated by the westerly gradient wind.

Vortex Rollup

The rolling up of the wing vortex sheet into discrete vortices was studied for selected passes of both the Lodestar and the Boeing 747. On the Lodestar, different color smoke grenades located at three spanwise locations on each wing produced filaments of smoke which traced the wrapping up of the vortex sheet. The smoke generators at four spanwise stations on each Boeing 747 wing served the same purpose.

Such tests served several purposes. The primary one of concern for this report was to attempt to mark various shells of the vortex, with different colors if possible, and then to observe the effect of the vortex breakdown decay mode on each of these shells. In addition, the rollup observations for the Boeing 747 were of interest for illuminating the physical effects of various vortex alleviation configurations, which is discussed further in the report by Hallock, et al (1977).

As an example of the results obtained, Figure 3-1 shows a montage of photographs of the Lodestar vortex rollup process for the first six seconds, for a case with flaps and gear down. The photographs were taken at half second intervals by a camera pointing directly upward. A cable above the camera, strung crosswise to the flight path, provided a reference for direction and position and is visible on each frame. The frames have been mounted in spatial sequence in Figure 3-1 to illustrate the apparent evolution of the wake behind the aircraft; actually all frames were taken of the same point in space and thus show the same vortex segments.

The figure shows the smoke filament from the wingtip spiraling around the smoke-marked vortex core while diffusing slowly. The filament retains its identity throughout the sequence, indicating that is is a small vortex itself, as would be expected for the flow from the wingtip which is associated with the spanwise end of the lift distribution. Donaldson and Bilanin (1975) have modified the method of Betz (1932) to compute the structure of the vortex wake from a flapped wing. They conclude that two discrete vortices can indeed occur, with core positions originating at the points where the slope of the lift distribution $|d\Gamma/dy|$ is a maximum – i.e., approximately at the outboard end of the flap and at the wingtip, as observed here. This explains the discrete appearance of the vortices in Figure 3-1, and also shows that a smoke grenade at the wingtip cannot be used to mark a "shell" of vortex structure.

A second smoke source installed inboard of the main smoke generators was also operating in the case shown in Figure 3-1. Its smoke was wrapped into the main vortex core within one chord length and was thereafter no longer distinguishable from the rest of the vortex in spite of its contrasting color.

The tip vortex should undergo breakdowns and instabilities in much the same way as the main vortex. Although such breakdowns are not seen in Figure 3-1, some instability in the smoke structure is visible, which appears to be connected with similar phenomena in the main vortices. Perhaps

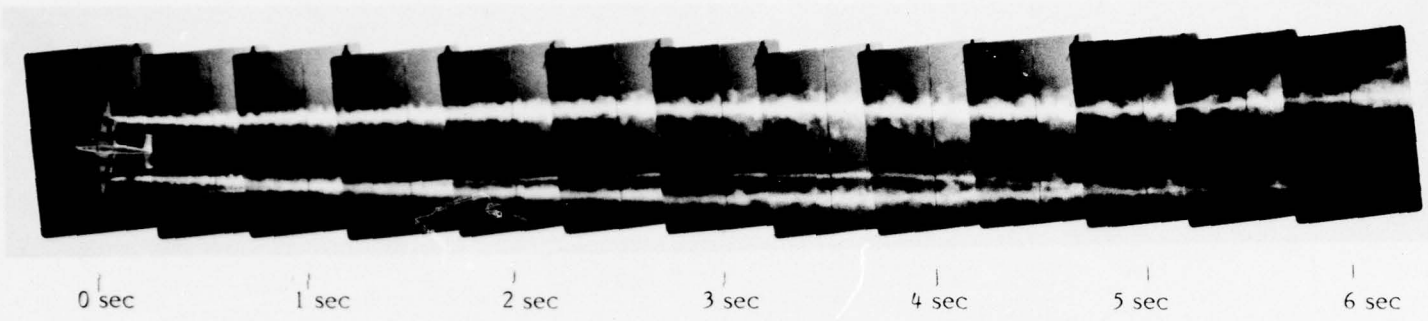

FIGURE 3-1. SEQUENCE OF PHOTOGRAPHS SHOWING ROLLUP OF LODESTAR VORTICES AS SEEN FROM BELOW.

(Although mounted in sequence to show the spatial evolution of the wake, the photos actually all show the same vortex segment at half-second intervals.)

turbulent interaction of the vortex cores is a contributor to the decay of the tip vortex.

Figure 3-2 shows two more rollup sequences, one with flaps down and the other with flaps up, both without the additional tip smoke. In the clean (flaps up) configuration the vortex should originate at the wingtip; the smoke, however, is being released at the outboard end of the flap. The result is that the smoke never enters into the vortex core, but rather wraps around it, giving a hollow shell-like, diffuse appearance to the vortex. Comparison of the two sequences in Figure 3-2 can then give rise to misleading results, such as the conclusion that the clean configuration vortex is larger in diameter than the one produced with flaps down. If the smoke generator had been placed at the wingtip for both runs, the opposite conclusion would have been reached. (An example of such a case appears in the Boeing 727 tests reported upon by Barber, et al (1974).) This comparison illuminates one of the weaknesses of flow visualization, and also shows that proper smoke source placement is important for effective long-term visualization of vortex behavior.

Vortex Transport and Decay

The behavior of the vortices for both the Lodestar and the Boeing 747 was determined by analysis of side and top view photographs of the smoke marked vortices, supplemented by the anemometer data in selected cases. For each run the behavior of the vortices was qualitatively categorized and the time of the first breakdown of organized structure by core bursting, linking, or ground contact was noted. Table 3-1 summarizes the vortex behavior data, together with information on aircraft configuration and relevant meteorology, for the Lockheed Lodestar. For these tests the green (starboard) vortex was sometimes difficult to see against the horizon sky/ground background, and thus less information is available for this vortex than for the better-marked red vortex.

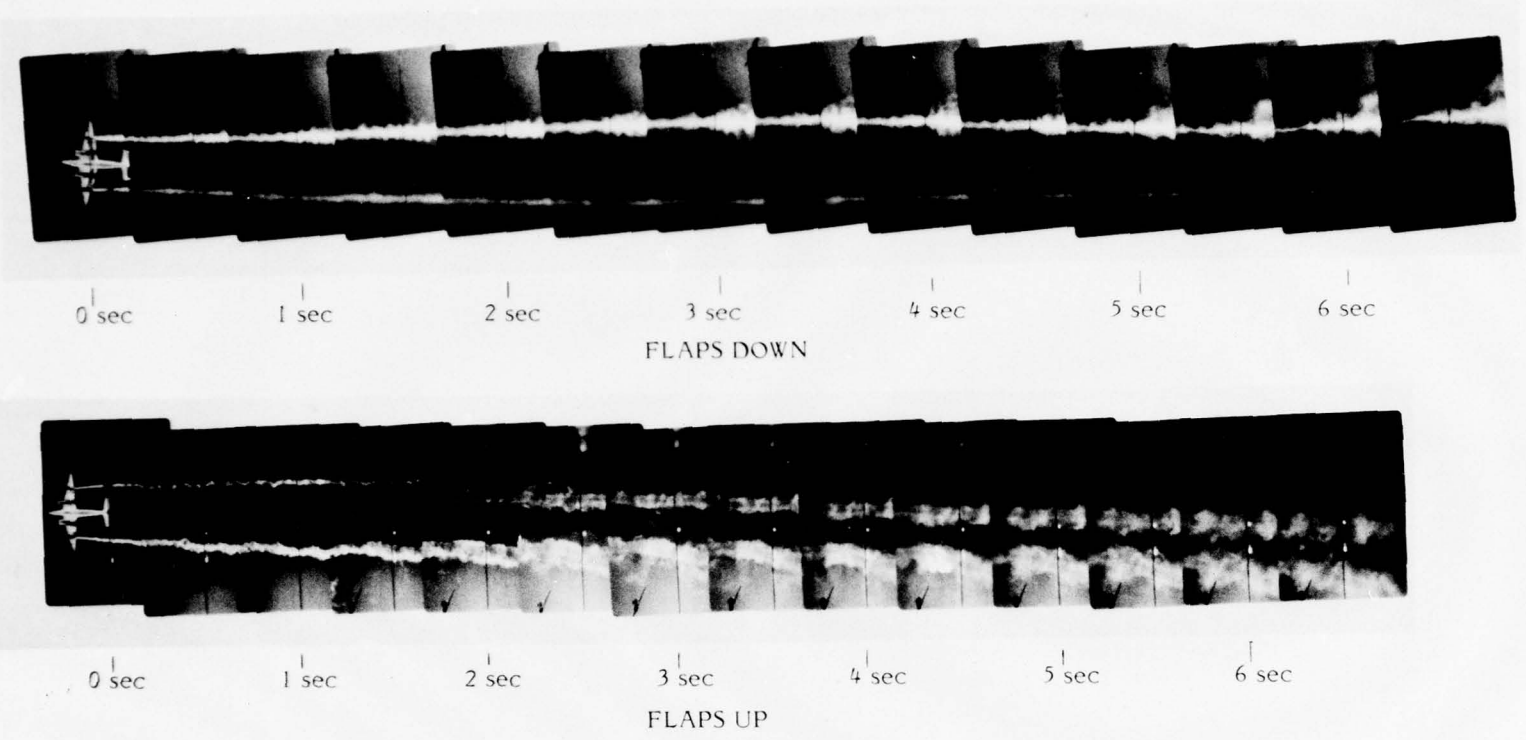

FIGURE 3-2. COMPARISON OF SMOKE VISUALIZATION OF LODESTAR VORTEX ROLLUP WITH FLAPS DOWN AND WITH FLAPS UP.

Table 3-2 is a similar summary for the Boeing 747 runs. The flow visualization was significantly poorer for this aircraft, and thus less than half of all runs had identifiable breakdown phenomena.

A glossary of terminology for interpretation of the descriptions of vortex behavior in Tables 3-1 and 3-2 is provided in Table 3-3. These tables show only those runs for which usable data could be derived from the photographs; a complete summary of all run conditions and meteorological conditions appeared previously in Tables 2-2 and 2-3

A couple of comments should be made about the data in Tables 3-1 and 3-2. First, the lapse rate γ and turbulence ϵ listed are those for the region of the atmosphere just below the generating aircraft. Usually the variation in γ and ϵ with height was not very rapid, and thus this γ and ϵ adequately defined the average atmospheric condition encountered by the descending vortices. There were a few exceptions however, with the most notable being the situation around 60 m AGL during runs 10-18 of the Boeing 747 on 2 December 1975. A strong gradient in turbulence was present at around that level, with turbulence below that level significantly greater than above it (note the large difference in turbulence between runs 13 and 14 in Table 2-3 as the turbulent layer grew and engulfed the flight level. The vortex burst times for runs 14 and 16 during this period were anomalous, and fitted the other data better if the lesser turbulence just above the flight level were used rather than the greater turbulence which was actually measured. Since the gradient was rather abrupt, a small error in the altitude of the meteorological aircraft vis-a-vis the Boeing 747 could have been the cause. All vortices generated near this level should have descended quickly into the turbulence below, and thus initial differences in turbulence should have acted for only a brief time at most, however.

Second, the photo record often ended before the vortex had decayed. Such cases are marked with lower limits for decay time, with such limits being the ends of the photographic records. The actual persistence time for these cases is unknown.

TABLE 3-1. SUMMARY OF VISUALLY OBSERVED BEHAVIOR OF LODESTAR VORTICES

(See Table 3-3 on Page 3-13 for definitions of abbreviations used. Numerals in the behavior columns represent times, in seconds, e.g., "Bu 24" means vortex burst at age of 24 seconds, "P Rises 20" means port vortex began rising at 20 seconds age. A breakdown time indicated as greater than some time (e.g., > 47) signifies that the vortex was still intact when the photographic record ended at that time.)

Run #	Time	Configuration				Meteorology		Behavior			
		Altitude (m)	TAS (m/s)	Flaps (%)	Gear	Γ (C/100m)	$\epsilon^{1/3}$ ($cm^{2/3}s^{-1}$)	Descent	Breakdown & Time Port	Breakdown & Time Starboard	Comments
10/24/75											
1	0748	15	54	0	Up	7	<1.5	--	>31	Bu 29	
2	0754	15	54	0	Up	7	<1.5	--	>42	>18	
3	0800	15	54	0	Up	7	<1.5	--	>38	>24	
4	0807	15	54	40	Up	7	<1.5	--	>34	Bu 25	
5	0813	15	54	40	Up	7	<1.5	--	>47	>9	
6	0819	15	54	40	Up	7	<1.5	WHR	Bu 55	>24	P Rises
7	0825	15	54	70	Up	7	<1.5	WHR	Bu 41	Bu 24	P Rises 20
8	0831	15	64	70	Up	7	<1.5	WHR	Bu 37	>28	
9	0826	15	54	70	Up	7	<1.5	LWHR	Bu 33	>28	P Rises 14
10/25/75											
10	0730	15	54	0	Up	4	0.6	--	Bu 34	>10	
11	0734	15	54	0	Up	4	0.6	--	Bu 33	--	
12	0738	15	54	0	Up	4	0.5	--	Bu 33	--	
13	0743	15	54	40	Up	5	1.2	--	Bu 38	>5	
14	0748	15	54	40	Up	5	1.2	--	Bu 43	--	
15	0753	15	54	40	Up	5	1.3	--	>38	>33	
16	0758	15	54	40	Up	6	1.1	--	>28	>57	
19	0925	15	54	40	Up	-2	1.8	LDBR	>32	>27	P Bounces 20, Rises 22
20	0930	15	54	40	Up	-2	1.8	LWR	--	--	P Rises 25
21	0934	15	54	40	Up	-2	1.7	LSD	Bu 25	--	P Center low, Bu on high points
22	0938	30	54	40	Up	-2	1.9	LWH	Bu 30	Bu 30	P High center, low sides
23	0942	30	54	40	Up	-3	2.2	LWG	Bu 30	--	P NG several places
24	0946	30	54	40	Up	-3	2.3	LWG	Bu 28	--	P Center high

Run #	Time	Configuration				Meteorology		Behavior			
		Altitude (m)	TAS (m/s)	Flaps (%)	Gear	γ (C/100m)	$\varepsilon^{1/3}$ ($cm^{2/3}s^{-1}$)	Descent	Breakdown & Time Port	Breakdown & Time Starboard	Comments
10/25/75											
25	0949	30	54	40	Up	-3	2.1	LWH	Bu 20	--	
26	0953	30	54	40	Up	-3	2.2	LWD	--	--	P NG 28
27	0957	30	54	40	Up	-4	2.1	L Rap	Bu G 40	--	P NG 26
28	1106	30	54	40	Up	-1	2.5	S	Bu 25	>16	
29	1109	30	54	40	Up	-1	2.5	LG Rap	G Lk 25	>10	
30	1113	30	54	40	Up	-1	2.8	S	Bu 12	--	
31	1117	61 Climb	54	40	Up	-2	2.5	L Rap	Bu 21	--	P NG
32	1121	61	54	40	Up	-2	2.6	LSG	Bu 45	--	P Rapid center descent
33	1124	61 Climb	54	40	Up	-2	2.4	LWD	Bu 24	>8	
34	1128	61 Climb	54	40	Up	-1	2.7	SD	Bu 35	>20	
35	1132	61	54	40	Up	-4	2.5	SD	Bu 17	>5	
36	1136	61	54	40	Up	-1	2.6	SD	Bu 20	-	
38	0715	30	54	40	Up	3	1.8	--	Bu 29	>29	
40	0722	15	54	40	Up	4	1.3	--	Bu 30	>25	
41	0726	15	54	40	Up	4	1.3	--	Bu 39	--	
43	0734	15	54	40	Up	5	1.7	--	Bu 24	>24	
44	0738	15	54	40	Up	6	1.7	--	>19	>19	
45	0742	15	54	40	Up	6	2.3	--	>15	>15	
10/26/75											
46	0841	15	54	70	Up	4	3.5	SR	Bu 30	>24	
47	0845	15	54	70	Up	4	2.9	SRG	Bu 24	>19	P Broken humps SDD?
48	0848	15	54	70	Up	3	2.2	SRG	Bu 22	>25	P Very rapid descent to 5m
49	0852	15	54	70	Up	3	2.3	SHR	Bu 27	--	P Descent to 5m
50	0856	15	54	70	Up	3	2.4	NR	Bu 25	>14	P Descent to 5m
51	0859	15	54	70	Up	3	3.9		G Lk 25	>14	
52	0903	15	54	70	Up	2	3.1	SG	G >20	--	
53	0906	15	54	70	Up	2	4.3	SG	Bu G12	>5	
54	0909	15	54	40	Up	2	3.2	WG	Bu 19	-	

TABLE 3-1. (Continued)

Run #	Time	Configuration				Meteorology		Behavior			
		Altitude (m)	TAS (m/s)	Flaps (%)	Gear	γ (C/100m)	$\epsilon^{1/3}$ ($cm^{2/3}s^{-1}$)	Descent	Breakdown & Time Port	Breakdown & Time Starboard	Comments
12/10/75											
1	0854	61	54	40	Up	0	2.4	LSG	>51	>42	
2	0859	61	54	40	Up	0	1.8	LS	>33	>33	
3	0903	61	54	40	Up	0	2.3	LSG	G Lk?40	>23	P Middle low, ends high
4	0906	61	56	40	Up	0	2.4	LSG	>40	--	P Center low
5	0911	61	54	40	Dn	0	2.1	LSG	G Lk 46	>24	P DD moves toward plane, bent at 15m
6	0915	61	54	40	Dn	0	2.3	LS Rap G	G Lk 27	G Lk 27	P Two DD bent toward aircraft at 20m
7	0919	61	54	70	Up	0	1.8	LS Rap	G Bu 35	>14	
8	0923	61	54	70	Up	-0	1.9	LS Rap	Bu 36	>22	
9	0928	61	54	70	Dn	0	1.2	--	>34	>34	
11	1037	30	54	40	Dn	0	3.3	--	Bu 30	>10	
12	1041	30(Ldg)	54	40	Dn	0	3.5	--	>7	-	
13	1045	30	54	40	Dn	0	3.1	--	Bu 39	--	
14	1049	30(Ldg)	54	40	Up	0	3.7	--	>20	>10	
15	1053	30	54	40	Up	0	4.0	--	>29	>4	
16	1057	30(Ldg)	54	40	Up	0	3.3	--	>29	>19	
17	1102	30	54	40	Up	0	4.2	--	>30	>5	
18	1106	30(Ldg)	54	40	Dn	0	3.3	--	>20	>5	
12/11/75											
21	0700	30(TO)	54	15	Up	1	1.1	--	>23	>23	
22	0704	30	54	15	Up	0	0.8	--	Bu 38	>38	
23	0708	30(TO)	54	40	Up	0	0.3	--	Bu 34	>34	
24	0712	30	54	40	Up	0	1.0	--	Bu 38	>38	
25	0717	15	54	40	Up	-1	0.9	-	Bu 39	>39	
26	0721	15	54	40	Up	-1	1.2	--	>31	>31	
27	0726	15	54	40	Up	-1	1.3	--	>24	-	
28	0824	30	54	40	Up	0	0.9	Rap GR	Bu 50	>39	

Run #	Time	Configuration				Meteorology		Behavior			
		Altitude (m)	TAS (m/s)	Flaps (%)	Gear	$\epsilon^{1/3}$ ($C/100m)(cm^{2/3}s^{-1}$)		Descent	Breakdown & Time Port	Breakdown & Time Starboard	Comments
12/11/75											
29	0828	30	54	40	Up	0	1.1	LWHRG	Bu 77	>38	P Center hump, G 77
30	0832	30	54	40	Up	0	0.9	WHRG	Bu 52	>34	
31	0836	30	54	40	Up	0	1.6	LWH	Bu 42	>45	
32	0841	30	54	40	Dn	0	0.8	Slo G	Bu 35	>45	
33	0845	30	54	40	Dn	0	0.7	LWG	Bu 40	>45	
34	0850	30	54	70	Up	0	0.9	WDG HR	Bu 60	Bu 60	
35	0856	30	54	70	Up	0	0.7	N	>48	>54	
36	0900	30	54	70	Dn	0	1.3	WD	Bu 42	Bu 36	
37	0952	15(Ldg)	54	40	Dn	0	3.7	LG	Bu 20	>35	P puffs 29
38	0956	15	54	40	Dn	0	4.0	LG	Bu 20	>29	P puffs 36
39	1000	15(Ldg)	54	40	Dn	0	4.1	LG	>20	>25	
40	1004	15	54	40	Dn	0	4.0	L	>14	>30	P puffs 29
41	1009	15(Ldg)	54	40	Dn	0	3.7	Big LG	G 8	>10	
42	1014	15	54	40	Up	0	3.6	LWG	Bu 18	>20	
43	1018	15(TO)	54	40	Up	0	3.3	Rap	--	-	
44	1021	15	54	40	Up	0	4.0	LDG	Bu 26	>10	P hump away from aircraft
45	1026	15	54	40	Up	0	3.5	LSDG	Lk Bu 20	>10	
46	1114	15	54	40	Dn	0	3.1	LSR	Bu 22	>21	
47	1118	15	54	0	Up	0	4.4	--	>25	>15	
48	1123	30	54	40	Up	0	4.4	LSG	Bu 29	>5	P Bu on humps
49	1126	30	54	0	Up	0	4.6	SG	>30	>5	P puffs 30
50	1130	30(Ldg)	54	40	Dn	0	4.0	L Rap	>10	>5	
51	1134	30(Ldg)	54	0	Dn	0	4.1	LDSG	>23	>5	
52	1137	30(Ldg)	54	70	Dn	0	3.8	G	>27	Bu 30	
53	1142	30(TO)	54	40	Up	0	4.0	LD	>18	>15	
54	1146	30(TO)	54	0	Up	0	3.7	G	>9	>13	

TABLE 3-2. SUMMARY OF VISUALLY OBSERVED BEHAVIOR OF BOEING 747 VORTICES

(See Table 3-3 on Page 3-13 for definitions of abbreviations used. Also, see comments in caption for Table 3-1.)

Run #	Time	Configuration					Meteorology		Behavior		
		Altitude (m)	TAS (m/s)	Flaps (deg)	Gear	Spoilers	γ (C/100m)	$\epsilon^{1/3}$ ($cm^{2/3}s^{-1}$)	Descent	Breakdown & Time	
										Port	Starboard
12/2/75											
4	0725	65	78	30/30	Dn	No	9	0.6	W	Bu 42	Bu 47
5	0730	122*	78	30/30	Dn	No	9	1.0	W	Bu 63	--
6	0735	122*	78	30/30	Dn	No	8	1.5	WD	Bu 57	Bu 57
14	0847	65	75	30/30	Dn	No	0	2.1	WD	Bu 74***	>70 ***
16	0859	61*	75	30/30	Dn	No	0	2.7	WD	>110***	Bu 89***
19	0942	38	76	30/1	Up	No	1	3.7		Bu 38	Bu 19
20	0947	67	75	30/1	Dn	No	0	3.1	W	>60	Bu 58
21	0951	64	75	30/1	Up	No	-1	2.7		Bu 29	Bu 29
22	0956	91*	75	30/1	Dn	No	-1	0.8	W	>60	>60
12/3/75											
23	0654	122*	79	30/30	Dn	No	8	0.6		Bu 47	--
24	0658	122*	119	0/0	Up	No	8	0.5	W	Bu 76	Bu 53
25	0703	122*	79	30/30	Dn	No	7	0.4	W	Bu 50	Bu 60
26	0707	122*	116	0/0	Up	No	7	0.6		Bu 66	Bu 80
27	0712	67(Ldg)	79	30/30	Dn	No	6	1.1	WD	Bu 60	Bu 50
28	0716	66	79	30/30	Dn	No	6	0.9		Bu 51	>50
30	0725	66	78	30/30	Dn	No	6	1.0		Bu 64	Bu 56
32	0801	65	84	10/10	Up	No	6	0.6	W	>55	>55
34	0811	59	77	10/10	Up	No	6	1.5	Rap	>70	Bu** 52
35	0816	63	77	30/30	Dn	No	6	1.9		>45	Bu 42
36	0821	68	77	30/30	Up	No	5	1.5		Bu 52	Bu 56
38	0831	61*	76	30/30	Up	No	5	0.7		Bu 52	Bu 57
42	0919	54	81	10/10	Up	No	1	1.0		>30	>30
47	1012	91*	73	30/30	Dn	No	0	1.5		>60	>60
48	1016	91*	73	30/30	Dn	Yes	0	1.4		>70	>75
49	1022	37	72	30/30	Dn	Yes	-1	3.9		Bu 10	Bu 10

* Nominal altitude

** Small core left behind.

*** See discussion in text.

TABLE 3-3. DEFINITIONS OF TERMS USED TO DESCRIBE VORTEX BEHAVIOR

Descent

W - Wavy - The vortex column is distorted along its length so that its shape appears wavy. The apparent wavelength is usually on the order of tens to hundreds of meters and the amplitude is a small fraction of the wavelength. Often small wavelength waves are seen traveling along the distorted core edge.

S - Sinuous - The vortex column is distorted along its length as in the wavy case, but the amplitude is a large fraction of the wavelength.

L - Lurching - Segments of the vortex appear to descend more rapidly than neighboring segments, deforming the vortex. The rapidly descending segments then appear to slow and the neighboring segments accelerate downward. The process is repeated alternately by adjoining segments, often producing an irregular shape.

D - Detraining - The vortex core appears to throw off patches of smoke when descending, and leaves them behind in a wake.

B - Bounces- The vortex descends rapidly and appears to bounce off an invisible layer close to the ground and gains altitude.

H - Halts descent - The vortex descends slowly toward the ground and apparently stops near the ground and maintains altitude.

R - Rises - The vortex slowly rises after having halted near the ground.

G - Ground - A section of the vortex core touches the ground.

NG - Near Ground - A section of the vortex core comes very close to the ground (within a few meters) but does not actually touch.

N - Normal - Well behaved vortex that descends and maintains a horizontal attitude and well-defined core.

Breakdown

Bu - Burst - Sudden breakdown of smoke-marked vortex structure.

Lk - Link - Joining of the two vortices at a point.

DD - Dust devil - The vortex behavior resulting from linking of a vortex with its below-ground image.

G - Ground -The breakdown occurs as a result of contact with the ground.

General

Rap - Rapidly

Slo - Slowly

P - Port vortex (left side)

S - Starboard vortex (right side)

From Tables 3-1 and 3-2, the vortex behavior can be determined as a function of turbulence level for three very broad local atmospheric stability categories: very stable, neutral to mildly stable, and unstable. These stability categories were defined for the region immediately below the aircraft into which the vortices were propagating. When stratified in this manner, the observations for both aircraft summarize as follows (see Table 3-3 for definitions of the terms used):

Very Stable Conditions. Under these conditions, the vortices descended in a wavy manner, with descent slowing and often halting in the vicinity of the ground. After halting, the Lodestar vortices rose up again. Sometimes the descent was rapid and the halting and rising occurred quickly enough to give the impression that the vortices had bounced off a layer close to the ground. As wavy or oscillating vortices approached the ground under these stable conditions the amplitude of the waves often appeared to be damped out and the vortex appeared to stiffen and straighten out any kinks that may have developed.

Neutral to Slightly Stable. Here the vortices descended in a lurching, wavy, or sinuous manner to the ground level. They often reached the ground at some point along their length, which immediately initiated a burst breakdown or ground link. The ground-linked vortices, which were only photographed for the Lodestar, resembled dust devils 20 to 30 meters in height. Only the half curved toward the aircraft was visible, indicating that axial flow toward the aircraft was picking up the dust. On a number of occasions the vortices descended at different rates along their length. Portions would rapidly dip, forming deep troughs which often burst near the ground at the point of maximum curvature. At other times the vortices descended rapidly while horizontal, and then in the vicinity of the ground certain portions rose up rapidly, forming humps which again usually burst at the point of maximum curvature.

Unstable Atmosphere. Under unstable conditions the vortices descended rapidly in a lurching, sinuous manner and often appeared to be

detraining fluid, leaving patches of smoke in a wake behind the vortex pair. The vortices contacted or almost contacted the ground on several occasions, which invariably initiated a burst breakdown near the ground.

Regardless of the atmospheric stability, the time of vortex breakdown (as defined by an obvious break in the smoke-marked vortex) was generally earlier in a turbulent atmosphere than in calm conditions.

These observations are a composite of results for both test aircraft and for all flight configurations, although the greater amount of Lodestar data tends to make them particularly representative of the Lodestar observations. The categorization by stability class is unique and has not been observed in prior experimental work, although Tombach, et al, (1974), noted the tendency for vortices to descend more rapidly in neutral conditions than in a stable atmosphere. As can be seen here, the descending behavior of the wake vortices becomes quite complex near the ground, with the vortex dynamics, atmospheric turbulence and stability, ground effect, and unstable vortex-vortex and internal mechanisms all playing a role. The usual simple models of vortex descent are quite inadequate to describe this behavior; because of its irregular, wavy nature, modeling of wake descent near the ground may thus not be possible in any detailed deterministic way.

It should be pointed out for completeness that the vortex behavior description discussed above applies to both vortices if both were visible, or to the one vortex which could be visualized. A few cases were observed where both vortices were visible but behaved differently, as for example would occur if the wake tilted or banked and the vortices then decayed differentially, but such behavior was not analyzed. The wind shear observations of Tombach, et al (1974) discuss such cases. The crosswinds during these tests tended to be small, so such behavior was not a major feature. Because of the difficulties with flow visualization it is possible that some of the rising of vortices which was noted is simply the asymmetric motion of the one visible vortex of a tilting vortex pair.

A limited number of runs were conducted under simulated take-off and landing conditions, so that the aircraft was climbing or descending when passing over the test array. The vortices produced in these situations rapidly approached the ground at an angle to the horizontal and contacted the ground sequentially at points along their entire length. These vortices appeared to break up immediately and than rapidly dissipate. The initiation time of this break up was much shorter than the time to first break up measured when the aircraft maintained constant altitude. No linking was observed in these situations, and normal core bursting was rare.

In contrast to the effects of attitude (and hence thrust), data scatter obscured the effects of landing gear or flap positions on vortex decay times. By inference, then, vortex breakdowns seem to be at most weakly influenced by the aircraft configuration.

The core breakdown and sinuous instabilities appear to be intimately intertwined in all of the observations of the Lodestar tests, and the actual mechanism initiating vortex decay is not always apparent. Previous work by Tombach, et al (1975) studied the sinuous instability near the ground theoretically and experimentally, and also noted the presence of both core bursting related to the sinuous instability as well as core breakdowns which occurred in no apparent correlation with the linking behavior. The current results show the same qualitative behavior for the Lodestar. Linking was not observed in the documentation photos of the Boeing 747 tests, although it was observed a few times (runs 5, 8, 51, 52, 53, and 54) at locations out of view of the cameras. For both aircraft, it was observed that ground contact, whether through linking or otherwise, invariably initiated a vortex breakdown.

Axial Flow

One interesting aspect of vortex behavior is the axial flow in the core, which is often assigned a contributory role in various vortex decay mechanisms. The Lodestar vortices, when marked by small buoyant balloons

as shown in Figure 3-3, invariably showed axial flow toward the aircraft, i.e., a wake-like axial flow. On the other hand, the axial flow in the Boeing 747 vortices was either jet-like (away from the aircraft) or there was no significant axial flow.

Jet-like flow in the cores was found behind the Boeing 747 when in takeoff configuration (10/10 flaps, either spoiler and gear position, aircraft climbing) or in landing configuration (30/30 flaps, gear down, no spoilers, aircraft descending). No significant axial flow was observed when the aircraft was "dirty" (30/30 flaps, gear down, no spoilers) and in level flight.

The balloon observations of axial flow direction were corroborated by visual observation of the ends of the smoke-marked portions of the vortices (where axial flow would cause a "spike" of smoke or a hollow core) and of dust flow in vortices contacting the ground.

In order to explain this behavior of the axial flow, the interaction of induced and profile drag in producing axial flow perturbations is of interest, since in the initial stages the effects are of opposite sign. As shown by Brown (1975) for the initial wake near the wing, the jet-like axial flow component is caused by flow developed by the induced drag and defined by the circulation, Γ and the aspect ratio A; while the wake-like axial flow is associated with the profile drag, defined by the wing profile drag coefficient C_{Do} and the mean chord $\bar{c}$. For an elliptically loaded wing of uniform chord shedding a simple vortex pair, Brown's results indicate that a net jet-like flow will result if

$$C_{Di}/C_{Do} > \pi^2/2 .$$

For the aircraft used in the present tests, with their complex wing and engine structures, this ratio will be different, but the general character of the behavior should be the same. Consequently, for a sufficiently clean aircraft one would expect an initial jet-like flow, while the flow would be more wake-like if the aircraft configuration were more dirty. Sufficiently

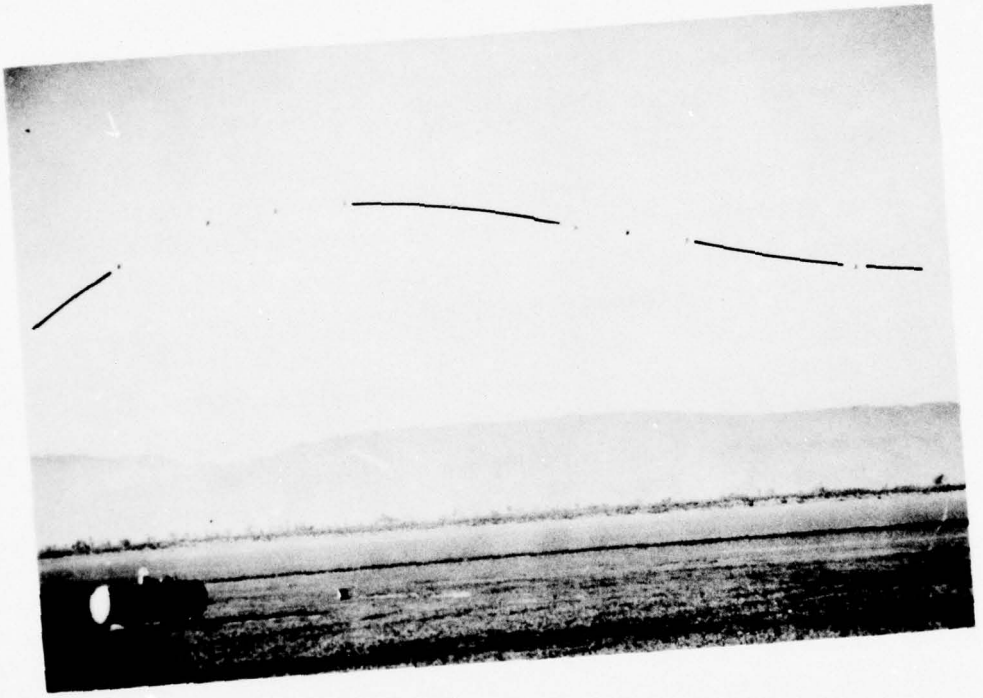

FIGURE 3-3. MARKING OF VORTEX BY SMALL BUOYANT BALLOONS

(The eight balloons show the location of the vortex even though all of the marking smoke has dissipated The line segments are drawn in to show the probable vortex location)

far downstream any initial jet-like component (if it exists) will transform to a wake-like flow, as discussed by Batchelor (1964), since the pressure in the wake will tend toward static, and thus the total drag must be represented by a wake-like momentum deficit.

When viewed from this perspective, the experimental observations suggest that the Lodestar is generally relatively "dirty," and thus has wake-like core flows, while the Boeing 747 is generally "clean" with jet-like flows initially. The one Boeing 747 case which shows no axial flow occurs when a relatively dirty configuration has enough thrust added to maintain level flight. It is likely that the turbulence added by the thrust is sufficient to cause rapid decay of any initial jet-like wake, and thus no significant axial flow was observed in the core by the time the balloons were captured

Local axial flow also occurred whenever a vortex breakdown or vortex pair linking occurred. In such cases the axial flow was away from the instability manifestation, in both directions along the vortex, indicating the presence of higher pressures at the burst or link point. The instability-induced axial flow was stronger than the normal axial flow in the vortex, and thus the local flow was totally dominated by the links or bursts

Axial flow need not be confined only to the core centerline, and shells of axial motion have been observed in tests of aircraft flying past smoke sources. The flow visualization techniques of these experiments could not illuminate non-centerline core flows.

Effects of Core Bursting

The smoke marking often showed a small filament of smoke remaining after a burst had occurred, which indicated the continued presence of organized vortical motion. The small balloons released into the cores also showed vortex motion to be present after a visible vortex breakdown. In several cases the balloons were still spinning in the vortex core at a vortex age of around 150 seconds, which is well in excess of the observed core

breakdown times. In another case, the balloons in the core were overtaken by a moving breakdown, and then remained firmly trapped in the now-invisible vortex core after the breakdown had passed. Prior work (e.g. Hallock, 1976) has also suggested that a vortex breakdown does not necessarily imply a destruction of organized vortex motion, but rather represents a rearrangement of vortex structure. The present work supports this concept, and indicates that the visually observed behavior of the smoke does not always provide a complete picture of the vortex lifetime.

In order to investigate this point further, selected anemometer records on vortex velocities occurring prior to and subsequent to vortex breakdown were examined. The cases studied were ones in which the photography showed a breakdown to have occurred above an anemometer.

A consistent pattern of behavior was observed, which is represented by the three sets of traces in Figure 3-4. Each trace represents the horizontal wind speed, transverse to the flight path, recorded by an anemometer as a function of time as the vortex traveled horizontally above it in ground effect. For each of the three cases shown, the top trace shows the vortex structure before a burst was seen on the photographs at the array, and the lower trace shows the vortex structure at the next anemometer reached by the vortex.

In each case, the effect of the vortex burst is to flatten the velocity profile by significantly reducing the peak velocity under the center of the vortex (to about 30% of its prior value), but without major effect on the speeds away from the center of the vortex. A definite vortex flow remains in all of the three cases shown, however, indicating that core bursting did not totally eliminate the vortex, and the persistence of the outer flow speeds suggests that such bursting may not significantly alleviate the vortex hazard to aircraft with wingspans larger than the core size.

A few of the cases studied showed total alleviation of all vortex velocities by a vortex breakdown, with no residual vortex structure remaining.

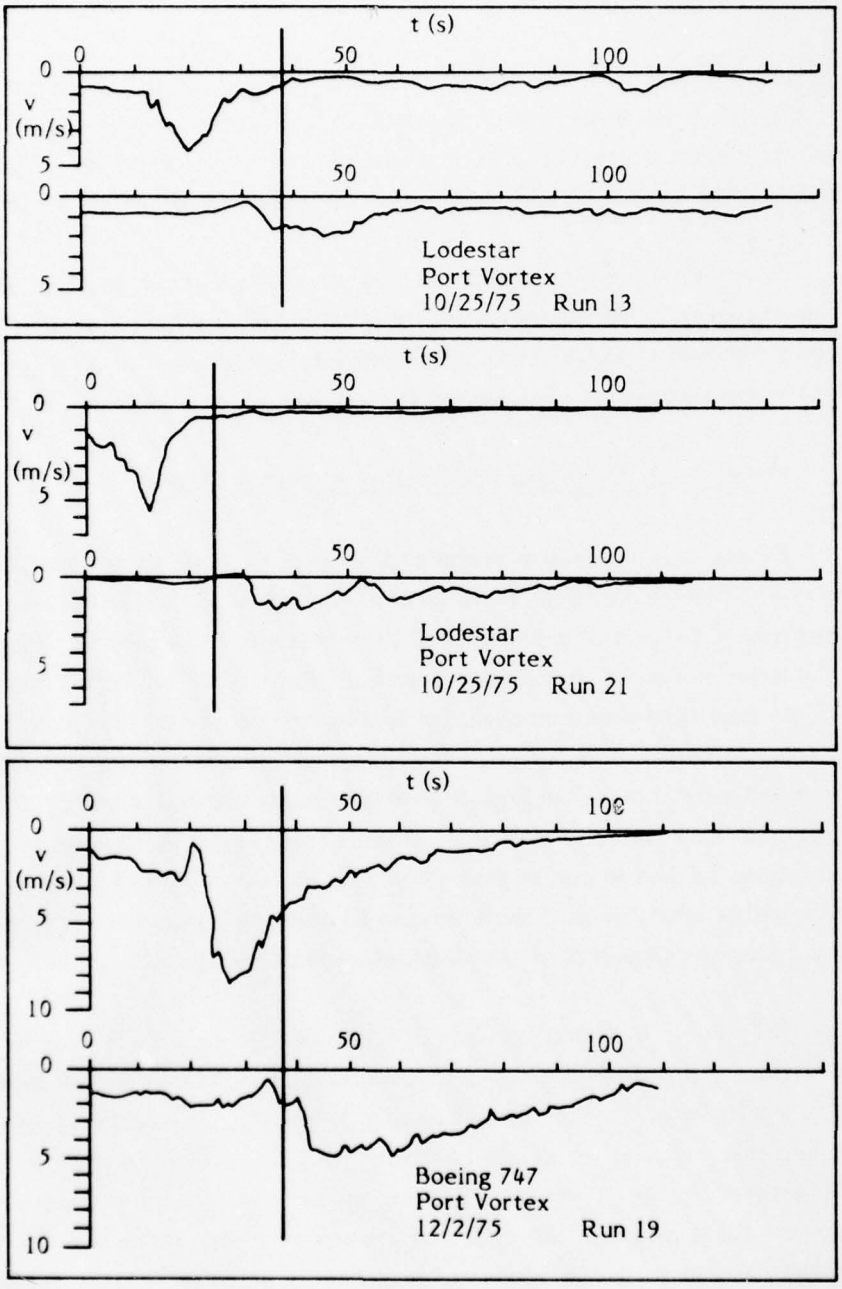

FIGURE 3-4. ANEMOMETER RECORDS OF VORTEX BREAKDOWN

(The top graph of each set shows the horizontal speed history at an anemometer before a burst; the lower trace shows the record at the next anemometer after the burst.)

The flow visualization showed no visible difference between the partial and total vortex decay breakdowns, except that the presence of a residual visible core corresponds (obviously) to a case of partial alleviation. Aircraft configuration was not an obvious factor in selecting one form over the other.

In order to assist in interpreting the vortex breakdown observations a brief discussion of vortex core stability would serve as a useful background. Such a discussion follows below, preparatory to development of an approach to core burst modeling in the succeeding section.

3.2 Simple Analytical Studies of Stability of Vortex Cores

Simple fluid mechanical models of an aircraft wake vortex were constructed to study the major features of the stability of inertial waves, the processes of turbulence generation and the possibility of energy dissipation by coupled motion of simple wave modes. For simplicity, vortex models with no axial flow were employed, the feeling being that while the axial flow affects the vortex development with time, the behavior of inertial waves which are a function of the local profile is probably controlled mainly by the tangential flow velocity profile. Thus it was likely that some of the phenomena related to core-bursting could be explained without considering axial profile interactions. The following discussion presents the key aspects of the analysis; supporting details are included in Appendix A.

The classic Rayleigh stability criterion applied to a vortex having no axial flow shows that axisymmetric disturbances are stable providing that $d\Gamma^2/dr > 0$ where Γ is the circulation at a given radius r. This particularly simple case can be visualized by noting that if a ring of fluid moves outwards while maintaining its angular momentum, then the centrifugal outward force will be less than the inward restoring force due to the pressure gradient if the Rayleigh condition is satisfied. Most vortices generated by aircraft are likely to satisfy this condition since Γ will not decrease as we move outwards.

Considering the more general case of linear waves possessing an azimuthal or helical component, the work of Kelvin (1889) shows that a simple Rankine vortex is stable to all disturbances, although damped long waves of wave speed between 1/20 and half the aircraft speed can exist.

Next, the relatively simple approach of analyzing total mean energy in the flow was studied. Adopting the usual high Reynolds number approach of stating that the interaction of the shear stress (in this case Reynolds stresses due to turbulence) and the flow distortion produces a rate-of-work term in the flow, one can show that this product of shear stress and distortion is always zero in a Rankine vortex, since in the inner rotational core the Reynolds stresses may exist but there is no flow deformation, while in the outer potential flow there are no Reynolds stresses. Thus there is no rate of change of mean flow energy due to these terms. There will always be energy dissipation due to laminar viscosity, of course, but this is small.

Although the energy decay for an ideal Rankine vortex is zero, this is not the case for a more realistic situation where the velocity profile is smooth near the radius of maximum velocity. In this case one has a region between the zero distortion inner core and the zero shear stress outer flow. In this annular region both Reynolds stresses and distortion occur, so that a mechanism exists by which energy can be removed from the mean flow.

A number of other analyses relating to possible instabilities of helical waves (in flow visualization these might look like the rotating screw-thread type of disturbance sometimes observed) were made using very simple base flow and disturbance models. These are developed in Appendix A. The object of these analyses was not to predict the core-bursting phenomenon, but rather to attempt to obtain rational insight into the phenomenon from simplified analytical models.

The analyses provided several conclusions which are summarized below:

Aircraft vortices usually satisfy the Rayleigh stability criterion and thus are stable to linear (small) axisymmetric disturbances

Fast damped or neutral axisymmetric waves can occur, however. and it is possible that some form of non-linear amplification could occur, resulting in "breaking" and consequent core-bursting.

The Rayleigh criterion does not exclude the possibility of unstable helical waves, and such waves could extract energy from a critical annulus where their angular velocity is the same as that of the fluid.

If there are inflection points in the core velocity profile then a helical wave system will certainly be unstable. The core velocity profile associated with a wrapped up scroll-like vortex sheet can contain such destabilizing inflection points

All the above analyses were conducted for zero axial velocity fields, so that many types of instability can occur even without postulating some critical axial flow profiles. Although it has not been proven, it is possible that some analog of Squire's Theorem for the axial and tangential fields exists. Squire's Theorem (Squire, 1933) established that, for a three-dimensional perturbation flow, the critical Reynolds number is no less than that for a two dimensional disturbance. In general, then, if a two-dimensional perturbation showed instability, then the three-dimensional perturbation would be unstable, too. In our case we are discussing two- and three-dimensional mean flows, not perturbations, but it appears possible that if the tangential profile is unstable, the introduction of an axial mean flow to this flow field would not substantially change the stability. This is not to say that the axial fields do not affect the flow development with time, but only that the stability analysis at a given station shows that many instabilities can occur even without axial mean flow fields.

Operationally, the implications of these analyses support the work of other investigators (e.g., Donaldson and Bilanin, 1975) indicating that many forms of waves are possible in a general aircraft type vortex, and that mechanisms can be postulated by which these waves can initiate core-bursting. In particular the wrapped-up vortex sheet can exhibit helical instabilities which will generate turbulence within the vortex, while the normal long axisymmetric waves, although stable or neutral in the linearized analyses, can undergo non-linear amplication and could be the precursors of core-bursting.

3.3 Laboratory Studies of Vortex Behavior

The helical instability mode described in the previous discussion, and the resulting generation of turbulence within the vortex, appears to be a significant factor in vortex decay. An experiment was designed to study this phenomenon while removing other effects insofar as as possible. This experiment was described briefly in Chapter 2, and a detailed discussion appears in Appendix B. Here, the main experimental results of that experimental vortex analog study will be described. This analog experiment in the water tank shed light on instability and transition within the vortex as well as on wake descent and interaction with the ground plane

The water tank experiments showed that, initially, the vortical scroll rolled up into a finite core vortex (Figure 3-5a). During the rollup, disturbances developed in the vortex sheet and became amplified (Figure 3-5b). (This response is somewhat similar to that observed in a free shear layer Kelvin-Helmholtz instability.) The wavelength of this laminar instability increased approximately proportionally to the square root of time until the amplitude was approximately equal to 1/10 of the vortex span, b_v. At this point there was a rapid transition to turbulence, (Figure 3-5c), with the turbulent transition moving radially both inwards and outwards from the annulus where the instability waves first developed. Within a short time the flow within the vortex cell appeared fully turbulent except for a small region near each vortex center.

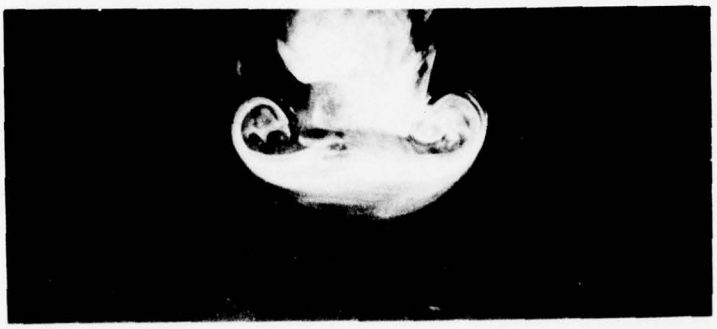

(a)

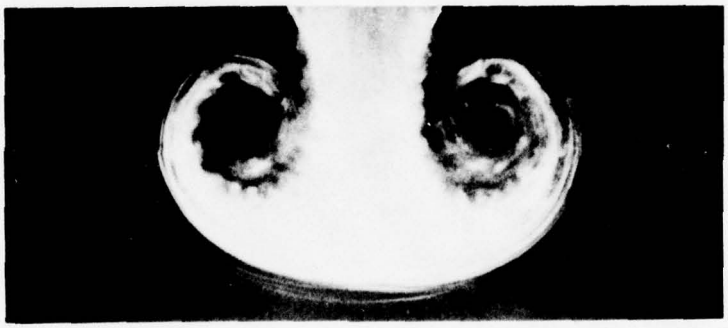

(b)

(c)

FIGURE 3-5. DEVELOPMENT OF VORTEX INSTABILITY IN WATER TANK TESTS

(a) Initial vortex rollup, (b) Later stage of rollup, with shear layer instability at inner boundary of smoke, and (c) Transition to turbulence. Vortex pair motion is downward in these photographs.

In further experiments, the initial turbulence in the cell was increased by installing sawtooth vorticity generators at the outlet of the vortex pair generator to simulate the initial turbulence in the aircraft wake vortex which might result from wing flaps, spoilers or engine exhaust. In this case the wavelength of the instability was twice as large as without the sawtooth and the rate of growth of the wavelength also increased. This is qualitatively what one might expect, indicating that initial turbulence will accelerate the turbulent transition in the vortex core.

These experiments indicate that any analytical modeling of core structure should include the effects of internally generated turbulence. However there was no evidence that this turbulence suddenly caused the size of the core to increase in a manner suggestive of a two dimensional core burst. Nor did the turbulence affect the translational motion of the vortex pair during the early stages of its descent.

Vortex Pair Descent and Interaction With Ground Plane

In the water tank experiments the gross character of the motion was only approximately that predicted by inviscid line vortex pair theory. As expected, it was observed that the vortices descended, separated as they approached the ground plane, and then moved apart along the ground plane. However there were very important distinctions between the real motion and the trajectory computed by a simple analysis such as that in Tombach, et al (1975). According to that analysis, which was based on computations by Lamb (1932), the vortices should approach the ground, and then move outwards until they are finally at a height equal to the original vortex semispan and moving outward at a velocity equal to the original downward velocity. This simple theory thus predicts that the vortices will never rise relative to the ground plane.

In the water tank experiments, however, it was noted that the vortex pair never moved as close to the ground as simple theory predicts, and the separated vortices eventually started to move upwards and away from the

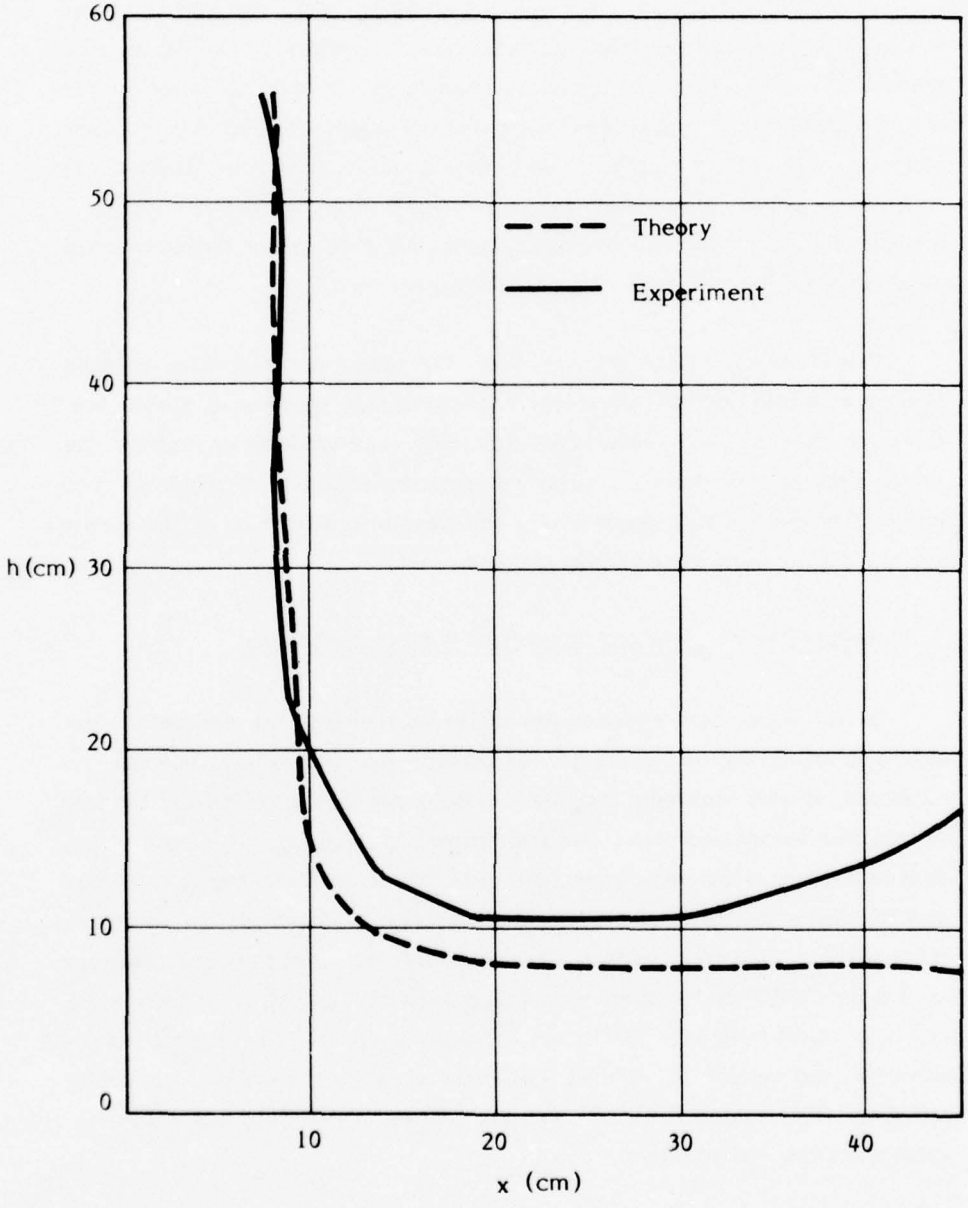

FIGURE 3-6. COMPARISON OF MEASURED VORTEX TRAJECTORY IN WATER TANK WITH POTENTIAL FLOW LINE VORTEX THEORY

(Vortex motion is downward and to the right.)

ground plane, as shown in Figure 3-6. In other words, the vortex appeared to "bounce" when in ground effect. When the vortex pair was generated closer to the ground, this rebound effect was even more pronounced.

The effect of ground plane roughness and boundary conditions was also studied. Three different states were tested. In the first the ground plane was simulated by the free surface of the tank. (The vortex pair motion was actually upwards in these tests but has been recast into normal wake vortex directions in this discussion.) This boundary condition simulates the potential wall condition, but does not impose a "no slip" condition at the surface since the water is free to move horizontally and thus does not simulate the effect of the ground-plane boundary layer. For the second case, a smooth rigid plate was used as the ground plane, and for the third, a rough rigid plate. It was expected that if the ground boundary layer affects the motion and causes dissipation of the vortex strength, then this effect should be distinguished in the experiments. In fact, the different ground boundary conditions had little effect on the vortex trajectories. The rigid ground planes do cause a gradual reduction in apparent vortex strength at later stages of the motion, however, with the rough ground plane causing somewhat stronger effects than the smooth one.

The rebound motion observed in the water tank is very similar to that observed in various flight tests, including those of the current program (c.f. comments in Tables 3-1 and 3-2). Tombach, et al (1975) (also Tombach and Crow, 1976) measured the lateral transport of vortices in ground effect, and noted that the transport speed slowed significantly after a definite distance of travel along the ground. Figure 3-7 compares those results, in non-dimensional form, with the water tank data from the present experiment. The agreement is excellent. The confirmation of this motion suggests that vortex rising, not decay, is the main cause for the slowing of transport observed in the flight tests.

An important operational variable is the circulation Γ, of each vortex, and the way it changes with time in ground effect. It was not possible to

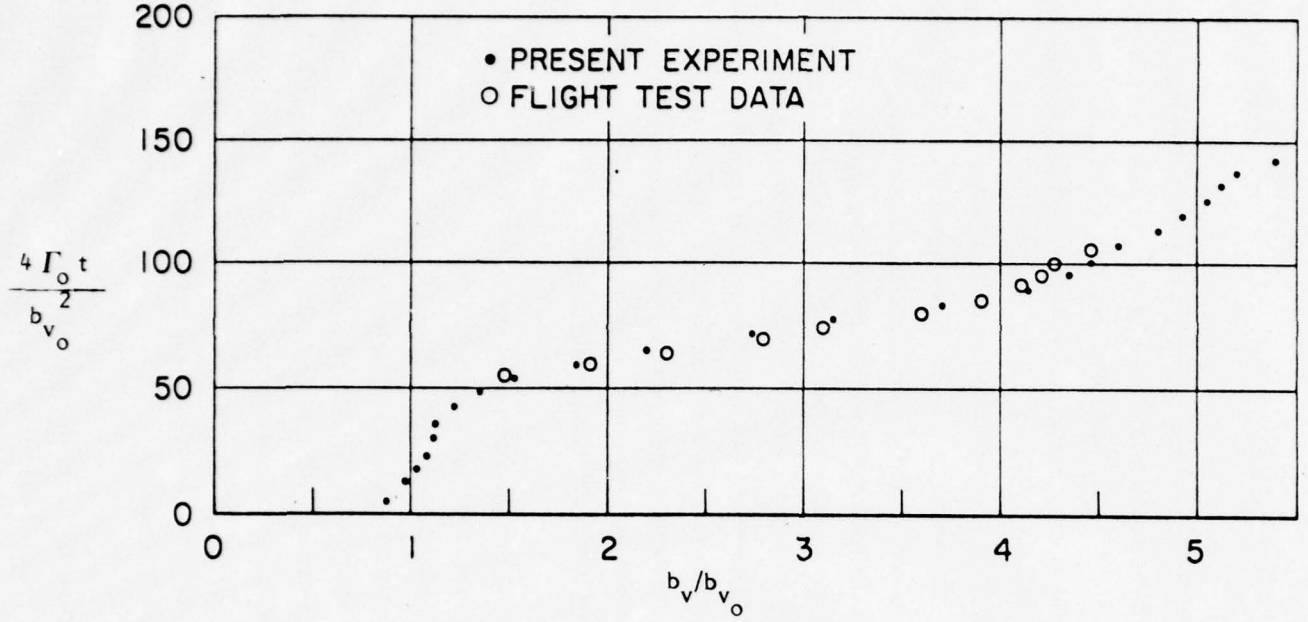

FIGURE 3-7. NORMALIZED WATER TANK VORTEX TRAJECTORY COMPARED WITH FLIGHT TEST DATA FROM TOMBACH, ET AL (1975)

measure Γ directly in these experiments, but an "apparent circulation" could be computed from the vortex trajectory. Using standard inviscid pair theory, the strength of a line vortex was calculated which gave the same propagation speed when located at the measured vortex core center position. For example, when the vortex separation is large, and the height above the ground is h, the apparent circulation Γ_a is given by

$$\Gamma_a = 4 \pi g h,$$

where g is the horizontal propagation speed.

Calculating Γ_a by this method produces curves of the type shown in Figure 3-8, which shows that the overall character of the curve of Γ_a versus time is indicative of a gradual circulation decay upon which is superimposed an oscillatory component. Since an increase of circulation with time is not possible, this curve suggests that caution must be exercised in inferring actual vortex strength from apparent circulation computed from the assumption that the vortex is a line pair.

The vortex behavior observed in these tests can be accounted for, however, by recognizing that the vorticity is contained in a core of finite radius, and that this core is continually distorted due to the induced flow fields. The flow visualization shows the core to be of approximately oval shape. Before encountering the ground plane this oval is oriented with its major axes at about 45° to the plane of symmetry with the lower lobe closest to this plane. As the ground plane is encountered and the vortex begins to move laterally, the core oval is subjected to a strongly distorted corner flow and the axes begin to rotate. This rotation of the core could account for the rebounding effect as well as for the oscillation in apparent circulation.

Implications

The water tank experiments have shown that there is an annulus within the core where turbulence is generated, and this turbulence spreads radially,

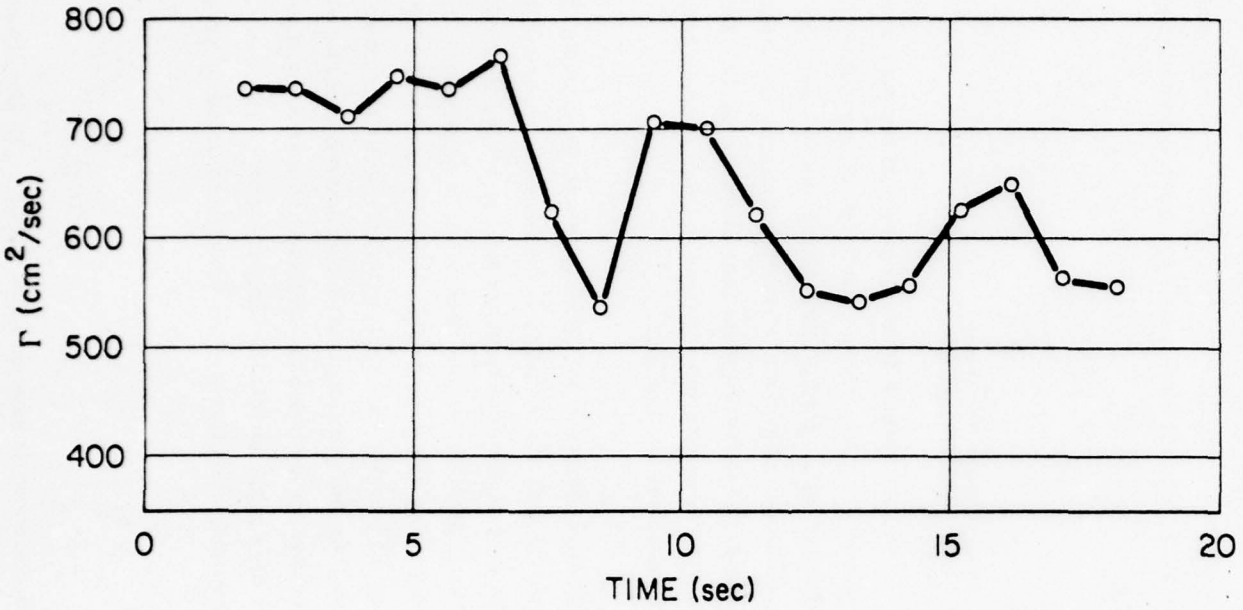

FIGURE 3-8. DECAY OF APPARENT CIRCULATION OF WATER TANK VORTICES.

although there is still a small inner core in which the flow appears to be laminar. Increasing the initial turbulence level of the fluid composing the core tends to make the wavelength of the instability waves larger, and to make the wavelength grow more rapidly with time. However this turbulence generation does not appear to be connected with core-bursting.

The motion of the vortex pair in ground effect is significantly different from inviscid line vortex predictions, and the vortices are observed to rise in ground effect and to approach a height which may be about 60% larger than their initial half-separation. As a consequence of the finite size oval-shaped core, the apparent circulation computed assuming a line vortex system is quite different from the actual circulation about a core.

From the operational point of view, these results show that initial turbulence within the cores certainly affects their development. The most important operational result is that the vortices do rebound and rise above their predicted height, even under uniform conditions. Thus it is not necessary to postulate wind shears, ambient turbulence or ground boundary layers to account for this motion when observed in flight tests. Also, computing of the apparent circulation from the trajectory using point vortex models can falsely imply a significant reduction in vortex strength.

3.4 Heuristic* Approach to Core-bursting

Because of the difficulties of predicting core-bursting by any direct fluid mechanical analysis, we propose a heuristic argument which appears to incorporate the main physical terms and has correlation with the data. The objective of this approach is to identify the factors which affect the time-to-breakdown of the vortex core, and to quantify the relationships between them and vortex lifetimes.

---

* Heuristic method – a method of solving a problem in which one tries each of several approaches or methods and evaluates progress toward a solution after each attempt.

Consider one particular case of core-bursting, that occurring on a single long rectilinear vortex. Thus it is assumed that the flow development in the vortex is not connected to the other member of the pair so that b_v, the vortex span, should not enter as a parameter. (Core-bursting can certainly be connected in some cases with the presence of the other member of the pair, especially during the occurrence of the sinuous instability. In such a case the perturbation fields induced by the neighbor vortex and by the curvature of the vortex itself probably cause an accelerated core development, thus producing core velocity profiles conducive to core-bursting. From an operational point of view, however, such breakdown is coupled with the sinuous instability, so that for estimates of time-to-breakdown the time estimate of sinuous instability applies. Other manifestations of core instability, unrelated to the sinuous instability, are thus the ones of interest for the present discussion.)

Now, starting from a given initial condition, which can be completely described by the tangential and axial velocity profiles at some effective time zero, assume that these profiles develop in some way with time so that at some stage the profiles have acquired a shape such that inertial waves can be sustained and amplified to produce the core-bursting phenomenon. Since there appears to be no acceptable method of predicting these critical profiles, we must experimentally determine the critical time required for a given initial condition to develop into a particular profile.

The mechanism by which the profiles develop is principally momentum transfer in a radial direction. This momentum transfer can occur only through laminar viscosity or turbulence. For a simple laminar vortex having no axial components this mechanism can be scaled by the introduction of laminar viscosity into the process. In the classical case (Lamb, 1932) the time scale is of the form r^2/ν, where r is a characteristic radius, and ν the (laminar) kinematic viscosity. For a radius of about one meter (representative of vortex cores for aircraft such as the Lodestar), this gives a time scale of order 10^5 seconds. Since experimentally observed vortex decay time scales are characteristically around 100 seconds or less, this indicates that laminar viscosity is not an important term in vortex decay.

Consider next momentum transfer through turbulence within the vortex. Assuming this turbulence is mechanically generated by the circulatory flow, then one model suggests that the effective turbulent viscosity, ν_T is given by $\nu_T = .005\,\Gamma$ (Squires, 1954). In this case, the time scale for the same vortex, with $\Gamma \sim 100\ m^2/s$, is of the order of one second. There is also additional turbulence present due to ambient atmospheric turbulence, which can be characterized by the turbulent dissipation rate ϵ, so a time scale for this is given by $(r^2/\epsilon)^{1/3}$. A characteristic magnitude of ϵ for moderate turbulence is about 50 cm^2/sec^3 so that the time scale associated with ambient turbulence is of the order of ten seconds.

Both of the turbulent terms are much more significant than the molecular laminar viscosity term, and are both of relatively comparable magnitude. The atmospheric turbulence term obeys a different ordering scale with respect to length than the mechanically generated turbulence. The time scale associated with ν_T goes like r^2, while that associated with ϵ goes like $r^{2/3}$. Consequently ambient turbulence should have a greater effect (smaller time scale) the larger the vortex radius, and thus should play a significant role in the vortex aging process. It has certainly been observed in numerous flight experiments that an increased ϵ is associated with reduced time-to-burst as well as reduced time-to-link (Crow Instability). In addition there have been a number of observations of high altitude single vortices in very calm stable air, where the vortex has been observed to persist in organized form for times in excess of 300 seconds. Thus it appears reasonable that ϵ should be a significant parameter affecting core-bursting times in the real atmosphere.

To provide further perspective on this, Donaldson and Bilanin (1975) report on numerical experiments of vortex profile development using second order closure techniques in which turbulent transfer is analytically modeled in detail. In these computer simulations turbulence is introduced into the core at a number of different radii. They found that the introduction of turbulence causes quite distinct differences in development from that of a simple laminar vortex. As expected, turbulence introduction near the center

causes the core of the vortex to grow much more rapidly than in the laminar case. Such a mathematical introduction of turbulence will cause the same type of effects as would be caused by the presence of ambient turbulence throughout the vortex, again suggesting that the time scales of vortex development should be quite significantly affected by ambient turbulence.

The vortex development, when viewed from earth-fixed coordinates, will also be essentially independent of the aircraft speed, U. To arrive at this conclusion, we assume the radial development of the tangential flow is a function only of time from formation, so that each "slice" of vortex behaves like an expanding circular disc. To first order, then, this slice is cylindrical and its stability is independent of the flight speed. On the other hand, to define the axial flow perturbations, which are driven by the axial pressure gradients, one must know the relative growth of each "vortex disc." This will depend upon the distance or time from the origin, which introduces the flight speed as the rate at which the wake is being generated. Thus the flight speed will only affect the growth of the vortices through axial/radial momentum coupling, but it should not, to first order, affect the stability.

To summarize the argument to this point, we have assumed that at some arbitrary time zero the vortex is fully described by its tangential velocity profile and by its axial velocity profile. Viewed in earth fixed coordinates, the axial and tangential profiles will develop with time in a generally diffusive way towards reducing velocity gradients and increasing the effective lateral scales. The factors controlling the time scale of the process will presumably be ϵ, the ambient turbulence dissipation, and Γ, the term which controls the mechanical turbulence generation through ν_T; while the inertial coupling between the tangential and axial velocity field will play a significant role in the mutual development of the profiles. At some time the tangential and axial profiles will have developed to the point where inertial waves can be formed and core-bursting will occur.

We now assume that, for a given generator aircraft under defined conditions, the core-burst will continuously occur at a given distance behind

the generator aircraft. Observations show that this is usually the case, although data presentations such as in Tombach (1975) or Tombach, et al (1975) show considerable scatter. The scatter results because core-bursting occurs locally on one segment of the vortex while portions of the vortex further downstream (that is, of greater age) remain organized, although usually not for long. This can be accounted for by assuming some degree of scatter in the critical time, due to non-uniformities in either the vortex generation or the ambient conditions. In particular, it is quite reasonable to expect a portion in a locally turbulent patch of atmosphere to burst more rapidly than a nearby segment in calmer air.

To specify the initial profiles, we wish to consider the minimum number of parameters sufficient to give some representative description of the flow. For the tangential flow we assume that the maximum tangential velocity, V_T, and the radius at which it occurs, r_T, provide the minimal first-order description. The actual profile could be considered to be some smooth curve defined by these parameters. For the axial flow we will assume the profile is approximately normal or bell-shaped and introduce the parameters V_W and r_W, being respectively the maximum centerline speed and the effective width of the axial flow distribution. A dimensionless quantity $S^* \equiv V_T/(V_T + V_W)$ is then like a swirl number, defined in such a way that $S^* = 0$ corresponds to flow with no swirl (pure wake flow) and $S^* = 1$ corresponds to swirl-dominated flow (pure two-dimensional vortex flow). A parameter $R^* \equiv r_T/(r_T + r_W)$ gives a measure of the tangential and axial length scales. Thus, the axial and tangential profiles can be expressed in terms of two dimensional quantities and two dimensionless quantities, that is V_T, r_T, S^*, R^*.

The time to burst, T_b, is thus a function of the initial parameters V_T, r_T, S^*, R^*, and a dissipative turbulence parameter. For convenience, since the ambient turbulence will generally be dominant, represent the total turbulence by ϵ, recognizing that now ϵ contains both the ambient dissipation as well as the smaller mechanically generated turbulence. It can then be shown that a possible general formulation for T_b is

$$T_b = \frac{r_T}{V_T} \left(\frac{V_T^3}{\epsilon r_T} \right)^{\alpha} F(S^*, R^*) .$$

The first term provides the proper dimensions based on the initial tangential flow scales, the second term provides the turbulence scaling and the third term contains the initial axial/tangential flow characteristics. The exponent α appears because the second term is dimensionless. A more general form for the second term would have been an arbitrary function of $V_T^3/\epsilon r_T$.

Before proceeding further we discuss some cases where a parameter is arbitrarily eliminated. If, for example, we assume that the tangential flow can be characterized by Γ alone (ignoring its scale r_T), then a similar analysis gives $T_b \sim \Gamma^{1/2}/\epsilon^{1/2}$. The arbitrary exponent no longer exists when the number of variables is reduced by one.

On the other hand, we can ignore Γ entirely and assume that the development is entirely connected to the initial radius and ϵ. This model occurs in the turbulent dispersion of a passive plume, although it does not seem probable here. However, adopting this approach we would obtain $T_b \sim r^{2/3}/\epsilon^{1/2}$.

Returning to the more general form, to finally solve the complete time-to-burst problem requires definition of the function $F(S^*, R^*)$ and determination of the exponent α. Lacking further information on the theoretical forms these should take, further analysis requires recourse to experiment. Since detailed experimental data on V_T, r_T, S^*, and R^* does not exist for cases where T_b has also been measured, some further assumptions about the form of the elements of the time-to-burst model will need to be made to allow currently available experimental data to be used.

3.5 Experimental Model of Core Breakdown

The preceding section gave some insight into the parameters and basic variables of a heuristic core-bursting model, and noted that the observables from most general flight testing are not adequate to determine the fundamental velocity scale parameters of the vortex systems. In addition, there are many real effects which always occur in the landing configuration of heavy transport aircraft which make the actual wake vortex systems far more complicated than the model of a simple turbulent vortex pair immersed in a neutral atmosphere of homogeneous turbulence. Particular significance here should be placed on the flap and spoiler settings of the aircraft, engine placement and power settings, the non-homogeneity of the atmosphere, and the presence of the ground plane. In fact, as pointed out by Donaldson and Bilanin (1975), the wake development is extremely sensitive to configuration details of the lift, drag and thrust producing mechanisms of the aircraft.

The theoretical analysis suggests that if the time-to-burst were measured as a function of turbulent dissipation while all other variables were held constant, a curve such as sketched in Figure 3-9 might result. In this curve there exists a flat portion at low ϵ where T_b does not vary strongly, since wake decay there would be principally due to mechanically generated turbulence. For larger values of ϵ turbulence will play an increasingly significant role so that the curve for T_b varies like $\epsilon^{-\alpha}$ for large ϵ, as postulated previously. The actual numerical values on the axes would depend on the initial r_T, V_T, and F (S*,R*).

The parameters S* and R* will be functions of the induced drag and profile drag of the wing. If the profile drag coefficient of the various wings studied does not vary much, then the function F (S*, R*) should have approximately the same value for general wings of comparable aspect ratio and lift coefficient. Making such an assumption would then allow use of existing experimental data, since the time-to-burst relation from the preceding section then simplifies to

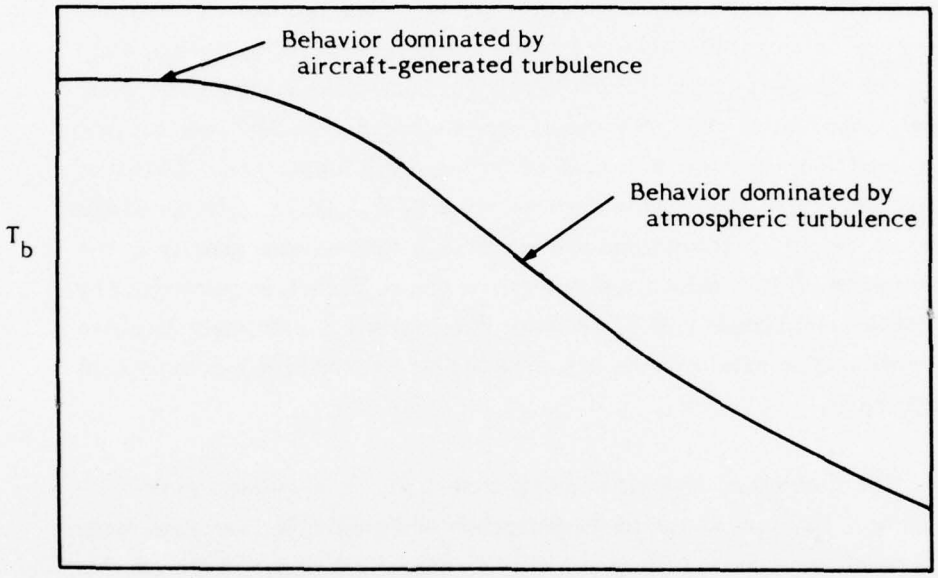

FIGURE 3-9. HYPOTHETICAL DEPENDENCE OF TIME-TO-BURST T_b ON AMBIENT TURBULENCE ϵ

$$T_b \sim \frac{r_T}{V_T} \left(\frac{V_T^3}{\epsilon r_T} \right)^{\alpha} ,$$

and, assuming a universal tangential velocity structure initially, so that $V_T \sim \Gamma_o / r_T$, gives

$$T_b \sim \frac{r_T^2}{\Gamma_o} \left(\frac{\Gamma_o^3}{\epsilon r_T^4} \right)^{\alpha} ,$$

where Γ_o is the initial circulation of the rolled-up vortex, say a few spans downstream of the wing. As a final assumption, assume that the vortex core size is proportional to the wingspan, which is reasonable since the core is made up of the wing boundary layer. Inserting $r_T \sim b$ into the equation then gives

$$T_b \sim \frac{b^2}{\Gamma_o} \left(\frac{\Gamma_o^3}{\epsilon b^4} \right)^{\alpha} .$$

Recall that the total turbulence has been represented by ϵ for convenience, and the ϵ is made up of both ambient and mechanical turbulence. Let ϵ now represent only the ambient portion again, and let k represent the equivalent turbulence due to mechanical generation. Although k should decrease with wake age, assume that, to first approximation, it is a constant for a given aircraft at the wake ages of interest for core-bursting. Including a constant of proportionality, G, the final form of the time-to-burst relation is then

$$T_b = G \frac{b^2}{\Gamma_o} \left(\frac{\Gamma_o^3}{(k + \epsilon) b^4} \right)^{\alpha} , \qquad (1)$$

with α still unknown.

The most probable values for α are multiples of 1/3, i.e., 1/3, 2/3, 1, etc., since $\epsilon^{1/3}$ is physically meaningful as a quantity proportional to the root-mean-square turbulent velocities in the atmosphere and $\epsilon^{2/3}$ is proportional to the energy spectral density of the turbulence. Recourse to experiment is necessary to define α as well as the constant G and the aircraft turbulence term k.

Experimental data available for analysis of the T_b versus ϵ relationship involves tests with four aircraft: a Cessna 170, an Aero Commander 560F, and the Lodestar and Boeing 747 of the current tests. This data includes measured time-to-burst, atmospheric turbulence and the gross aircraft parameters of weight, flight speed and flap settings. Thus T_b and ϵ are determined. Γ_o can be inferred from the vortex spacing, and b is given. No quantitative data on axial velocity is available for these flight tests, and none is required by the present model.

To make the data amenable to analysis, the configurations considered had to be compatible between aircraft and could not vary significantly for the same aircraft. Review of the data indicated that the configurations for each aircraft were relatively invariant from run to run, from the perspective of bursting times, with two exceptions. As one exception, the 30/1 flap configuration for the Boeing 747 results in a significantly different spanwise lift distribution than the clean and normal flaps-down configurations (recall that the 747 flaps span most of the wing). As the second exception, the clean Lodestar configuration has a different lift distribution than the flaps down condition. Consequently, data for the Boeing 747 30/1 flap configuration and the Lodestar clean configuration was excluded from the analysis. The airspeed, and hence the vortex circulation, for the Boeing 747 clean runs was also significantly different from the other runs, and was initially excluded from the analysis. Different power settings did not appear to noticeably influence bursting times, based on study of this limited data base, and thus power was not considered as a factor in the analysis. (Power settings do affect the near-field dispersion of the visualization smoke, however.)

The resulting data base for the analysis is shown graphically in Figure 3-10 for each of the four aircraft under discussion. The Cessna 170 and Aero Commander 560F data shown are from the original experimental records for the experiments described by Tombach (1973) and Tombach, et al (1974), respectively. All of the data has a good distribution over a wide range of $\epsilon^{1/3}$ except for the 747 points, whose clustering in two groups will have some impact on the statistical analysis later. The data has a slight bias toward underestimation of T_b, especially at longer times, because decay of the visualization smoke density often precluded observations of breakdowns. This effect was particularly significant for the Boeing 747 tests.

Lines representing behavior of the nature of $T_b \sim \epsilon^{-1/3}$ have been drawn on the figure, and appear to correlate well with the general trend of the data, although the scatter is considerable and vortex breakdown times vary significantly from one run to the next under apparently identical conditions. One obvious factor causing this is the spatial and temporal inhomogeneity of the atmospheric turbulence, which does not affect the averaged parameter ϵ. Another factor is the vertical variability of turbulence in the highly stratified atmospheres near the ground which prevailed during some of the tests. This resulted in vortices descending through a continually varying turbulence field. This turbulence field is also anisotropic, as was discussed by Tombach, et al (1975), and thus it is unlikely that a single turbulence index could provide a complete representation of its effects.

As suggested by Equation 1, functions of the form $T_b = \left(\frac{K}{k + \epsilon}\right)^{\alpha}$ were fitted to the experimental data. As suggested by the lines in Figure 3-10, the best fit was obtained for $\alpha = 1/3$, although the sensitivity of the fit to the value of α was fairly weak. Table 3-4 summarizes the results of the fitting procedure. The correlation of the data with the assumed functional form is fairly good with a mean standard error of estimate of around 10 seconds, which is more governed by the degree of data scatter than by the best curve fit. Thus 67% of the experimental observations lie within about 10 seconds of the functional form used. (For $\alpha = 1$, the standard error of

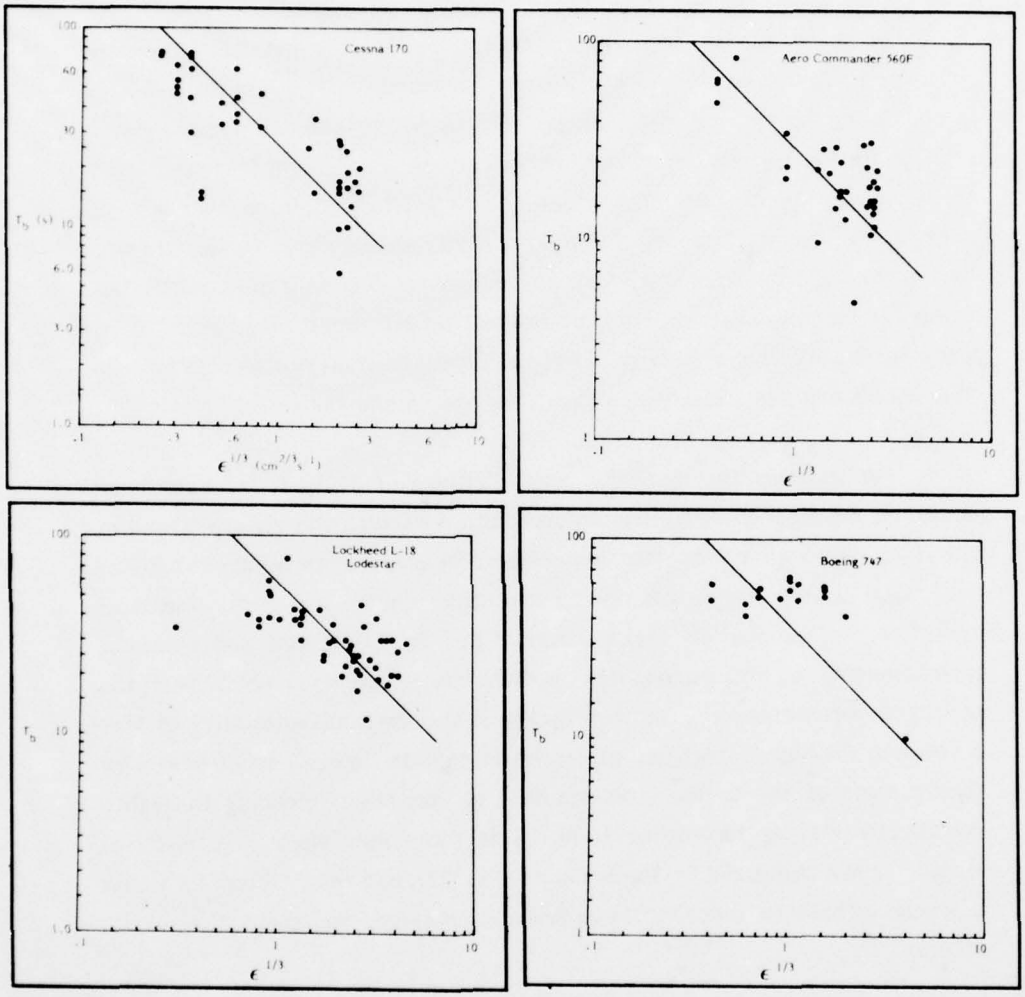

FIGURE 3-10. DATA ON TIME TO BURST VERSUS TURBULENCE USED IN THE ANALYSIS

(The lines represent $T_b \sim \epsilon^{-1/3}$.)

TABLE 3-4. STATISTICAL CONSTANTS OF FIT OF FORM $T_b = [A/(k+\epsilon)]^{1/3}$ TO THE EXPERIMENTAL DATA

Aircraft	Configuration	No. of points	A (cm^2)	k ($cm^2 s^{-3}$)	Correlation Coeff.	Std. Error of Est. (s)
Cessna 170	Clean	43	38,300	0.023	.76	13.7
Aero Commander 560F	Clean	33	39,100	0.089	.84	9.5
Lockheed L-18 Lodestar	Flaps down	50	394,000	3.87	.64	9.6
Boeing 747	Flaps down	21	1,020,000	5.66	.82	8.5

estimate averaged about one second longer.) The correlation coefficient (or coefficient of determination) is fairly high for all but the Lodestar

The constant k, which can be interpreted as the effective residual aircraft-generated turbulence in the wake, is quite small for the Cessna 170 and Aero Commander 560F, which were flown in the clean configuration with flaps retracted. In terms of $\epsilon^{1/3}$, the value of k for these aircraft corresponds to an ambient $\epsilon^{1/3}$ of 0.2 to 0.4 $cm^{2/3}s^{-1}$ (normally considered as negligible turbulence). For the Lodestar and Boeing 747, which were flown with landing gear and flaps extended, the value of k is significantly higher, and has the same effect as an ambient $\epsilon^{1/3}$ of 1.6 to 1.8, which is typically classed as light turbulence.

The constant A varies significantly over the range of aircraft considered, and generally increases as the aircraft scale increases. Comparing the tested time-to-burst relation with the complete relation in Equation 1, it can be hypothesized that

$$A = G^3 b^2,$$

where G^3 is (hopefully) invariant from aircraft to aircraft. Note that Γ_o disappears from Equation 1 for the particular case of $\alpha = 1/3$. Table 3-5 shows the computation of G for each aircraft. The value of G is very nearly 0.3 for all aircraft except the Lodestar, for which G is 0.46. The different value of G for the Lodestar, which has significant flaps on the inboard third of the wing and thus might have a different form of the drag-related function F(S*,R*), is not surprising. In addition, the Lodestar data had the poorest correlation with the assumed functional form, which makes the value of A less reliable. The relative constancy of G for aircraft ranging from the small Cessna 170 to the giant Boeing 747 is surprising, however, and provides considerable support to the reasoning behind the heuristic analysis.

Thus a reasonable overall estimate for G is, say, 1/3. The probable bias in the data for long times is a consequence of the difficulty of good

TABLE 3-5. CALCULATION OF THE PROPORTIONALITY CONSTANT G IN THE RELATION $T_b = G\left[b^2/(k+\epsilon)\right]^{1/3}$

Aircraft	Configuration	b (cm)	$G = (A/b^2)^{1/3}$
Cessna 170	Clean	1100	.32
Aero Commander 560F	Clean	1490	.26
Lockheed L-18 Lodestar	Flaps down	2000	.46
Boeing 747	Flaps down	5960	.31

flow visualization when flaps are lowered, is worse for the Boeing 747 than the Lodestar (because of the different flow visualization method used on the Boeing 747), and is conveniently handled through the aircraft turbulence parameter k. For slightly conservative (high) estimates of T_b, select k = 0.05 $cm^2 s^{-3}$ for any clean configuration aircraft and k = 4 $cm^2 s^{-3}$ for any aircraft with flaps and gear down. Thus the general time-to-burst relation developed here becomes

$$T_b \approx \frac{1}{3}\left(\frac{b^2}{k+\epsilon}\right)^{1/3} , \qquad (2)$$

with k selected as noted above.

Figure 3-11 shows the same data as in Figure 3-10, with the best fit curves for each aircraft (from Table 3-4) as well as the composite equation (Eq. 2) drawn on each plot. It can be seen that the composite function does not fit the data as well as the individual curves for each aircraft, indicating that not all factors which vary from one aircraft to another are handled by the simplified analysis used here. The deviations are greatest for the two twin-engine propeller aircraft, but not in a constant manner.

Equation 2 can also be written in non-dimensional form as

$$\tau_b = \frac{1}{3\,\eta_b} , \qquad (3)$$

where

$$\tau_b = \frac{T_b\,\Gamma_o}{2\pi b^2} , \qquad (4)$$

and

$$\eta_b = 2\pi\left[\frac{(k+\epsilon)b^4}{\Gamma_o^3}\right]^{1/3} . \qquad (5)$$

Here, Γ_o has been reintroduced as a parameter which is required for the non-dimensionalization.

A plot of τ_b versus η_b, with all of the time to burst data plotted on it, is shown in Figure 3-12. Some points for the clean 747 configuration have

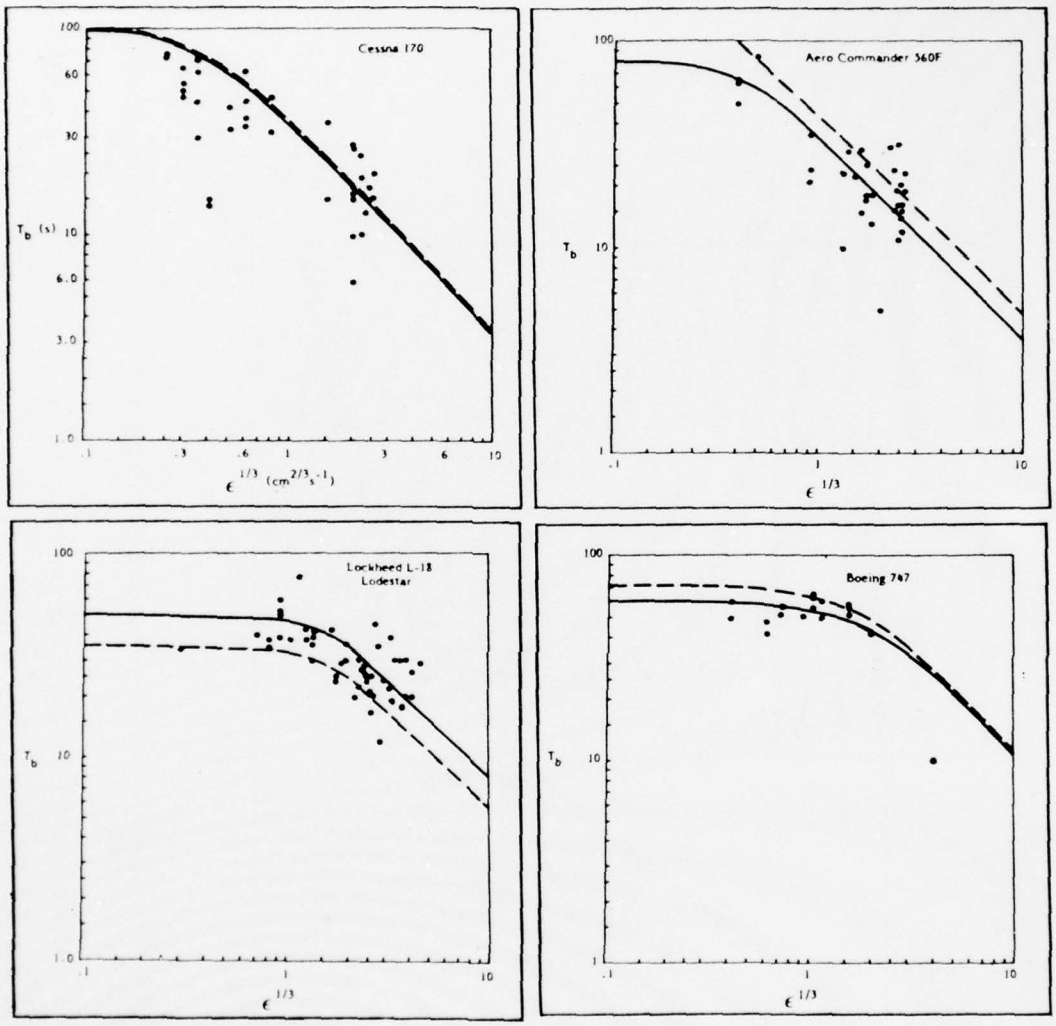

FIGURE 3-11. FITTED CURVES FOR TIME-TO-BURST DATA FOR EACH AIRCRAFT

(From Table 3-4 (solid lines), and composite function from Equation 2 (broken line). The logarithmic scales emphasize the deviations below the curves.)

AD-A042 478 AEROVIRONMENT INC PASADENA CALIF F/G 20/4
AIRCRAFT VORTEX WAKE DECAY NEAR THE GROUND.(U)
MAY 77 I TOMBACH, P B LISSAMAN, J B MULLEN DOT-TSC-1008
UNCLASSIFIED AV-FR-668 FAA-RD-77-46 NL

2 OF 2
AD A042478

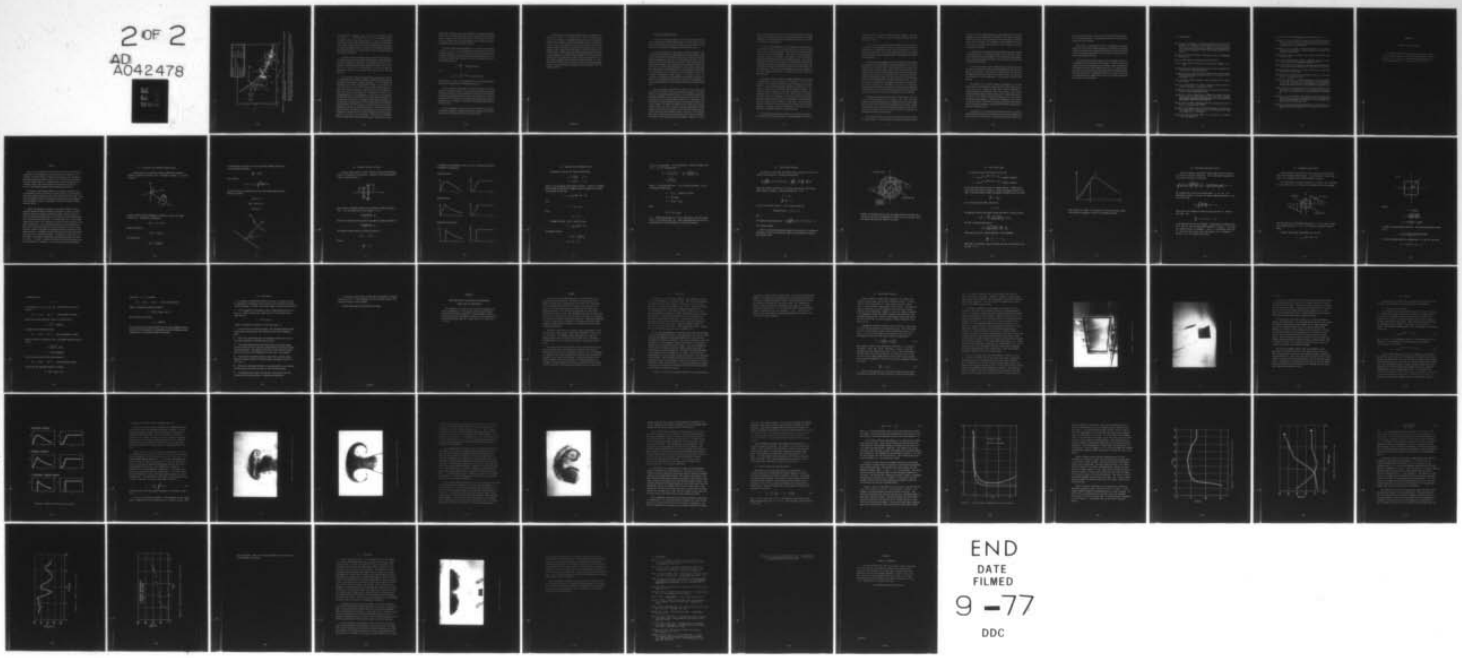

END
DATE FILMED
9 -77
DDC

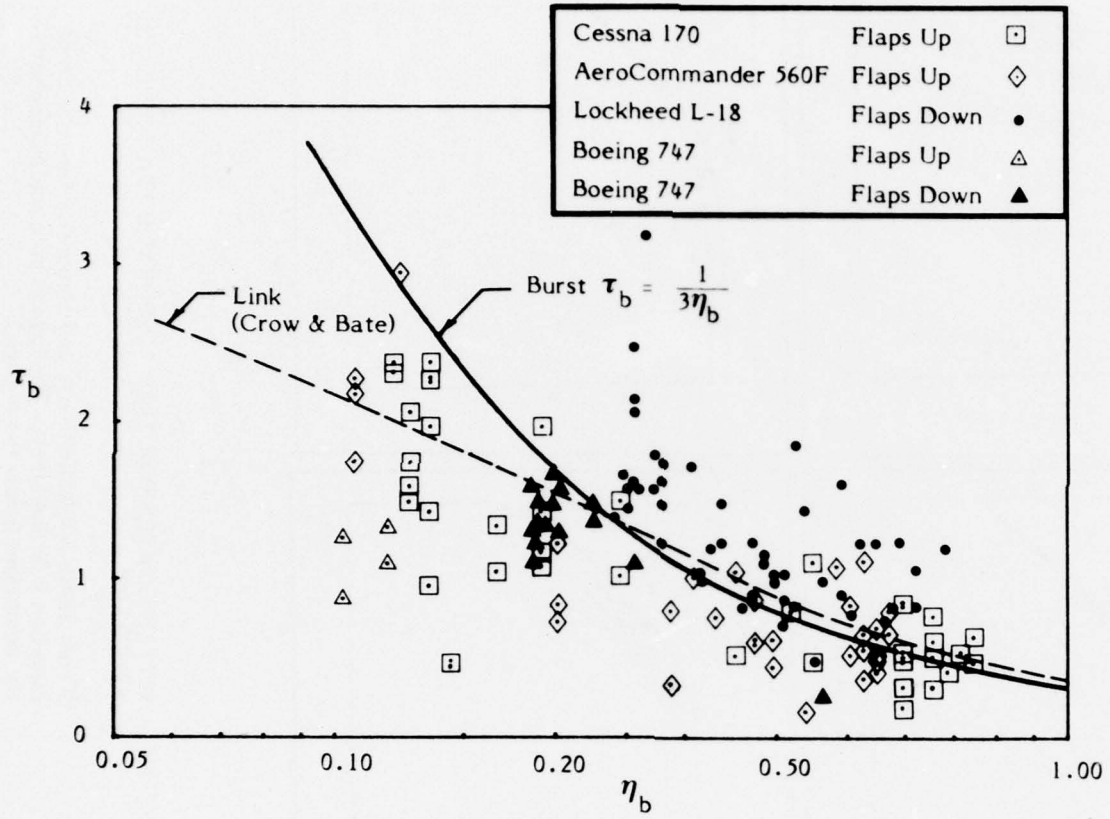

FIGURE 3-12. COMPOSITE PLOT OF TIME-TO-BURST DATA IN DIMENSIONLESS FORM, AND COMPARISON WITH MODEL (SOLID LINE)

(Also shown is the time-to-link formula of Crow and Bate (broken line) assuming elliptical span loading to relate η and η_b, and setting the turbulence constant k = 0. The logarithmic scale for η_b emphasizes deviations to the left of the curves at small values of η_b.

also been added to this figure, using k = 0.05 $cm^2 s^{-3}$ and measured b_v and U to compute Γ_o. Here again there is a definite clustering of points according to aircraft type, showing that the τ_b and η_b non-dimensionalization alone does not fully describe all aircraft effects on vortex breakdown. There is a general trend for the clean configuration data (open points) to lie below the general best fit line and for the flaps-down configuration data (filled points) to lie near or above that line; this is most pronounced at small η_b (low turbulence).

An arbitrary choice of a larger value of k, hence a larger value of η, for clean aircraft could improve the fit, but would have to be recognized as an ad hoc adjustment in parameters. Nevertheless, the simple curve in Equation 3 is generally good for predicting vortex breakdown times within a factor of 2, except for very small values of η_b, where, however, the experimental data tend to be biased toward shorter T_b as discussed previously.

It is of interest to compare this approach with that previously taken by Crow and Bate (1976) for sinuous instability to estimate the time-to-link, T_l as a function of atmospheric turbulence dissipation ϵ. In their analysis the normalized time-to-link and normalized turbulence are defined by $T_l \Gamma/(2\pi b_v^2)$ and $2\pi (\epsilon b_v^4/\Gamma^3)^{1/3}$, which are similar normalizing terms to those used in the present analysis, except for the use of b_v instead of b. There are theoretical distinctions which distinguish the present core-bursting approach from the linking analysis. First, in the core-bursting case, the significant length scale according to our simple approach should be r_T, the initial vortex radius scale. To represent this as being proportional to b, the wing span, is an approximation. Thus we might expect that for different wing arrangements the relationship of r_T to b would be different, so that our assumption is valid only as a preliminary estimate. Second, the Crow-Bate model eliminates flight speed on the grounds that, at the scale of sinuous instability, the core growth of the vortices is insignificant, thus they may be regarded as cylinders of very small radius. Third, the core breakdown analysis includes aircraft induced turbulence, which is unlikely to be of scale

large enough to influence the sinuous instability. The analysis approaches differ, also. The time-to-link analysis of Crow and Bate provides a rational stability analysis which gives the form of the universal curve from theoretical grounds. The time-to-burst approach here is empirical and relies on experiment to provide the unknown constants.

The time-to-link relations developed by Crow and Bate can be recast in terms of τ_b and η_b if it is assumed that the lift distribution on the wing is elliptical, so that $b_v = \frac{\pi}{4} b$. (This assumption should be used with caution; experimental data have shown actual ratios to differ significantly from $\pi/4$ sometimes, even with flaps retracted.) In this case the lifespan relations of Crow and Bate reduce to

$$\tau_b = \frac{0.35}{\eta_b} \qquad \text{(strong turbulence)}$$

and

$$\eta_b = 1.33\ \tau_b^{1/4} e^{-1.30\tau_b} \qquad \text{(weak turbulence)}$$

assuming that $k = 0$ for η_b in the linking relation. The composite function derived from these equations is also plotted on Figure 3-12.

The time-to-burst relation (Eq. 3) is almost identical to the strong turbulence time-to-link formula. It is important to note, however, that the mechanisms leading to vortex breakdown and to linking are quite different, and the relevant scaling parameters are not, in general, the same. Thus the agreement of the constants in the two relations is somewhat fortuitous, and would not occur, for example, if non-elliptic wing loading had been used for relating b and b_v.

In weak turbulence, the time-to-link and time-to-burst curves differ considerably, although the breakdown data tends to agree better with the linking curve for the specific selection of parameters used.

The significance of the core-bursting time analysis on the prediction of the decay of vortices is more complex than it was for the linking time analysis. With linking, it is reasonable to assume that a link rearranges the vortex structure sufficently to significantly reduce any hazard to a following aircraft. Such is not always the case with core-bursting, however, The experiments performed during this study showed conclusively that a visually apparent vortex core-burst did not necessarily indicate the demise of the vortex structure. Rather, observations of the buoyant balloons showed the continued presence of a vortex after bursting had occurred, and, in several instances, the laser velocimeter, acoustic sensors, and anemometer array also showed continuing vortex structure well after bursting. It is clear, however, that the velocities in the vortex and the overall circulation appear to reduce after core bursting; examples are given by Hallock (1976) and Hallock, et al (1977).

4. CONCLUDING OBSERVATIONS

To assess the utility and significance of the main conclusions of this rather complex, many-faceted research program, it seems useful to stand back from the details of this particular study alone and to look at how its results fit into the whole of knowledge about aircraft wake vortices.

To set the framework, it seems that the details of behavior of the vortex wake have tended to resist investigation to an amazing degree. Many years of intense effort have yielded some concrete results of utility for operational applications, but have also revealed the description of vortex behavior to be more complex than once assumed. This is at once both surprising and predictable – surprising, because one would have thought a few years ago that a well-defined formulation of vortex behavior would have been completed by now; predictable, because vortex phenomena are governed to a great degree by the vagaries of the atmosphere, which are of themselves unpredictable except, possibly, in a statistical sense. To compound the challenge, each experimental study seeking to quantify the physics of one phenomenon has also been succcessful in discovering one or more new phenomena which are also important and warrant another round of study.

Prior to the program described in this report, only one vortex wake behavioral characteristic had been successfully conquered to the point where, within reasonable statistical factors, it could indeed be predicted if the proper atmospheric variables and aircraft parameters were known. This characteristic is the sinuous instability, which was first recognized in the mid-1950's, was initially modeled by Crow in 1963, and became known as the "Crow" instability. The effect of turbulence on this instability was noted by Tombach in the early 1970's, and Crow and Bate subsequently included turbulent excitation into an extension of the Crow model. Finally, work by Tombach, Bate, and Crow tailored the model to conditions near the ground. Thus, now, a model exists which can define the time at which a vortex pair will annihilate itself in almost any given atmospheric condition, if it elects

to decay by this particular mode. The time estimates given by this model tend to be within better than a factor of two of those observed in in-flight experiments. This level of agreement is probably as good as one can expect for randomly excited phenomena.

If vortex linking through the Crow instability were always assured, then at least the upper limit to vortex wake lifetimes would be defined. This is not the case, unfortunately. Often the vortex pair seems to be immune to the sinuous instability – some cases in stable atmospheric conditions are noted in this report – and continues to exist until aging or internal vortex breakdowns terminate its organized motion. A particularly significant case occurs when, in some sort of asymmetrical flow field, one vortex decays and leaves its mate behind. Then, for reasons unknown, the remaining vortex seems to be blessed with much longer life than normal. On the other hand, at other times vortex breakdown acts swiftly in advance of the Crow instability, and destroys or at least alters, the flow field of an affected vortex.

This program set out to study the breakdown phenomenon, in the hope of emulating the success achieved in the prediction of the sinuous instability. It was obvious from the onset that the analysis would be more difficult – many had already attempted mathematical modeling, with mini mal success, and thus a semi-empirical approach would be necessary. The results, now that the program is over, are intriguing and a model of the breakdown exists. The success has been diluted, though, by definite confirmation that vortex breakdown, as it has been defined by everyone who has looked at smoke marked vortices, is not necessarily a mechanism which destroys a vortex, nor even weakens it significantly. Thus the ultimate destroyer of vortices which avoid linking with each other has still not been captured – it could be a cascade of breakdowns, a new form of mutual interaction, or possibly even decay by turbulent diffusion.

To provide a setting for those who need to use aircraft vortex research results for practical, operational purposes, it seems appropriate to provide a

capsule summary of what was found during this program, with some commentary on how it affects the state of useful, applicable knowledge about aircraft wakes.

First, it was shown analytically that instabilities of the form which contribute to vortex breakdown could exist without axial disturbances or axial flow, and are almost sure to exist if axial disturbances occur. At the scale of a water tank, with axial flow suppressed, larger scale unstable disturbances did not grow, although turbulence was generated from smaller scale disturbances.

A heuristic argument suggested that the scale parameters defining the rate of growth of major disturbances, and hence setting the time of vortex breakdown, are the initial vortex velocity field after the vortices have formed, and the turbulence field in which the vortices are immersed. Four parameters (two velocities and two lengths) define the former; atmospheric turbulence and residual aircraft turbulence in the wake define the latter. Using such an argument, a single curve was constructed from properly scaled data for time-to-breakdown for four highly dissimilar aircraft – a Cessna 170, an Aero Commander 560F, a Lockheed L-18 Lodestar, and a Boeing 747. The scatter in the data is considerable, but the curve fit is statistically significant and the breakdown time estimate thus provided is generally good within a factor of two of the measured values, which is accuracy comparable with that achieved by the more rigorous modeling of the Crow instability.

The flight tests proved conclusively what had been suspected for some time – that vortex breakdown is a change in state of the vortex and manifests itself by velocity and core size changes, but that this state change does not always mean the end of the organized vortical motion. Various measurements showed a significant vortex present long after a vortex breakdown had occurred; at other times, they indicated that breakdown had indeed effectively neutralized the vortex.

This discovery weakens the utility of flow visualization as an indicator of vortex presence. It has been known all along that improperly placed

smoke, or smoke in insufficient quantity, would diffuse before the vortex decayed, but it was hoped that the dramatic and relatively explosive diffusion of smoke from a vortex breakdown did indeed signal the end of the vortex. This is now known to be definitely untrue, although the occasional fine filament of smoke remaining after a visible breakdown has been pointing this out all along.

A few details of information about the breakdown were also obtained from the flight tests. As expected, turbulence in the wake due to engine thrust hastened the onset of breakdowns. Also, the effect of flaps is equivalent to increasing the ambient turbulence, and thus shortens vortex lifetimes in weak ambient turbulence.

It was also noted that vortex breakdowns are accompanied by high pressure in the cores, with local axial flow heading away from the burst point in both directions. The axial flow in the Boeing 747 vortices was in the opposite direction from the flow in the Lodestar vortices. No effects of this difference on vortex breakdowns or other behavior could be seen, however.

The transport of the vortices through the atmosphere is one of the easier aspects of vortex behavior to study, and thus received some attention in this study also. During the flight tests, dramatic differences in descending behavior were noted from hour to hour and day to day. Further analysis showed atmospheric stability to play a role in defining the nature of the descent, with stability suppressing irregular motion and inhibiting descent (and even stopping it). Quantitative modeling of vortex descent, with proper treatment of the effects of buoyancy and turbulent entrainment, has so far eluded investigators, although around a half-dozen models of some aspects of this behavior exist.

A mechanism for the slowing down of the lateral motion of a vortex in ground effect was identified in the water tank tests, and was correlated with prior aircraft tests. The cause is a rising of the vortex, which results from

rotation of the non-circular vortex core, rather than a dissipative mechanism, as previously believed. An analytical formulation for the trajectory awaits further work, however.

Some areas of wake behavior were not investigated during these experiments, and still lack adequate explanation and analytical formulations suitable for operational use. Prime among the items not studied is the whole area of asymmetrical wake behavior, as in wind shear, and the related area of the isolated, long-lived vortex.

The data collected during this program was considerable and not all of it was analyzed with full intensity for this report. Additional analysis, in conjunction with the simultaneous laser and acoustic sounder measurements of the Boeing 747 wake, will be reported upon shortly in a separate report. In addition, the vortex anemometer data, which has not been analyzed to its fullest, potentially offers considerable information on vortex structure near the ground and plans are being made for the use of suitable mathematical tools to extract this information.

5. BIBLIOGRAPHY

Barber, M.R., R.L. Kurkowski, L.J. Garodz, G.H. Robinson, H.J. Smith, R.A. Jacobsen, G.W. Stinnett, Jr., T.C. McMurtry, J.J. Tymczyszyn, R.L. Devereaux, and A.J. Bolster (1975): Flight test investigation of the vortex wake characteristics behind a Boeing 727 during two-segment and normal ILS approaches. NASA TM X-62,398, FAA-NA-75-151, January.

Batchelor, G.K. (1964): Axial flow in trailing line vortices. J. Fluid Mech. 20, 645-658.

Betz, A. (1933): Behavior of vortex systems. NACA TM 713.

Brown, Clinton E. (1973): Aerodynamics of wake vortices. AIAA J. 11, 531-536.

Chevalier, H. (1973): Flight test studies of the formation and dissipation of *trailing vortices.* J. Aircraft 10, 14-18.

Corsiglia, V.R., R.A. Schwind, and N.A. Chigier (1973): Rapid scanning, three dimensional hotwire anemometer surveys of wing tip vortices. J. Aircraft 10, 752-757.

Crow, S.C. (1970): Stability theory for a pair of trailing vortices. AIAA J. 8, 2172-2179.

Crow, S.C., and E.R. Bate, Jr. (1976): Lifespan of trailing vortices in a turbulent atmosphere. J. Aircraft 13, 476-482.

Donaldson, C. DuP., and A.J. Bilanin (1975): Vortex wakes of conventional aircraft. NATO AGARDograph No. 204.

Garodz, Leo J. (1970): Measurements of Boeing 747, Lockheed C5A and other aircraft vortex wake characteristics by tower fly-by technique. Aircraft Wake Turbulence and Its Detection, John H. Olsen and Milton Rogers (eds.), Plenum Press, New York, 265.

Hallock, James N. (1976): Monitoring wake vortex strength decay near the ground. J. Aircraft 13 (10), 830-832.

Hallock, J., D.C. Burnham, I.H. Tombach, M.R. Brashears, A.D. Zalay, and M.R. Barber (1977): Report on joint FAA-NASA Boeing 747 wake vortex experiment. To be published.

Kelvin, Lord (Sir W. Thomson) (1889): On the vibrations of a columnar vortex. Phil. Mag X, 155.

Lamb, Sir Horace (1932): Hydrodynamics. Dover Publications, N.Y.

Lissaman, P.B.S., S.C. Crow, P.B. MacCready, Jr., I.H. Tombach, and E.R. Bate, Jr. (1973): Aircraft vortex wake descent and decay under real atmospheric effects. Federal Aviation Admin. Rpt. No. FAA-RD-73-120, AeroVironment Inc., Pasadena, Ca.

MacCready, P.B., Jr. (1966): Operational application of a universal turbulence measuring system. American Institute of Aeronautics and Astronautics Paper 66-364.

McGraw-Hill Dictionary of Scientific and Technical Terms (1974). New York, N.Y. 687.

Mullen, J.B. and T. Maxworthy (1976): A laboratory model of dust devil vortices. Dynamics of Atmospheres and Oceans 1, 181-214.

Squire, H.B. (1933): On the stability of three-dimensional distribution of viscous fluid between parallel walls. Proc. Roy. Soc. A142. 621-628.

Squire, H.B. (1954): The growth of a vortex in turbulent flow. Aeronautical Research Council No. 16, 666.

Tombach, I.H. (1973): Observations of atmospheric effects on vortex wake behavior. J. Aircraft 10, 641-647.

Tombach, I.H., E.R. Bate, Jr., and P.B. MacCready, Jr. (1974): Investigation of the motion and decay of the vortex wake of a light twin-engine aircraft. Rpt. No. AV FR 439 for U.S. Department of Transportation, Transportation Systems Center, by AeroVironment Inc., Pasadena, Ca.

Tombach, I.H., S.C. Crow, and E.R. Bate, Jr. (1975): Investigation of vortex wake stability near the ground. Air Force Office of Scientific Research Rpt. No. AFOSR TR-75-1501, AeroVironment Inc., Pasadena, Ca.

Tombach, I., and S. Crow (1976): Some aspects of aircraft wake behavior near the ground. Preprint, AMS 7th Conference on Aerospace and Aeronautical Meteorology and Symposium on Remote Sensing from Satellites. Nov. 16-19, Melbourne, Fl.

Widnall, S.E. (1975): The structure and dynamics of vortex filaments. In: Annual Review of Fluid Mechanics, M. Van Dyke, et al (eds.), 7, 141-165.

APPENDIX A

STABILITY OF VORTEX CORES

This appendix is based on notes prepared by Steven C. Crow as part of the subcontract activities of Poseidon Research during the course of this study. It substantially follows the text of Poseidon Research Note No. 4, 25 August 1975, by S.C. Crow.

Summary

Apart from the familiar mutual induction instability, we have distinguished three mechanisms for vortex decay near the ground: core bursting, turbulent erosion or aging, and ground friction. Bursting and aging are manifestations of *vortex core instability*, modified perhaps by nonlinear effects. Bursting has been studied during the AeroVironment flight tests, while aging and ground friction were examined in the Poseidon Research vortex visualization facility.

According to the Rayleigh stability criterion, isolated vortices of aerodynamic interest are stable to small *axisymmetric* disturbances. These disturbances propagate as fast waves along the vortex cores. Core bursting probably results from nonlinear amplification and breaking of these axisymmetric waves, so bursting is outside the scope of linear stability theory.

Neither the Rayleigh criterion nor the other theorems of vortex stability forbid the growth of helical disturbances, and they are probably the origin of turbulent erosion and aging. Helical waves can extract energy from the mean flow in the transition zone between solid-body rotation and potential flow. The exceptional case is the Rankine vortex, which has no such transition zone and is therefore stable to all small disturbances. A core velocity distribution with an inflection point in the rotational region is certainly unstable to helical instabilities, though it satisfies the Rayleigh stability criterion for axisymmetric waves. A wrapped-up vortex sheet has one or more such inflection points and is therefore unstable. A cylindrical vortex sheet, in particular, is unstable to modes having azimuthal wavenumbers of three or greater. We expect to observe the growth of these helical modes and their conversion to turbulence in our flow-visualization experiments.

A. 1. Structure of an Isolated Columnar Vortex

A simple vortex is a flow with circular streamlines, having an azimuthal component of velocity $V(r)$ independent of angle θ or axial location z:

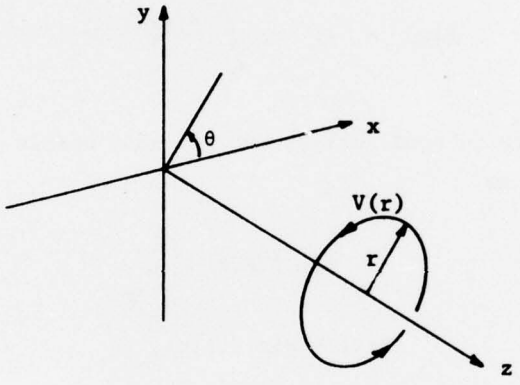

We shall assume the axial component of velocity is zero in the unperturbed state. Circulation is defined as

$$\Gamma(r) = 2 \pi r V(r),$$

angular velocity as

$$\Omega(r) = V(r)/r,$$

and vorticity as

$$\zeta(r) = \frac{1}{r} \frac{d}{dr}(rV).$$

In the absence of viscosity, the only nontrivial dynamics equation is the radial momentum balance

$$\frac{dP}{dr} = \frac{\rho V^2}{r} ,$$

with solution

$$P(r) = P_\infty - \rho \int_r^\infty \frac{V^2(r')}{r'} dr' .$$

All such flows are in equilibrium, but are they stable against perturbations of the form

$$u(r,\theta,z,t) \quad ,$$

$$V(r) + v(r,\theta,z,t), \quad$$

$$w(r,\theta,z,t) \quad ?$$

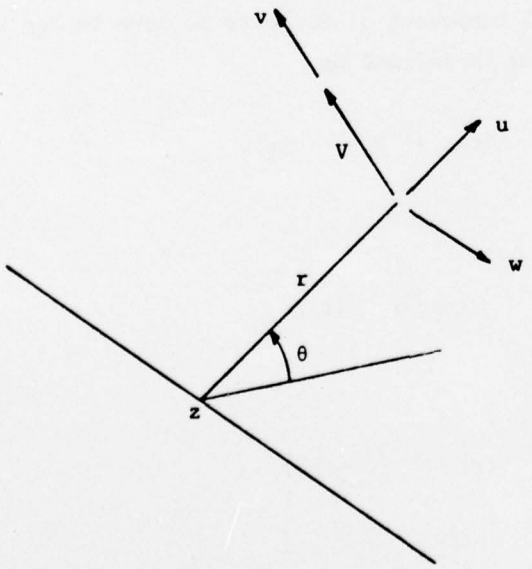

A.2. Rayleigh Stability Criterion

The most famous index of vortex stability was derived by Rayleigh (1916) for *axisymmetric* disturbances. Consider a fluid ring displaced from its original radius r_1:

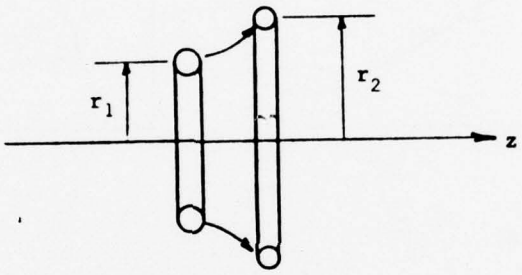

By the Kelvin circulation theorem, its circulation remains constant at $\Gamma(r_1)$. The centrifugal force on an element dV is

$$\rho \frac{[\Gamma(r_1)/2\pi r_2]^2}{r_2} \, dV,$$

whereas the restoring force exerted by the ambient pressure gradient is

$$\rho \frac{[\Gamma(r_2)/2\pi r_2]^2}{r_2} \, dV.$$

The element returns toward its original location if

$$\Gamma^2(r_2) > \Gamma^2(r_1),$$

that is

$$\frac{d\Gamma^2}{dr} > 0.$$

According to the Rayleigh criterion, all the following are stable to axisymmetric disturbances:

Gaussian Vortex:

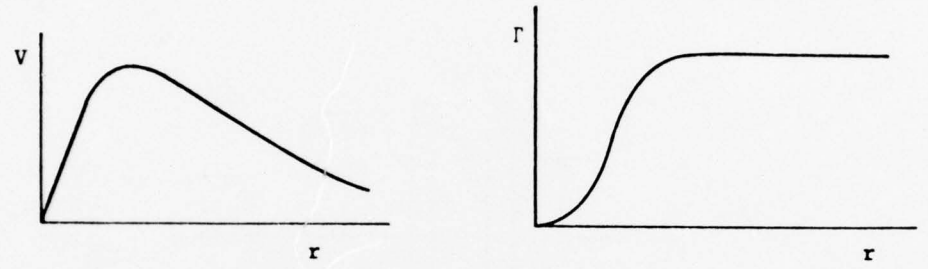

Rankine Vortex:

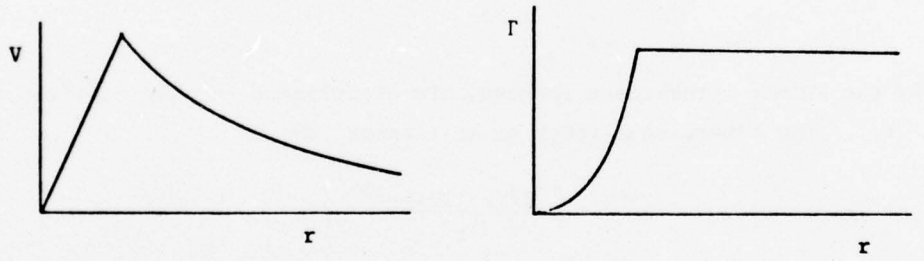

Cylindrical Vortex Sheet:

A.3. Stability of the Rankine Vortex

The Rankine vortex has the velocity distribution

$$V = \frac{\Gamma r}{2 \pi R^2} \qquad r < R,$$

$$V = \frac{\Gamma}{2 \pi r} \qquad r > R,$$

where R is the radius of the vortex core and Γ here is a constant. Kelvin (1889) showed that the Rankine vortex is stable to *all* small perturbations of the form

$$u = f(r)\, e^{i(kz + m\theta - \omega t)}.$$

Thus

$$\omega = \omega_r + i\, \omega_i,$$

with

$$\omega_i = 0.$$

Axisymmetric waves $(m = 0)$ have the form

$$u = f(r)\, e^{ik(z - ct)},$$

with phase velocity

$$c = \frac{\omega}{k} \rightarrow \frac{\Gamma}{2^{3/2} \pi R}$$

as $kR \rightarrow 0$,

that is, for long waves. It is interesting to compare the phase velocity c with the airplane speed U:

$$\frac{c}{U} = \frac{\rho \Gamma U}{2^{3/2} \pi R \rho U^2} = \frac{\rho \Gamma U b}{2^{5/2} \pi \frac{R b}{S} \frac{1}{2} \rho U^2 S}$$

$$= \frac{C_L S}{2^{5/2} \pi R b},$$

where S is the wing area and b is the vortex separation. For an elliptically loaded wing,

$$R = 0.1\, b \quad \text{(Spreiter \& Sacks)},$$

$$b = \frac{\pi}{4} \times \text{span},$$

$$S = (4/\pi)^2 b^2 A_R^{-1}.$$

Then

$$\frac{c}{U} = 0.91\, C_L A_R^{-1},$$

so c ranges from perhaps 0.1 to 0.5 U, depending on the lift coefficient C_L and aspect ratio A_R. These high-speed waves are often visible and seem to have something to do with core bursting.

A.4. Global Energy Equation

An easy way to show that the Rankine vortex is stable is to use the global energy equation for inviscid rotating flow:

$$\frac{d}{dt} \iint \frac{1}{2} \rho \, (\overline{u}^2 + \overline{v}^2 + \overline{w}^2) \, dA = \iint (-\rho \, \overline{uv}) \left(\frac{dV}{dr} - \frac{V}{r} \right) dA,$$

where the integrals extend over the vortex cross-section, and the bars denote angular averages. In the *solid-body core* $r < R$,

$$V = \alpha r,$$

$$\frac{dV}{dr} - \frac{V}{r} = 0.$$

In the *potential-flow region* $r > R$, it can be shown that

$$\text{Reynolds stress} = -\rho \, \overline{uv} = 0.$$

Thus

$$\text{Perturbation energy growth rate} = \frac{d}{dt} \iint \frac{1}{2} \rho \, (\overline{u}^2 + \overline{v}^2 + \overline{w}^2) \, dA = 0$$

for a Rankine vortex.

Notice that the energy equation admits the possibility of turbulence production in an annular transition region between solid-body rotation and potential flow:

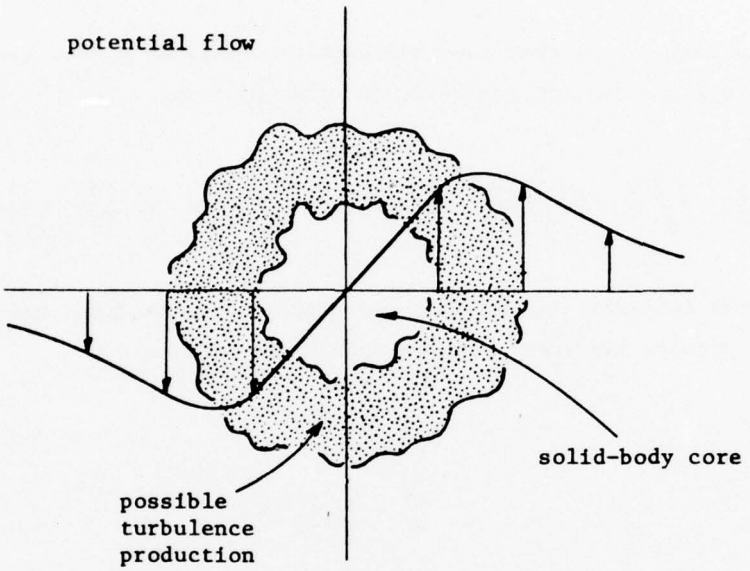

Neither the Rayleigh criterion nor the energy equation precludes instability of *helical* (non-axisymmetric) modes even in a Gaussian vortex, and nobody has shown such modes do not exist.

A.5. The Critical Layer

By assuming velocity disturbances of the form

$$u = f(r)\, e^{\omega_i t}\, e^{i(kz + m\theta - \omega_r t)} + \text{Complex Conjugate},$$

$$v = g(r)\, e^{\omega_i t}\, e^{i(kz + m\theta - \omega_r t)} + \text{Complex Conjugate},$$

we can make more explicit use of the energy equation. Suppose there exists a *critical layer* of radius r_c, where the angular rotation rate ω_r/m of the wave pattern equals the angular rotation rate of the fluid:

$$\frac{\omega_r}{m} = \Omega(r_c).$$

For a *neutrally stable* mode, that is for

$$\omega_i = 0,$$

the Reynolds stress can be shown to have the form of a delta-function:

$$-\rho\, \overline{uv} = \frac{\rho\, \overline{u}_c^2}{2}\, \frac{2\,\pi\, k^2\, r_c^3\, \zeta_c}{(k^2 r_c^2 + m^2)\, \omega_r}\, \delta(r - r_c).$$

The rate of energy production is

$$\rho\, \overline{u}_c^2\, \frac{2\,\pi^2\, k^2\, r_c^3\, \zeta_c}{(k^2 r_c^2 + m^2)\, \omega_r}\, \left(\frac{dV}{dr} - \frac{V}{r}\right)_c,$$

which must be zero for neutral stability. The requirement

$$\frac{dV}{dr} = \frac{V}{r} \qquad r = r_c$$

means that the azimuthal velocity profile must have an *inflection point* at some $r < r_c$:

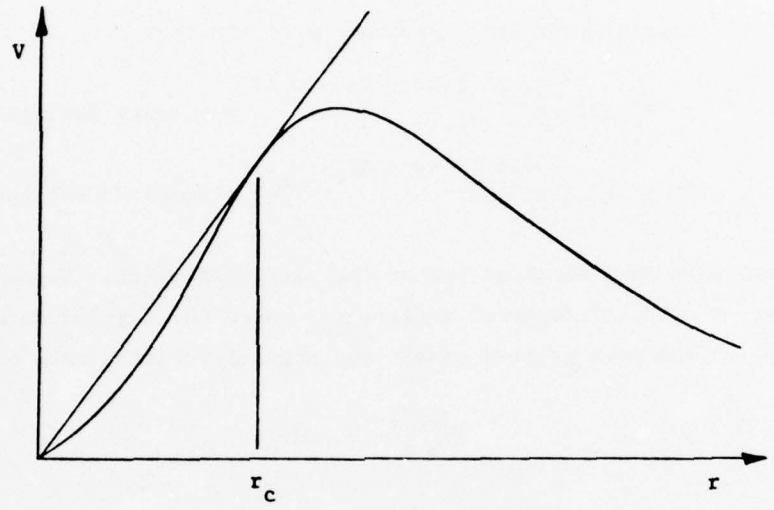

Such profiles are likely to be unstable to helical modes even though they satisfy the Rayleigh criterion for axisymmetric modes.

A.6. Generalized Rayleigh Criterion

We have attempted to generalize the Rayleigh stability criterion to account for helical disturbances. After considerable manipulation of the Euler equations, we find that

$$\omega_i \int_0^\infty \frac{r^2\,\overline{u^2}}{r^2k^2 + m^2} \left\{ \frac{2\,k^2\,m\,r\,\zeta}{r^2k^2 + m^2} - m\,\zeta' \over (m\Omega - \omega_r)^2 + \omega_i^2 + \frac{4\,k^2\,(V\zeta)\,(m\Omega - \omega_r)}{[(m\Omega - \omega_r)^2 + \omega_i^2]^2} \right\} dr = 0.$$

The integral must be zero for unstable modes $\omega_i > 0$. For $m = 0$ (axisymmetric modes), we recover the familiar Rayleigh stability criterion in the form

$$\omega_r\,\omega_i \int_0^\infty \frac{\overline{u^2}\,(V\zeta)}{(\omega_r^2 + \omega_i^2)^2}\, dr = 0,$$

which shows that axisymmetric modes can grow only when $V\zeta$ takes on both signs. But

$$\frac{d\Gamma^2}{dr} = 8\,\pi^2\,r^2\,V\zeta \lesseqgtr 0,$$

so the Rayleigh criterion is confirmed. Unfortunately the general case $m \neq 0$ does *not* yield a similar mode-independent criterion. In the case of a Gaussian vortex, for example, ζ and $-\zeta'$ are positive, and so is $V\zeta$. All we can say is that ω_r/m must exceed $\Omega(r)$ in regions of non-zero $\zeta(r)$ for instability to occur.

A.7. Cylindrical Vortex Sheet

The cylindrical vortex sheet is easy to analyze and illustrates many of the foregoing general points. It also should be a good rough model of the wrapped-up vortex sheet behind an airplane.

The cylindrical vortex sheet consists of a dead-air core surrounded by a potential vortex. A vortex sheet separates the two flow regimes:

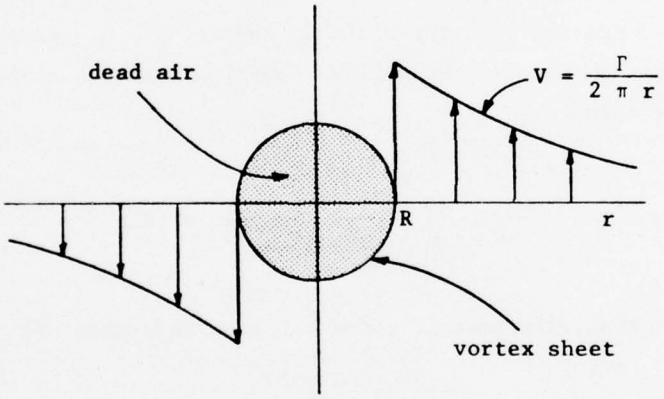

The flow satisfies the Rayleigh criterion for $m = 0$ but has a (singular) inflection point at $r = R$, so it should be unstable to helical modes.

Consider radial sheet displacements of the form

$$\eta = \eta_o e^{i(kz + m\theta - \omega t)};$$

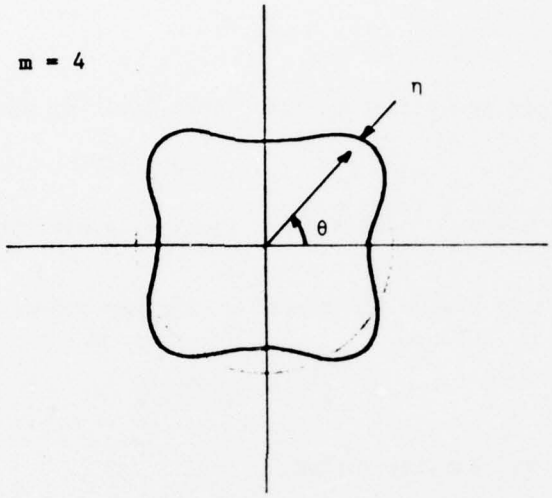

Define

$$\Omega = \frac{\Gamma}{2 \pi R^2} ,$$

$$F = \frac{I_m(kR)\, K'_m(kR)}{K_m(kR)\, I'_m(kR)} ,$$

$$G = kR\, K'_m(kR) \,/\, K_m(kR),$$

in terms of modified Bessel functions. The eigenvalue equation proves to be

$$\omega = \frac{m\,\Omega \pm \Omega\,[m^2 - (1-F)\,(m^2 + G)]^{1/2}}{1 - F} ,$$

so we have unstable waves for combinations of m and kR such that

$$m^2 - (1-F)\,(m^2 + G) < 0.$$

It transpires that

$$m \geq 3$$

for instability to occur for any kR. Some limiting cases are of interest:

(a) $m = 0, \quad kR \to 0$ (long axisymmetric waves).

These are neutrally stable and travel at a phase velocity

$$c = \frac{\omega_r}{k} = \frac{\Gamma}{2^{3/2} \pi R} ,$$

the same as for the Rankine vortex.

(b) $m = 0, \quad kR \to \infty$ (short axisymmetric waves).

These are stable but dispersive, with a wavenumber-dependent phase velocity

$$c = \left(\frac{R}{2k}\right)^{1/2} \frac{\Gamma}{2 \pi R^2}$$

$$= \frac{\Gamma}{2^{3/2} \pi R (kR)^{1/2}} .$$

Short waves travel more slowly than long waves.

(c) $m \neq 0, \quad kR \to 0$ (purely azimuthal waves).

In this case the eigenvalue equation is simple:

$$\omega = \frac{m \Omega}{2} \pm \frac{\Omega}{2} (2m - m^2)^{1/2} .$$

Waves with $m \geq 3$ are unstable.

(d) $m \neq 0$, $kR \to \infty$ (short helical waves).

Again the eigenvalue equation is simple,

$$\omega = \frac{m\,\Omega}{2} \pm \frac{\Omega}{2}\,(2kR - m^2)^{1/2},$$

and instability occurs when

$$m > (2kR)^{1/2}.$$

The cylindrical vortex sheet exhibits both the long axisymmetric waves that seem to be associated with bursting and the short azimuthal waves characteristic of turbulence formation and aging.

A.8. Conclusions

a) According to the Rayleigh stability criterion, a vortex is stable to axisymmetric disturbances if the square of its circulation increases radially outwards. Aircraft vortices are likely to satisfy that criterion.

b) Such axisymmetric disturbances travel at high speeds along the vortex core. Waves of length much longer than the core diameter have a phase velocity

$$c \simeq 0.9\, C_L\, A_R^{-1}\, U,$$

usually a significant fraction of the aircraft speed U.

c) In the context of trailing vortices, core bursting probably arises from nonlinear amplification and breaking of these fast axisymmetric waves.

d) Even in its generalized form, the Rayleigh criterion does not exclude the possibility of unstable helical waves.

e) The energy equation shows that disturbances can extract energy from the mean flow in the transition region between solid-body rotation and potential flow. The Rankine vortex has no such transition region and so is stable to all disturbances, but that case is exceptional.

f) Near-neutral disturbances extract energy from a critical layer, where the angular velocity of the wave equals the angular velocity of the fluid.

g) Helical or azimuthal instability is assured when the core velocity profile contains an inflection point in the rotational region.

h) A wrapped-up vortex sheet contains one or more such inflection points and is therefore subject to azimuthal instabilities.

i) A cylindrical vortex sheet, in particular, is unstable to helical modes with $m \geq 3$. It also exhibits the fast axisymmetric waves that seem to eventuate in core bursting.

j) Helical modes cause core turbulence and aging.

APPENDIX B

WATER TANK STUDY OF THE MOTION OF TWO-DIMENSIONAL VORTEX PAIRS IN GROUND EFFECT

This appendix is a report on the laboratory experiments with a water tank analog of the vortex pair which were performed by Poseidon Research under subcontract to AeroVironment during the course of this study. The material presented is based substantially on Poseidon Research Report No. 4, May 1976, by S.J. Barker and S.C. Crow.

Abstract

A new technique for generating a pair of line vortices in the laboratory has been developed. The mean flow of these vortices is highly two-dimensional, although most of the flow field is turbulent. This two-dimensionality permits the study of vortex motions in the absence of the Crow mutual induction instability and other three-dimensional effects. The vortices are generated in a water tank of dimensions 15 x 122 x 244 cm. They propagate vertically and their axes span the 15 cm. width of the tank. One wall of the tank is transparent, and the flow is visualized using fluorescein dye. High speed photography is used to study both the transition to turbulence during the vortex formation process and the interaction of the turbulent vortices with a simulated ground plane.

Transition occurs first in an annular region surrounding the core of each vortex, starting with a shear layer instability on the rolled up vortex sheet. The turbulent region then grows both inward and outward radially until the entire recirculation cell is turbulent. A "relaminarization" of the vortex core appears to take place somewhat later.

The interaction of the vortex pair with the ground plane does not follow the predictions of potential flow theory for line vortices. Although total circulation is apparently conserved, the vortices remain at a larger distance from the ground than expected and they eventually "rebound" or move away from the ground. Differences between a free surface boundary condition and a smooth or rough ground plane are discussed. The ground plane interaction is qualitatively very similar to that of aircraft trailing vortices observed in recent flight tests.

B.1. Introduction

The problems of aircraft wake turbulence have stimulated a number of recent measurements of vortex wake flows. Some of these measurements were made using full scale aircraft to generate the vortices (Caiger and Gould, 1971; Bate, 1974; Tombach, et al, 1974). Other wake velocity measurements were made in wind tunnels (Mason and Marchman, 1972) or in towing basin facilities (Miller and Brown, 1971; Lezius, 1973). These measurements are subject to effects of probe interference, whereby the presence of a physcial velocity probe in the vortex wake causes the vortex to move away from the probe. There have been some recent measurements of wake vortex velocity profiles using laser anemometry, where the results are not subject to probe interference (Baker, et al, 1974; Orloff and Grant, 1975). These measurements compare reasonably well with the theoretical predictions of Saffman (1973).

All of these measurements of vortex wake velocities have been made in three dimensional flow fields. Far downstream of the lifting surface, there are two significant three dimensional effects that make such measurements difficult to interpret. Free stream turbulence in the flow facility (or in the atmosphere) causes the vortices to be displaced randomly about their mean location in space. This "vortex wandering" has the effect of making the vortices appear larger than normal in time-averaged velocity measurements. The effects of vortex wandering are discussed in detail in Baker, et al. (1974). The second three dimensional effect is the mutual induction instability, first described by Crow (1970). This instability causes the vortices to form "kinks" along their length, which eventually result in a linking of the vortex pair into a series of vortex rings. It is nearly impossible to measure accurately in the laboratory the trajectories followed by vortex wakes in the presence of these two effects.

The goal of the present study was to determine the trajectories and

decay rates of vortex pairs in ground effect at moderately high Reynolds numbers. In view of the three-dimensional effects mentioned above, the best way to accomplish this was to create a two-dimensional vortex pair and study the flow field as a function of time. This simulated the flow in a plane transverse to a trailing vortex wake, at a distance behind the aircraft of $x = Ut$. To obtain the highest possible Reynolds number at laboratory scale, the experiment was done in water. Water is also more suitable for making photographic measurements using flow visualization techniques.

B.2. Experimental Apparatus

Several laboratory studies have been made of both laminar and turbulent vortex rings, such as that of Maxworthy (1974). A vortex ring can easily be generated in a water tank by ejecting a small amount of fluid through a sharp-edged circular orifice. The resulting rings are repeatable, and will propagate many times their original diameter before dissipating. However, it is not as simple to generate a two dimensional vortex pair which propagates large distances from the generating mechanism. Some previous attempts at this have failed, and their failure was at first attributed to three dimensional "end wall" effects.

A fundamental difference between a vortex ring and a vortex pair is in the size and shape of the recirculation cell. The recirculation cell for a vortex ring is a small toroid surrounding the axis of the vortex. For a 2-D vortex pair, the recirculation cell is an oval enclosing both vortices, whose shape is given by Lamb (1932):

$$0 = \frac{\Gamma}{2\pi}\left(\frac{x}{2s} + \log\frac{r_1}{r_2}\right). \qquad \text{(B-1)}$$

This equation relates to two vortices of circulation $\pm\Gamma$ located at coordinates $(s,0)$ and $(-s,0)$. The radii r_1 and r_2 are the distances from each vortex to the point (x,y) on the cell boundary. The semi-axes of the recirculation cell are 2.09s and 1.73s, so that the cell carries a much larger volume of fluid than that of a vortex ring of similar dimensions. Such a vortex pair will propagate vertically at a speed

$$\frac{dh}{dt} = \frac{\Gamma}{4\pi s} \; . \qquad \text{(B-2)}$$

A device which generates a 2-D vortex pair must supply not only the necessary vorticity, but also the fluid to fill the recirculation

cell. The "puffing" technique used to form vortex rings does not satisfy the latter requirement. Therefore, attempts to create vortex pairs in this manner result in two vortices that are unable to propagate away from the generator. After the "puff" has stopped, the vortices quickly draw together and dissipate.

Preliminary experiments in the present study pointed out this difficulty, and led to the following technique for generating vortex pairs. To completely suppress the mutual induction instability time and avoid end wall effects, it was decided to make the vortices 15 cm. in length and approximately 15 cm. initial spacing. The experimental tank was thus chosen to be 15 cm. across, 122 cm. deep, and 244 cm. long (Figure 1). These dimensions permit the vortex trajectories to be measured in ground effect until they have reached a separation of eight times their original spacing. The vortex generating mechanism is located 24 cm. from the bottom of the tank and is shown in Figure 2. There are two thin vertical plates spanning the 15 cm. width of the tank, forming a channel 12 cm. wide and open at both top and bottom. When the experiment is ready to begin, a horizontal plate blocks this channel near its bottom (Figure 2). This plate rapidly accelerates to a constant vertical velocity, pushing the fluid in the channel ahead of it. Fluid leaving the top end of the channel forms two vortex sheets beginning at the two sharpened ends of the channel walls. These vortex sheets immediately begin to roll up into a vortex pair.

After the horizontal plate has moved upward a distance of 4 cm., it is abruptly retracted into the back wall of the tank. During this retraction motion the plate maintains its constant upward velocity. This "disappearance" of the plate allows the vortex pair to leave the generator and propagate through the tank. If the plate does not retract, the vortices immediately draw together and dissipate. The retraction allows the upwash in the vertical channel to decay slowly rather than abruptly, thus providing the necessary fluid for the vortex recircula-

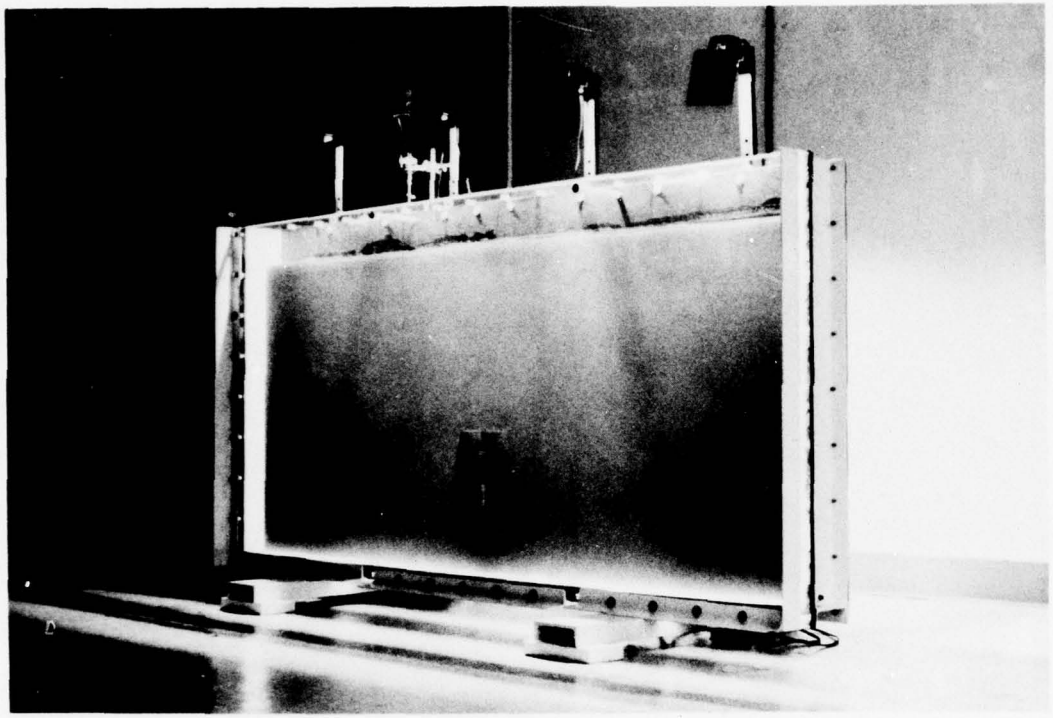

Figure B-1. Experimental flow tank.

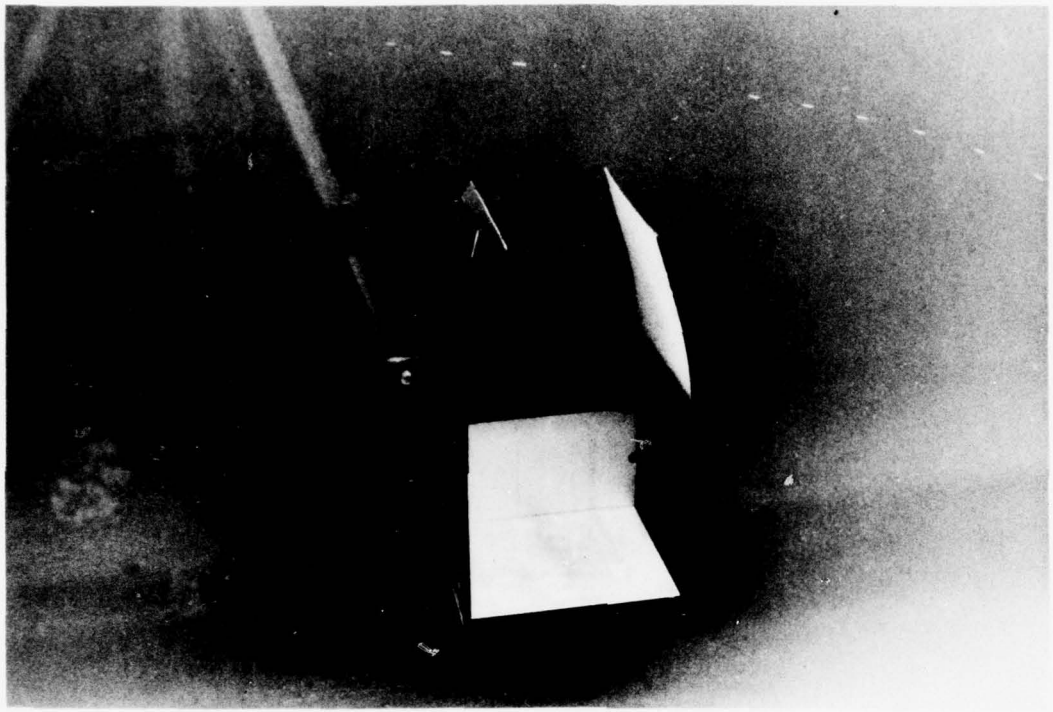

Figure B-2. Vortex generator mechanism.

tion cell.

The mechanical apparatus for executing the somewhat complex motion of the horizontal plate is located in a flooded box on the outside of the back wall of the tank. The vertical motion is driven by a constant speed AC motor which pulls a connecting rod through a seal in the flooded box. After the horizontal plate has moved upward 4 cm., a trip lever in the flooded box actuates a spring-loaded retraction mechanism. The plate retraction takes place in about 0.1 second.

The front wall of the tank is made of 5 cm. thick plexiglass to permit flow visualization. For high speed motion pictures, best results are obtained using fluorescein dye against a flat black background. The dye is illuminated from above by four 600 watt quartz lamps. (Heating of the water by these lamps was carefully avoided.) Before the experiment begins, the vortex generator is partially filled with the dye, which then provides excellent contrast during the vortex motion. Motion pictures are taken at speeds of 64 and 200 frames per second, and then projected on sheets of paper at speeds between 1 and 24 frames per second. The trajectories of the two vortex cores are traced on the paper, and time marks are added.

The vortices propagate upward rather than downward in this experiment to facilitate the study of the ground plane interaction. With this geometry we can observe three different boundary conditions on the ground plane. We have the free surface boundary condition (zero stress), the rigid smooth wall ground plane, and the rough wall ground plane. Furthermore, it is more practical to vary the distance between the vortex generator and the ground plane by changing the water depth than by moving the generator itself.

B.3. Results

The discussion of results will be divided into two parts: vortex instability and transition, and vortex trajectory measurements.

3.1 Instability and Transition

There has been much speculation about whether the flow in the cores of a vortex wake far downstream of the lifting body is largely laminar or turbulent. According to the Rayleigh stability criterion, any vortex will be stable as long as the absolute value of the circulation increases monotonically with radius. Most vortex velocity distributions of aerodynamic interest (Figure 3) are stable by this criterion. However, the Rayleigh criterion applies only to axisymmetric disturbances of the form

$$u' = f(r)\, e^{i(kz - \omega_r t)}\, e^{\omega_i t}, \qquad \text{(B-3)}$$

where z and r are coordinates parallel to and perpendicular to the vortex axis. This criterion says nothing about the more general "helical waves", of the form

$$u' = f(r)\, e^{i(kz + m\theta - \omega_r t)}\, e^{\omega_i t}. \qquad \text{(B-4)}$$

Kelvin analyzed the special case of the Rankine vortex (Figure 3) and found it to be stable to all disturbances, including helical waves. However, the Rankine vortex is a special case involving an abrupt change from solid body rotation in the core to a potential vortex outer region. Crow (1975) has shown by means of a global energy equation that helical disturbances can extract energy from the mean flow in the transition region between the core and potential vortex. In particular, the cylindrical vortex sheet (Figure B3) was analyzed and shown to be unstable to helical disturbances of wavenumber m greater than or equal to 3. From these considerations we might expect two dimensional vortices to

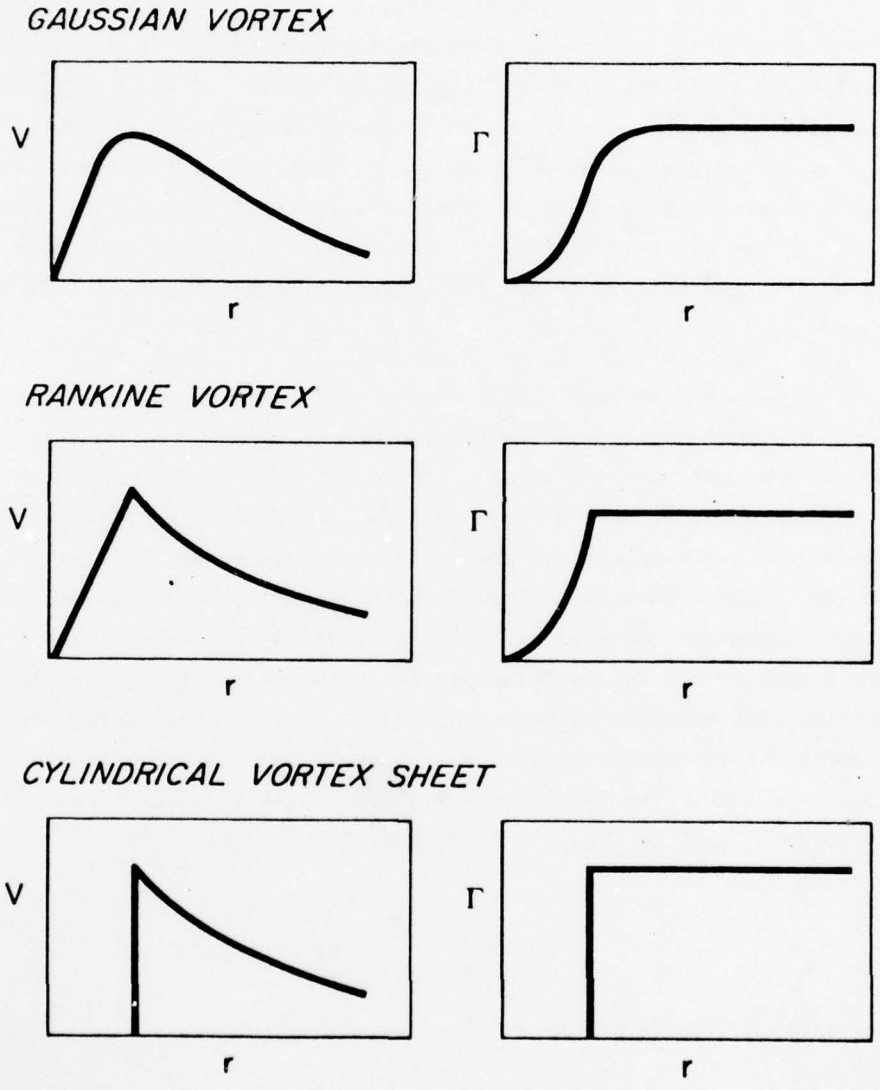

Figure B-3. Model vortex velocity distributions.

be unstable in an annular region surrounding the core.

The initial velocity profile created in this experiment does not correspond to any of the axisymmetric profiles of Figure 3. As the horizontal plate moves upward, two vortex sheets are generated and immediately begin to roll up. The velocity profile of the early vortex thus has a number of steps in it, with circulation increasing discontinuously at each step. Similar steps will occur in the near field of the aircraft trailing vortex wake, but in this case they arise from the roll up at the two ends of a single horizontal vortex sheet.

Figures B4 and B5 are flow visualization photographs of a vortex pair during the roll up process. The vortex circulation, as determined by the propagation velocity of the pair (eq. B2), is 240 cm^2/sec. The vortex Reynolds number, defined as Γ/ν, is 25,000. Relatively low speed vortices were used in the studies of roll up and initial instability. We see that an amplified disturbance occurs on the vortex sheet throughout the roll up. This instability is similar in appearance to the Kelvin-Helmholtz instability of a free shear layer, such as that observed by Brown and Roshko (1974). The eddies seen by Brown and Roshko occur even at very high Reynolds numbers in a fully turbulent flow. The wavelength of these eddies is proportional to the "vorticity thickness" of the free shear layer, defined by

$$\delta_\omega = \frac{1}{|\omega|_m} \int_{-\infty}^{\infty} |\omega| \, dy \, . \qquad \text{(B-5)}$$

Brown and Roshko found the measured wavelength of the eddies to equal $2.9\ \delta_\omega$.

The flow in the present experiment is time dependent and the length used to normalize the eddy wavelength must be a function of time. Since

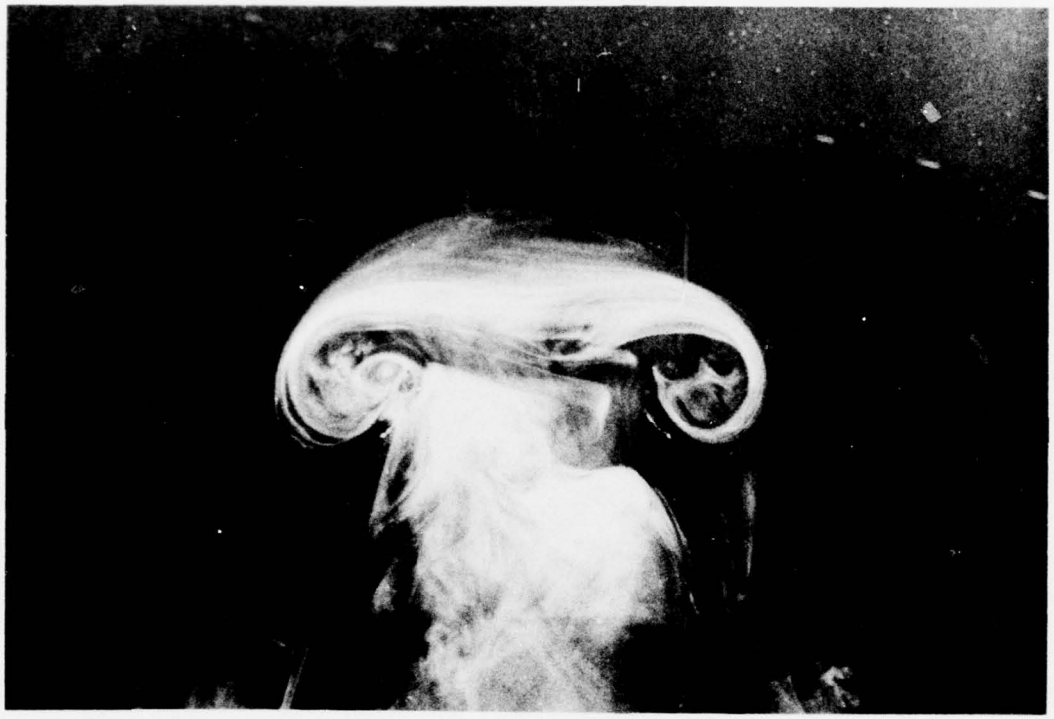

Figure B-4. Vortex formation -- early stage of roll-up.

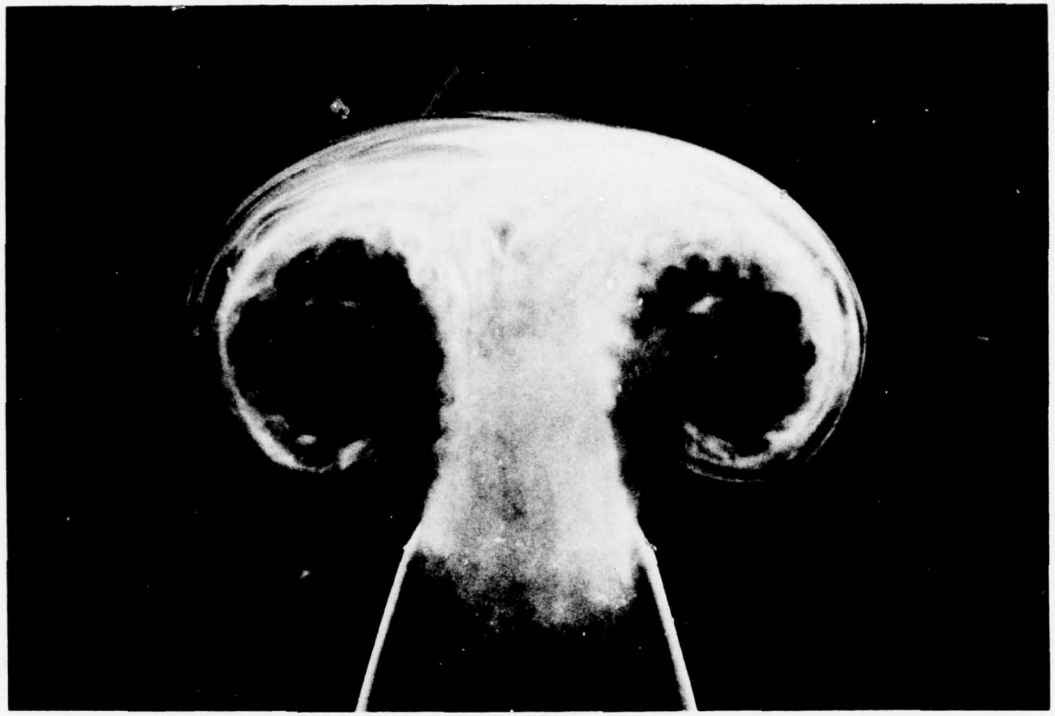

Figure B-5. Vortex formation -- later stage of roll-up.

the wave-like instability was observed only for times less than about 2 seconds, the boundary layer thickness on the inside walls of the channel plates can be crudely approximated by $\delta = 4\sqrt{\nu t}$. Movies of the initial roll up process were taken at 200 frames per second and analyzed one frame at a time to determine the eddy wavelength λ as a function of time. When λ is plotted versus $4\sqrt{\nu t}$, the slope of the best fit straight line is 2.6. This is in rather good agreement with the Brown and Roshko value of 2.9 considering the gross differences between the two experiments.

The boundary layer at the ends of the two channel plates is thin and laminar. To thicken this boundary layer and observe the effect upon the initial instability, sawtooth vorticity generators were installed on the ends of the plates. The teeth were spaced 0.6 cm. apart and protruded 0.3 cm. perpendicular to the channel walls. Two significant differences were observed in the movies with the sawteeth installed. The instability waves were not seen at all until more than one second after the motion had begun. Without the teeth, these waves can be seen as early as 0.2 seconds. In addition, the wavelength of the instability was almost twice as large with the sawteeth as without. When λ is plotted versus $4\sqrt{\nu t}$ as before, the slope of the straight line becomes 4.7. These two changes are qualitatively what we would expect for the shear layer instability.

As the roll up proceeds further, the initial instability wave grows to an amplitude of approximately one-tenth the spacing between the vortices (Figure 5). At this point a rather sudden transition to turbulence occurs, and within another 0.2 seconds the vortices appear as in Figure 6. The motion pictures show that transition begins in the annular region of the instability waves and progresses both inward and outward radially. The flow in the vortex recirculation cell remains fully turbulent until the vortices have dissipated, except for a small region near the center of each vortex. This inner region appears to

Figure B-6. Vortex pair after transition to turbulence.

remain laminar and grow slowly in radius during the evolution of the vortex. Although it can be seen in Figure 6, a still photograph cannot distinguish the laminar region as well as the movies do.

The fact that transition begins in an annular region is in agreement with the prediction of the stability calculation discussed above. The laminar appearance of the core region of the vortex can be correlated with observations of aircraft trailing vortices. Aircraft vortices are often visualized by vapor condensation in the low pressure vortex cores, as in contrails. In such cases the flow visualization is only in the inner core region where the flow may indeed be laminar. The turbulent region surrounding the core is not visualized, hence observers may be tempted to conclude that the vortices are predominately laminar. In other recent studies of aircraft vortices near the ground, (including the study described in this report), smoke was sometimes injected both into the core and the outer region. In this case, the rapid diffusion of smoke outside the core showed the outer region to be clearly turbulent, as in the present experiment.

At this point, it is appropriate to discuss the two dimensional nature of the mean flow in the experiment. Since the vortex axes are bounded by walls at both ends, the end wall boundary layers are possible sources of three dimensional effects. The pressure distribution of the mean flow has falling pressure towards the center of each vortex, which tends to produce a secondary flow in the end wall boundary layers. This secondary flow would be radially inward, and could thus cause fluid from the boundary layer to be "pumped" into the core of each vortex. This pumping into the cores would reduce the total circulation of the vortex, increase the thickness of the core, and also produce an axial mean flow along the vortex lines inward from the walls towards the center.

Three independent observations show that this boundary layer effect is insignificant. (1) Dyed fluid that is initially on or near the end walls is not sucked into the core of the vortex as it passes by. (2) Small air bubbles can be injected into the vortex cores and will remain

there due to the pressure minimum. They distribute themselves uniformly along the vortex axes and show no mean axial motion towards the center of length. They do move randomly back and forth along the axes in a manner very similar to the motions of small balloons trapped in the cores of aircraft vortices (as described in the main portion of this report). (3) The total circulation does not change while the vortices are out of ground effect – their separation and propagation velocity remain constant.

Simple dimensional analysis also suggests that boundary layer effects should not be important. The vortices are not stationary with respect to the end walls in the experiment, so that the wall boundary layers will not grow to a steady state thickness as an Ekman layer would. The boundary layer thickness is thus proportional to $\sqrt{\nu t}$, where t is the time for the recirculation cell to pass over a point fixed on the wall. This time is approximately 0.5 seconds, so that the boundary layer thickness is on the order of 0.07 cm.

3.2 Vortex Trajectories in Ground Effect.

The behavior of aircraft wake vortices in ground effect is extremely important in determining the possible dangers of vortices left near the runway by arriving and departing aircraft. If the wake vortices behaved as potential line vortices, their trajectories could be predicted quite readily. Lamb (1932) gives the solution of the problem of a pair of line vortices interacting with an image pair of opposite sign. The x-axis becomes the "ground plane" and the vortices propagate at velocities

$$\dot{s} = \frac{\Gamma}{2\pi} \frac{s^2}{hr^2} \quad ; \quad \dot{h} = \frac{\Gamma}{2\pi} \frac{h^2}{sr^2} \quad . \tag{B-6}$$

Here s and h are the x and y coordinates of the vortex in the upper right quadrant, and $r^2 = s^2 + h^2$. The trajectories can be written in the form

$$s_o^2(s^2 + h^2) = s^2h^2 \ , \qquad \text{(B-7)}$$

where s_o is the half-spacing of the vortices when they are far above the ground. After the vortices have spread apart some distance in the ground effect, they should approach a distance above the ground of s_o.

In the present trajectory measurements, two different water depths were used in the tank. Since the core radius will grow with the time from generation, the different depths will demonstrate the effects of core radius upon ground effect trajectory. Two values of the vortex circulation were also used to check for dependence upon Reynolds number. The circulations, as determined by the propagation velocity $\dot{h}$ far from the ground plane, were 250 and 750 cm^2/sec. The corresponding vortex Reynolds numbers (Γ/ν) were 25,000 and 75,000.

Since it was also desired to determine the effect of the ground plane boundary condition upon the trajectory, three different simulated ground planes were used. One of these was a free surface, with the boundary conditions $\frac{\partial u}{\partial y} = 0$ and $v = 0$ at the surface. The second ground plane was a horizontal sheet of smooth plexiglas immersed in the water. The third was the "rough ground plane", a sheet of plexiglas with grooves cut across the 15 cm. width. It was expected that the boundary layers on the two rigid planes would gradually reduce the circulation of the vortices in ground effect.

Figure B7 shows an experimental vortex trajectory compared with the line vortex trajectory of eq. B7. The experimental trajectory is the average of the trajectories of the two vortices of the pair. The initial circulation of the vortex is 750 $cm.^2/sec$. The ground plane in this case is the free surface. The vortices follow the line vortex trajectory closely for the first 30 cm. of vertical motion, or until they are 25 cm. below the surface. At this point they begin to spread apart sooner than the line vortex prediction and they remain farther

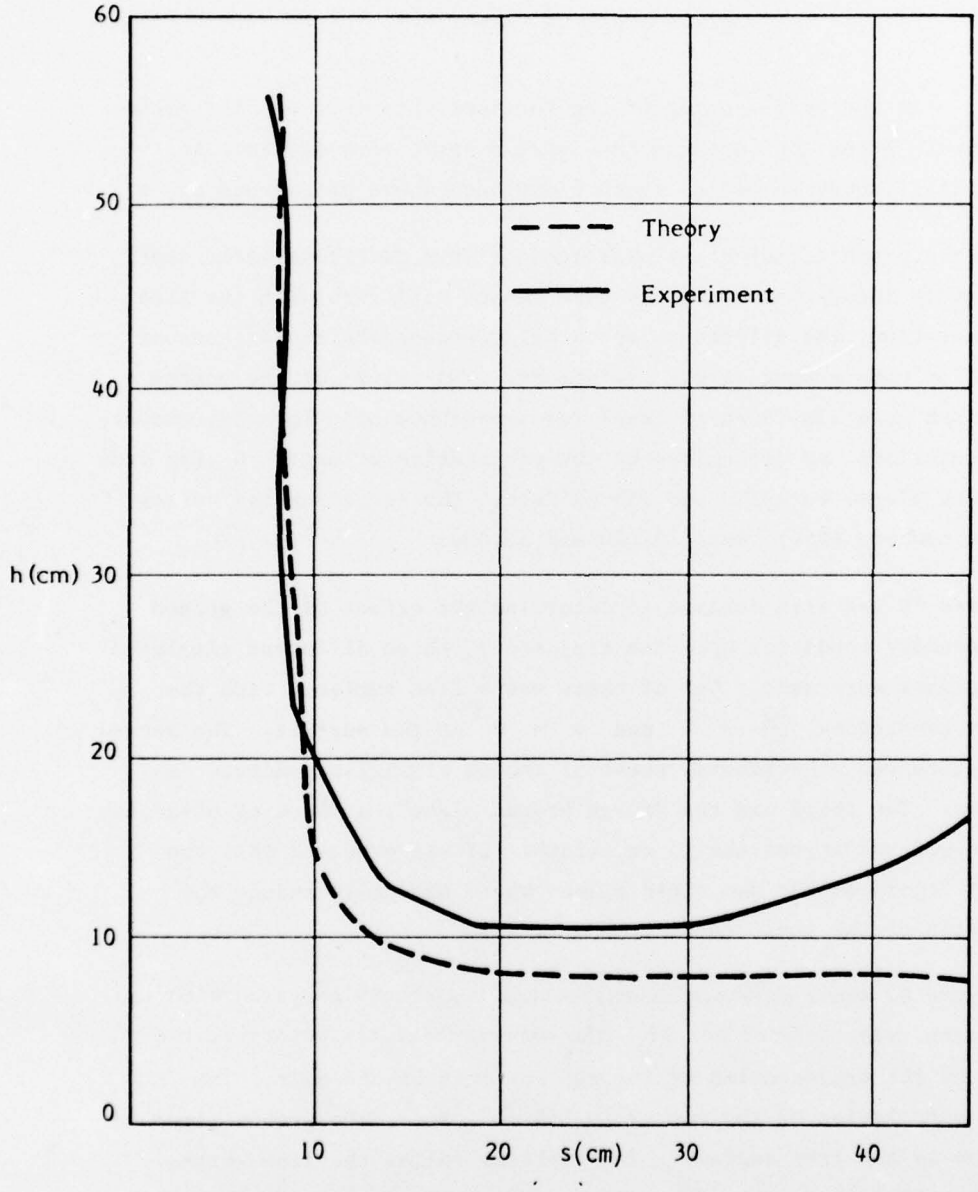

Figure B-7. Vortex trajectory compared with line vortex theory.

below the surface as they spread. When the half-separation of the vortices reaches about 30 cm., they suddenly begin to move away from the surface. This unexpected motion away from the surface, which we will call "rebounding", is very repeatable and always occurs simultaneously in both vortices of the pair. It is not caused by the imaging effect of the side walls of the tank, since these walls are 90 cm. away from the vortices when the rebounding begins. The downward vertical velocity induced by the side wall image pair has been calculated and is negligible. Recent measurements of ground effect trajectories of full scale aircraft vortices (Tombach, et al., 1975) also exhibit the rebounding phenomenon, especially when the aircraft is flying very near to the ground.

Figure 8 shows a vortex trajectory measured under the same conditions as in Figure 7, except that the distance from the generator to the surface is half as great. There are two distinct differences between these trajectories. The pair generated closer to the surface reaches a depth of 8 cm. before rebounding begins, whereas the other pair only reached a depth of 11 cm. When the near-surface vortex pair begins to rebound, it does so more severely and then levels off again at a distance of about 14 cm. from the surface. This result is also in qualitative agreement with the flight test data. All of these results can be attributed to the effects of finite core radius, which will be discussed below.

Figure 9 shows the coordinates of the vortex pair of Figure 8 plotted as functions of time. The slope of the s versus t curve changes suddenly during the rebounding period, at about 8 seconds. In view of this, it should also be of interest to plot the "apparent circulation" of the vortex versus time. We define apparent circulation to be the value of Γ determined from the line vortex trajectory formula:

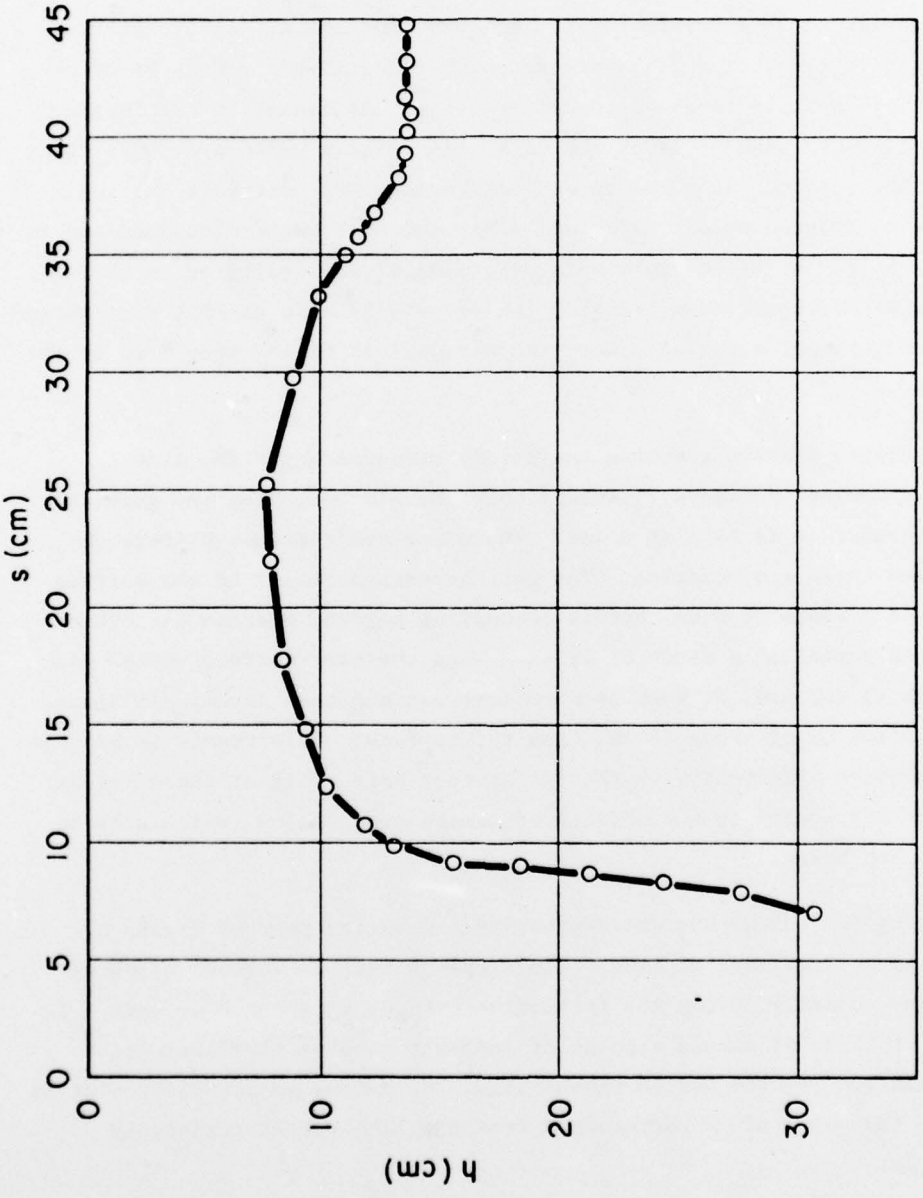

Figure B- 8. Vortex trajectory with generator near surface.

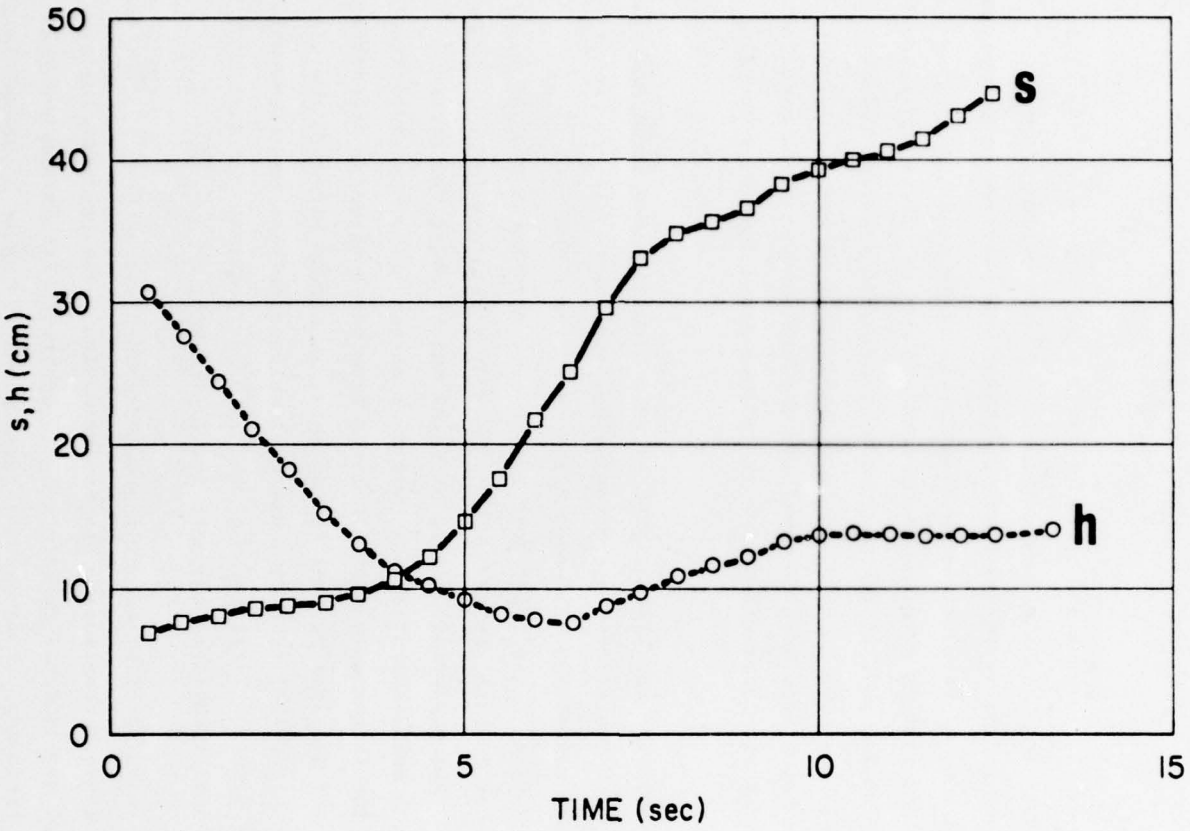

Figure B- 9. Vortex coordinates vs. time.

$$\Gamma = 4 \pi q \frac{s\, h\, (s^2 + h^2)}{(s^6 + h^6)^{1/2}} \qquad \text{(B-8)}$$

Here q is the propagation speed of the vortex, $(\dot{s}^2 + \dot{h}^2)^{1/2}$. This formula does not give the true circulation of the vortex since the exact shape of the vorticity-containing core has not been accounted for. A typical plot of apparent circulation versus time is shown in Figure B-10. The circulation remains nearly constant for the first six seconds, during which the pair is propagating vertically at constant velocity and separation. The circulation then undergoes a series of oscillations which are repeatable both in amplitude and frequency. These oscillations occur during the interaction with the ground plane and the rebounding process.

Trajectories can also be plotted in a dimensionless form, and then compared with the flight test experiments. In Figure B11, we have plotted the normalized half-separation s/s_o as a function of the normalized time $\Gamma_o t/s_o^2$, for both the present experiment and the flight test data of Tombach, et al (1975). The flight data are for an Aero Commander 560A twin engine aircraft flying at eight meters above the ground. The initial half-separation s_o was five meters. The apparent circulation for the flight data was calculated from the horizontal propagation speed of the vortices as they spread apart in ground effect. The time origin of the flight test data has been shifted so that the first point coincides with the first point of the laboratory data. The agreement between these normalized trajectories is striking.

The presence of either of the rigid ground planes has little effect upon the gross properties of the vortex motion. The trajectories are nearly the same and the oscillations in apparent circulation occur at the same frequency. However, the rigid planes do cause a gradual loss of apparent circulation as the vortices spread out in ground effect. The loss amounts to about 20% for the smooth plane and slightly more for

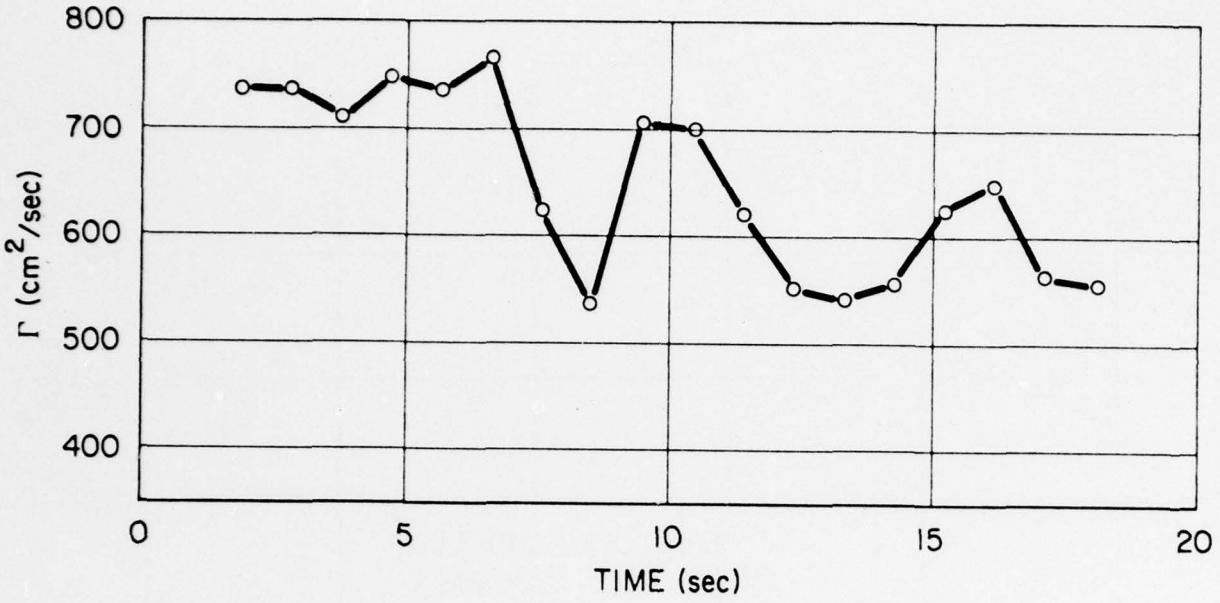

Figure B-10. Apparent circulation vs. time.

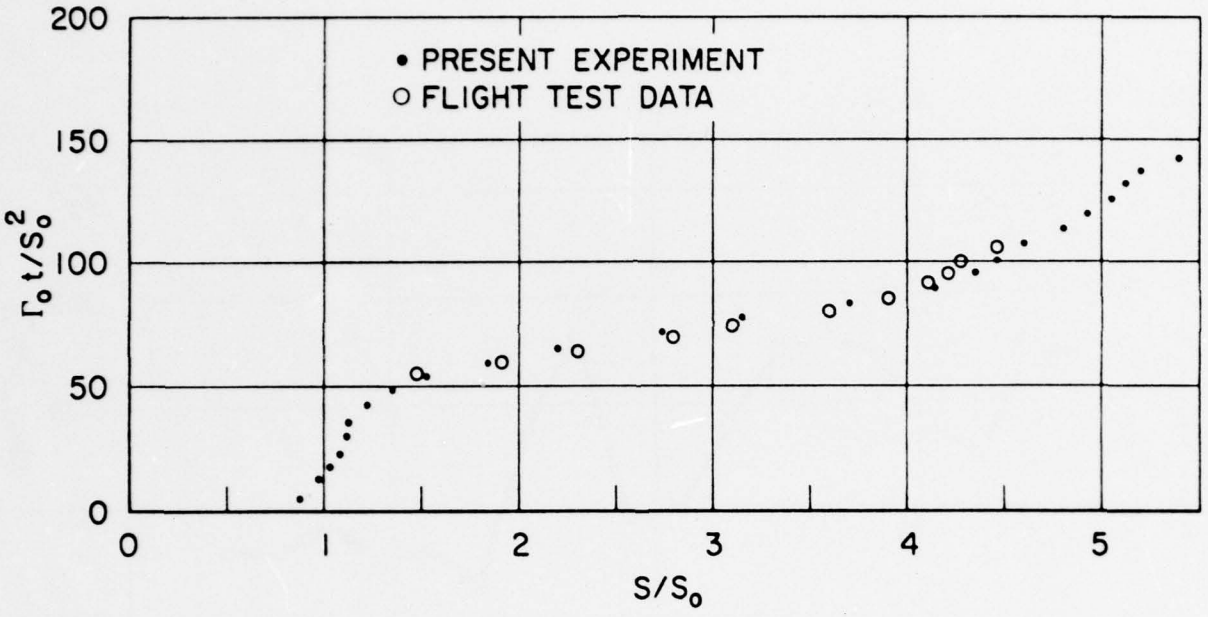

Figure B-11. Normalized vortex trajectory c.f. flight test data.

the rough plane. There is no obvious dependence of this loss upon Reynolds number in the data.

B. 4. Conclusions.

The most unexpected result of this experiment is the "rebounding" effect, which consistently takes place after the vortices have spread in ground effect to about four times their original separation. The agreement with the flight test trajectories shows that this is a real effect and not an artifice of the experiment. The explanation of the rebounding almost certainly lies in the effects of finite core radius. The dynamics of a vortex pair of finite core radius interacting with an image plane are complex, but it is intuitively apparent that a circular core will be deformed into a non-circular shape when it nears the surface. In fact, the eccentricity of the vortex can be seen in Figure 12, which shows a dyed vortex pair close to the surface. Once a vortex core is deformed, it would be expected to become unsteady in shape and vorticity distribution. An elliptical vortex core might have a tendency to rotate as it moves along the image plane. This would lead to changes in both the distance of the vortex center from the surface and the propagation velocity of the center. Such an effect could explain both the rebounding and the periodic oscillation of the apparent circulation.

If we model the vortex core as an ellipse in solid body rotation, we can predict the period of the oscillations. The result of this crude model is a period of three seconds, which is in fairly good agreement with the plotted data of Figure 10. The eccentricity of the vortex cores has also been predicted by a numerical simulation study currently in progress at Poseidon Research. In fact, the core shapes predicted by the numerical simulation are almost exactly those seen in the experiment.

In future studies we shall measure fluid velocities in the vortex flow field and determine the dimensions of the vortex cores. The dependence of the trajectories upon the exact vorticity distribution can then be determined. The agreement between the present normalized trajectory plot and that of the flight tests (Figure 11) may indicate that the ratio

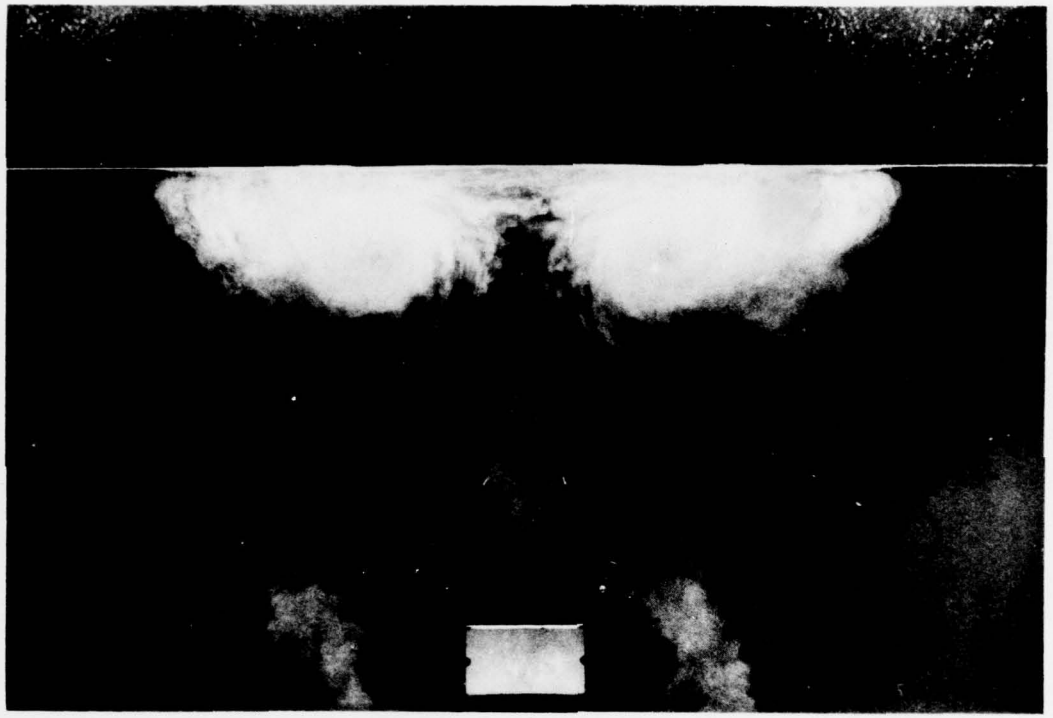

Figure B-12. Vortex pair in ground effect.

of core radius to initial vortex spacing is roughly the same in the experiment as in the flight tests. The trajectories of vortices generated at a greater depth do not agree so well with the flight tests, presumably because these vortices have a larger ratio of core radius to separation when they reach the surface. Previous numerical studies have shown that a large core radius can lead to instabilities in which the two vortices tear each other apart. The movies of the present experiment show a core instability taking place after the rebounding process, which might result from this mechanism.

This experimental technique has been shown to be extremely useful in simulating large scale two dimensional vortex dynamics in the laboratory. Effects of finite core radius can be observed in the laboratory and are also found in flight test data. These effects had not been expected before the experiment.

B.5 BIBLIOGRAPHY

Baker, G.R., S.J. Barker, K.K. Bofah, and P.G. Saffman (1974). Laser anemometer measurements of trailing vortices in water. J. Fluid Mech. 65, Part 2, 325.

Bate, E.R., Jr. (1974). A study to determine the structure of trailing vortices from full scale flight test data. Aero-Vironment Inc. Final Report No. AV FR 441, Pasadena, Ca.

Brown, G.L. and A. Roshko (1974). Density effects and large structure in turbulent mixing layers. J. Fluid Mech. 64, Part 4, 775.

Caiger, B. and D. Gould (1971). An analysis of flight measurements in the wake of a jet transport aircraft. In: Aircraft wake Turbulence and Its Detection, 1st ed., Plenum Press, New York, 125.

Crow, S.C. (1970). Stability theory for a pair of trailing vortices. AIAA J. 8, 2172

Crow, S.C. (1975). The stability of vortex cores. Poseidon Research Note #4. (Also Appendix A of this report)

Lamb, H. (1932). Hydrodynamics. 6th ed., Dover, New York, 223.

Lezius, D. (1973). Study of the far wake vortex field generated by a rectangular airfoil in a water tank. AIAA paper no. 73-682

Mason, H. and J. Marchman (1972). The farfield structure of aircraft wake turbulence. AIAA Paper No. 72-40.

Maxworthy, T. (1974). Turbulent vortex rings. J. Fluid Mech. 64, Part 2, 227.

Miller, E. and C. Brown (1971). An experimental study of trailing vortex wakes using a large towing tank. Hydronautics Tech. Report No. 7105-1.

Orloff, K. and G. Grant (1973). The application of a scanning laser-Doppler velocimeter to trailing vortex definition and alleviation. AIAA Paper No. 73-680.

Saffman, P.G. (1973). Structure of turbulent line vortices. Phys. Fluids 16, (8), 1181.

Tombach, I.H., E.R. Bate, Jr., and P.B. MacCready, Jr. (1974). Investigation of the motion and decay of the vortex wake of a light twin-engine aircraft. AeroVironment Inc. Final Report NO. AV FR 439.

Tombach, I.H., S.C. Crow, and E.R. Bate (1975). Investigation of vortex wake stability near the ground. Air Force Office of Scientific Research Report TR-75-1501

APPENDIX C

REPORT OF INVENTIONS

The work performed under this contract has increased understanding of the behavior of aircraft wake vortices near the ground and resulted in the development of a simple model to describe the gross mechanisms of the vortex breakdown phenomenon. However, after a diligent review of the work performed under this contract, it has been determined that no new innovation or discovery resulting in an invention or improvement to an invention was made.

☆U.S. GOVERNMENT PRINTING OFFICE: 1977—701-218/61

200Copies